FURTHER TESTS OF CAST C4 BLADES IN THE VORTEX WIND TUNNEL

by

D.J. CLOSE, B.E.

A Thesis submitted for the Degree of Master of Engineering Science in the Faculty of Engineering of the University of Tasmania.

September, 1960.

ACKNOWLEDGMENTS

This work was carried out in the Civil Engineering Department of the University of Tasmania. The author wishes to thank members of the staff of the University and of the Aeronautical Research Laboratories, Melbourne. In particular the author wishes to thank Professor Oliver, Professor of Civil Engineering at the University of Tasmania for his help and encouragement, and Mr. A. Robinson who assisted in all the experimental work.

SUMMARY

Extensive tests on the Vortex Wind Tunnel fitted with sand cast blades of free vortex design, have been carried out.

The performance of the blades is much better than obtained in previous tests (Ref. 3) and this is attributed to modifications made to the tunnel.

Whenever possible, the results from the tests are compared with two dimensional cascade data (Refs. 4, 6 and 15), and radial equilibrium studies are made on the flow. The agreement between the actual blade performance and the cascade data, is good, considering that the blades themselves are not of design shape. The flow appears to have almost reached a state of radial equilibrium $\frac{1}{2}$ chord lengths downstream of the blade rows.

By examining data on secondary flows, (Ref. 10, 11, 16 and 17), and results from the Vortex Wind Tunnel, a picture of secondary flow formation is presented.

CONTENTS

CONTENTS (Contd.) Page

CONTENTS (Contd.)

α_i - Air inlet angle to inlet guide vanes (degrees).

α_o - Air outlet angle from inlet guide vanes (degrees)

α_1 - Air inlet angle relative to rotor (degrees)

α_2 - Air outlet angle relative to rotor (degrees)

α_3 - Air inlet angle to stator(degrees)

α_4 - Air outlet angle from stator (degrees)

β_i - Inlet guide vanes blade inlet angle (degrees)

β_o - Inlet guide vanes blade outlet angle (degrees)

β_1 - Rotor blade inlet angle (degrees)

β_2 - Rotor blade outlet angle (degrees)

β_3 - Stator blade inlet angle (degrees)

β_4 - Stator blade outlet angle (degrees)

θ - Blade camber angle (degrees)

ξ - Blade stagger angle (degrees)

i - Air incidence angle onto blade (degrees)

δ - Air deviation angle from blade (degrees)

ε - Air deflection through cascade (degrees)

ϕ - Angle between tangent line on blade pressure surface, and chord line (degrees)

ξ_{rel} - Relative stagger angle along blade (degrees)

δ_D - Design deviation from Constant's or Reeman's Rule (degrees)

i^* - Howell nominal incidence (degrees)

ε^* - Howell nominal deflection (degrees)

δ/δ_D - Deviation ratio

$i-i^*/\varepsilon^*$ - Incidence ratio

$\varepsilon/\varepsilon^*$ - Deflection ratio

V_a - Axial Velocity (ft./sec.)

V_i - Inlet Air Velocity (ft./sec.)

V_u - Air velocity in circumferential direction (ft./sec.)

U_m - Rotor speed at mid blade height (ft./sec.)

U_T - Rotor speed at tip (ft./sec.)

$\overline{V_a/U_m}^\circ$ - Non dimensional axial velocity, averaged in circumferential direction

ΔP - Total head (ft.)

ΔP_s - Static head (ft.)

ρ - Air density (slug/cu.ft.)

$\Delta P / \frac{1}{2}\rho U_m^2$ - Non dimensional total head

$\Delta P_s / \frac{1}{2}\rho U_m^2$ - Non dimensional static head

$\bar{\psi}_m$ - Non dimensional total head, averaged in circumferential direction

ψ_m - Overall total head

ϕ_m - Overall flow

C_D - Coefficient of drag

s - Blade spacing

c - Blade chord length

s/c - Space : Chord ratio

r - Length in radial direction

C_θ - ~~Length~~ Angle in circumferential direction

z - Length in axial direction

F_r - Friction force in radial direction

INTRODUCTION

In 1956 and 1957, tests were made on the Vortex Wind Tunnel fitted with sand cast and machined blades of free vortex design. The performance achieved was poor, the maximum efficiency being 80 per cent and the maximum pressure rise 0.60. The performance of the machined blades was a little better than that of the cast blades.

The poor performance of the cast blade set was thought to be due to the following factors.

(i) Deviation of the blade shape from design, due to distortion on cooling during manufacture.

(ii) Air leaks at the rotor hub, which were present for both the cast and machined blade sets.

(iii) Incorrect blade setting

The subject of this report, is a comprehensive series of tests carried out on the sand cast blade set. An attempt was made to determine the angles of the blade set, and every care was taken to set the blades accurately and to prevent air leaking into the tunnel at the rotor hub.

Whenever possible, results from the tests have been compared with the Howell data mentioned in Ref. 6. Comparisons have also been made between the performance of the rotor and stator at mid-blade height and the results of tests on the standard S1 Cascade, described in Ref. 4.

Some emphasis has been placed on the study of secondary flows in the Vortex Wind Tunnel and by comparing them with those noted by other workers, a picture of the formation of secondary flows is presented.

Since the Vortex Wind Tunnel was moved to a new location immediately before the test, details of the initial calibration of the tunnel are included.

PART I

DESCRIPTION OF TUNNEL AND OF CAST BLADE SET

1. Description of Tunnel

The tunnel section and its position in the Fluid Dynamics Laboratory of the University of Tasmania, are shown in Figures 1 (a) and (b).

Briefly, the air enters the tunnel radially inward through a wire gauze, and is turned into an annular duct through a 90 degree bend, after which it moves axially through the tunnel working section. The working section has core and shell diameters of 27 and 45 inches respectively, giving a hub:tip ratio of 0.6. After passing through the inlet guide vanes, rotor and stator, the air moves through a parallel section of length 54 inches, which is followed by a diffusing section of length 13 feet. The diffuser is formed by the shell flaring out in an included whole angle of 5½ degrees, the core remaining cylindrical. Outlet is radially outward, the flow being controlled by a sliding throttle, which is in turn controlled by three chain driven driving screws.

The compressor is driven by a 40 H.P. direct current motor with a Ward Leonard speed control. Speed is measured by a calibrated strobodisk

illuminated by a fluorescent tube, and torque is measured by weighing the torque reaction of the driving motor on a set of scales.

An instrument carriage is provided so that instruments may be stationed at different radial positions and set at various yaw angles downstream of each of the blade rows.

All the blades are provided with one inch diameter cylindrical machined bosses at the mid chord position. The inlet guide vanes and stators are mounted in holding rings which are fitted into the outer shell. Hand operated driving screws rotate these rings so that two complete blade spaces (6 inches at mid blade height) can be traversed past a stationary instrument.

The system whereby the rotor blades are held in the rotor is shown in Fig. 2. The holding washer prevents movement of the blade in the radial direction, while the flange is screwed to the main rotor disk to hold the blade at the required stagger, after setting. The rotor leading edge is flush with the upstream edge of the rotor disk, while the trailing edge extends one half inch, that is, 1/6 chord lengths downstream of the downstream edge of the rotor disk.

The spacing of the blade rows may be altered by inserting shell rings of different widths into the outer casing.

A pitot static tube is placed upstream of the inlet guide vanes, and wall tappings are located upstream and downstream of each of the blade rows, and at the end of the parallel section downstream of the stator, Axial slots in the shell and core of the tunnel allow instruments to be inserted downstream of each of the blade rows, for detailed testing. The axial positions of the measuring stations are given more precisely in Table V, page 12, while the circumferential location is shown in Fig. 1(a).

Pressures are measured on a multitube alcohol manometer, inclined at an angle of arsine $\frac{1}{4}$ to the horizontal.

The greater clearance between the tunnel and the adjacent wall and roof, as compared to its previous location, should give more even inlet conditions.

More complete descriptions of the tunnel are given in Refs. 1, 2 and 3.

2. Details of Blading

The design dimensions and blade angles are included in Table III, page 9. Details of the design are given in Ref. 1.

The design blades are the well known C4 profiles on circular arc camber lines. The mid blade section on rotor and stator is the standard S1 Cascade, referred to in Ref. 4, comprising C4 aerofoils of 10 per cent maximum thickness. The stagger angle is 29.5 degrees and the camber angle is 31.1 degrees. The degree of reaction is 50 per cent at a flow $\phi_m = 0.76$. Fig. 3(b) shows a sketch of the aerofoil section used in the S1 Cascade and the profile co-ordinates. Fig. 3(a) shows, diagrammatically, the blades angles β_1, β_2 etc. and the air angles α, α_2 etc.

The blades, which are of constant chord length of 3 inches, are twisted about the line of maximum camber, which is straight and radial,

giving nominally free vortex flow at the design point.

The blades, as tested, differed from these design dimensions, as discussed in the next section.

To prevent air leaking into the tunnel through clearances of 0.020 and 0.060 inches, upstream and downstream of the rotor between the rotor disk and the core section, the following precautions were taken to seal off the core section from atmosphere. The core ends were blocked by masonite disks, with rubber sealing rings glued between them and the core, around their bearing surfaces. Molten paraffin wax was poured into the ends of the hollow struts which support the core section. The only effect of the clearances should be some recirculation through them.

3. Details of Cast Aluminium Blade Set

3.1 Measurement of Blades

Sections of the blades were measured by mounting them in a dividing head on the table of a milling machine and tracing a dial gauge, fitted with a point contact, over the profile. The reference point used was where the trailing edge arc appeared to join the pressure surface of the C4 profile. The blade was traversed underneath the dial gauge, readings being taken every 0.1 inches near the trailing and leading edges, and every 0.2 inches elsewhere.

The blade was then rotated 180 degrees and a point similar to that on the pressure surface was used as reference point on the suction surface. The blade was traversed in a similar manner to that adopted for the pressure surface.

To enable one surface to be located with respect to the other, and the leading edge point to be fixed relative to the trailing edge point, the maximum thickness and chord length were measured with a micrometer and a set of vernier calipers.

3.2 Construction of Blade Angles

The blade was drawn five times full size, and the two surfaces located with respect to each other by assuming that the maximum thickness occurred at 0.30 of the chord length as given by the co-ordinates in Fig. 3.

The method of construction used is shown in Fig. 4. Three positions, set near the leading edge, near mid chord and near the trailing edge were chosen, and the mid-thickness points at each, calculated. The mid-thickness points should have been calculated for sections perpendicular to the camber line. However, since the camber line was then unknown, in the case of the low cambered and relatively straight inlet guide vanes and stators, sections in the direction OY were used. For the relatively high cambered and twisted rotor blades, the directions of the camber line at each positionwere guessed and the sections were drawn perpendicular to these directions.

A circular arc was drawn through these points by constructing the perpendicular bisectors CAE and DBF, and extending them until they intersected at G, the centre of the arc. The circular arc camber line was then drawn through the three mid-thickness points. The same

three positions, as nearly as could be estimated, were chosen, to construct the camber line on all sections.

An arc was drawn tangent to the pressure and suction surfaces near the trailing edge, to form the trailing edge arc. The point of intersection of the substituted camber line and the trailing edge arc, was assumed to be the trailing edge point, T. The intersection of the camber line with an arc of radius equal to the measured chord length of the blade, and having its centre at the trailing edge point T, was assumed to be the leading edge point L. Line TL was then the chord line. Angle TGL, which was equal to the camber angle θ, was measured. A line was drawn tangent to the pressure surface, intersecting TL at J, and its angle with TL, ϕ, was measured. This angle was required later, for blade setting.

When more than one section of a blade was measured, the angle between TL and the reference line OX was obtained. OX represented the table of the milling machine which was kept in the same position relative to the blade when more than one section was measured. For the different sections of a blade, this angle gave their relative stagger angles.

The graphical method shown in Fig. 4, was used to measure all the angles, but in several cases the angles were checked by analytical geometry, using the same procedure as outlined above. This method, although eliminating graphical measuring errors was tedious, and in any case the angle ϕ, between the tangent to the pressure surface and TL could only be determined by constructing part of the blade.

Angles at the mid blade height of six blades each from the inlet guide vane, rotor and stator sets were constructed in this way. Blade angles were also measured at the free end and one inch from the boss end of one blade from each group, and one other blade from each group was measured at one inch intervals along its length.

At the stations where more than one blade was measured, the mean of the measured angles was calculated, and the maximum spread of results was found to be $\pm$ 0.5 degrees in camber angle and 0.2_5 degrees in stagger angle. The majority of the measured angles were in a range half as wide. Where the blade angles of a section were computed by both the graphical and analytical methods, the differences were less than 0.3 degrees in camber and 0.2 degrees in stagger. When the corresponding section on several blades was measured by the graphical method the mean value of the blade angles differed from the angles of one of the sections calculated using the analytical method, by less than 0.1 degrees in both camber and stagger.

Tests carried out in conjunction with the overall testing of the compressor suggested that individual differences between the blades were negligible. Assuming that the blades are similar, the method of representing them is shown by the comparisons in the above paragraph to have been accurate and common to sections examined.

In the analysis of results, air angles are referred to the two

dimensional cascade data, presented in Refs. 4 and 6. Difficulty is encountered in finding the source of differences between the performance of the blades in the Vortex Wind Tunnel, and the performance predicted from the two dimensional cascade data. One of the reasons for this is undoubtedly the differences in the flow pattern of a three dimensional as compared to a two dimensional cascade. However, another source of difference is that the measured blade angles of the cast aluminium blade set, do not bear the same relation to the profile as do the blade-angles referred to in Refs. 4 and 6, and shown in Fig. 3.

The surface roughness of the blades was found by tracing the dial gauge with the point contact over a small area of a blade surface. This method is rather crude, but showed the surface roughness to be the order of 0.001 inches to 0.002 inches from the mean, although there were some indentations on odd blades which were much larger.

The following table, Table I, gives the measured blade angles at one inch intervals along the blades. Where more than one section was measured, the average of the angles is recorded and shown by an asterisk.

TABLE I

Distance from Core - in

		0	1	2	3	4	4.5	5	6	7	8	9
I.G.V.	θ°	35.5*	32.4_5	31.2	30.9	30.4	29.5*	29.65	28.8	27.6_5	25.7*	
	ξ_{rel}°	-3.7*	-2.8	-2.6	-1.9	-0.8	-1.55*	-0.8	-0.5_5	+0.3	0.6*	
Rotor	θ°		47.7*	43.5_5	39.4	33.9_5	31.5*	31.0	26.8	21.9_5	18.9	19.0*
	ξ_{rel}°		-6.2*	+0.6	4.7	9.2	11.5*	13.9	15.8_5	20.7_5	23.1	25.5*
Stator	θ°	33.2*	32.0	29.9	31.8	31.3_5	32.9*	31.2	32.5	32.0	31.2_5*	
	ξ_{rel}°	8.2*	6.25	4.5	4.0	2.2	1.4_5*	-0.1	-0.5_5	-1.6_5	-2.7*	

4. Examination of Predicted Performance

Because of the differences between the cast and design blade shapes, it was decided to investigate several settings of the blade rows, to obtain the best from the point of view of row matching.

Three of the row settings examined, are shown in the table below. Setting I, is with the blades set as if they were of the design shape. Settings II and III are with the rotor at increased and decreased stagger, and with the inlet guide vanes and stator set to give the best range of incidence along the blade lengths.

TABLE II

Distance from Core - in

	0			4.5			8			
Settings	I	II	III	I	II	III	I	II	III	
ξ°	-16.6_5	-11.9	-12.2	-14.5	-9.7_5	-10.05	-12.75	-8.0	-8.3	Inlet Guide Vanes
β_i°	0.25	5.0	4.7	0.2_5	5.0	4.7	0.2_5	5.0	4.7	
β_o°	33.5_5	28.8	29.1	29.2_5	24.5	24.8	25.7_5	21.0	21.3	
i°	0.2_5	5.0	4.7	0.2_5	5.0	4.7	0.25	5.0	4.7	
ξ°	4.2_5	6.5_5	2.5_5	29.7	32.0	28.0	41.3	43.6	39.6	Rotor
β_1°	29.4_5	31.7_5	27.7_5	45.4_5	47.7_5	43.7_5	50.8_5	53.1_5	49.1_5	
β_2°	-20.9_5	-18.6_5	-22.6_5	13.9_5	16.2_5	12.2_5	31.7_5	34.0_5	30.0_5	
i°	-6.1	-3.5_5	-0.1_5	-4.3_5	-3.6_5	0	-0.6_5	-0.8_5	3.0	
ξ°	37.1_5	31.0	34.0	29.7	23.5_5	26.5_5	25.5_5	29.4	32.4	Stator
β_3°	53.5_5	47.4	50.4	46.1_5	40.0	43.0	41.4_5	35.3	38.3	
β_4°	20.7_5	13.6_5	16.6_5	13.2_5	7.2	10.2	9.6_5	-0.4_5	2.5_5	
i°	-4.5_5	0.6	-0.6	-4.1_5	0.4	0.1	-2.6_5	1.1	2.1	

The predicted rotor performance curves, calculated from the Howell data in Ref. 6, are shown in Fig. 5. The corresponding performance curves for the original design are also included as a comparison. They show that Setting I gives the lowest pressure rise with the highest flow at the design point, while Setting III gives the highest pressure rise with the lowest flow at the design point. Setting II gives intermediate conditions at the design point. Matching along the rotor blade height at the design point is best at Setting III.

For this reason, Setting III would probably give the best compressor performance. However, there is generally little difference between the three settings, and Setting I was chosen, since it was at this nominal setting that the previous tests were conducted.

For Setting I, the inlet guide vane stagger was altered from -13.9 degrees which was the design setting at mid blade height to -14.5 degrees which gives better rotor incidence at nominal conditions.

5. Mounting of Blades

The blades were set at the mid-blade height. On previous occasions, the setting station had been near the blade tips. It is felt that the effect of any errors in setting, or in actual blade twist will be minimised by using mid blade height as the setting station.

The blade setting device consisted of a straight edge mounted on a frame, which was clamped to the blade holding rings in the case of the inlet guide vanes and stator, and to a shell ring in the case of the rotor. To set the inlet guide vane and stator blades the shell rings were removed from the tunnel. The rotor blades were set with the rotor mounted on the shaft.

For the required stagger angle, the angle that the line tangent to the pressure surface made with the axial direction was measured by drawing the blade profile. The straight edge, mentioned in the above paragraph was set to this angle. For Setting I, the straight edge was set as for blades of the design shape.

With this setting, the blade was moved until its pressure surface was tangent to the straight edge. Errors involved in setting the blades should be less than 0.05 degrees.

Table III below gives a comparison between the design blade angles and those for Setting I, which of course, are angles measured by the method discussed on Pages ,5 and 6. The leading dimensions of the tunnel are also included.

TABLE III

	IGV		Rotor		Stator	
No. of Blades	38		37		38	
Hub Diameter	27"		27"		27"	
Tip Diameter	45"		45"		45"	
Hub Clearance	0.020"-0.060" (2/3 to 2% span)		0,030" (1% span)		0.030" (1% span)	
Tip Clearance	0.025" (0.8% span)		0.033" (1.1% span)		0.020" (2/3% span)	
Aspect Ratio	3		3		3	
	Design	Measured	Design	Measured	Design	Measured
$S/_C$ at Mid Blade Height	1	0.99	1	1.02	1	0.99
Hub Stagger Angle	-17.2°	-16.6_5°	4.2°	4.2_5°	37.2°	37.1_5°
Mid Blade Stagger Angle	-13.9°	-14.5°	29.5°	29.7°	29.5°	29.7°
Stagger Angle 1" from Tip	-12.2_5°	-12.7_5°	41.9°	41.3°	25.1°	25.5_5°
Hub Camber Angle	34.4°	33.8°	52.5°	50.4°	32.9°	32.8°
Mid Blade Camber Angle	27.8°	29.5°	31.1°	31.5°	31.1°	32.9°
Camber Angle 1" from Tip	24.5°	26.0°	19.7°	19.1°		31.8°
	IGV		Rotor		Stator	

PART II

PRELIMINARY TESTS, METHOD OF DETAILED TESTING, INSTRUMENTATION AND PRESENTATION

1. Preliminary and Static Tests

1.1 Measurement of No Load Torque

Before the test rotor was installed in the tunnel, a rotor with blades removed was mounted on the shaft and torque measurements were taken for a range of speeds up to 650 r.p.m. Speeds higher than this could not be tested as small deviations in straightness caused the shaft to vibrate alarmingly.

The no load torque curve, shown in Fig. 6, has been extrapolated to 750 r.p.m., at which speed, the error in no load torque may be as high as $\pm$ 0.5 ft. lb. At 750 r.p.m. this represents an error of $\frac{1}{2}$ per cent for the flows tested. However, as torque is only used as one check on efficiency, this error is not very critical.

1.2 Investigation of Inlet Conditions

Pitot static tube traverses were made at the top, bottom and two sides of the tunnel, one chord length (i.e. three inches) upstream of the inlet guide vanes leading edge. As instrument carriages are not provided at these stations, the instrument was held in the hand. The radial position of the instrument was measured using a steel rule, and it was held in an axial direction by eye.

Errors in the radial position should be 0.1 inches at most, and except for the station at the bottom of the tunnel where the experimenter had to lie on his back, yaw angles of the instrument should be not greater than 5 degrees. Chapter 4 of Ref. 5 indicates that a yaw angle of 10 degrees in the setting of a pitot static tube, gives readings of total pressure 1 per cent low, and of static pressure 2 per cent low. Thus the difference between true and measured velocity, due to yawing the instrument, should be less than 1 per cent.

Tests at 300, 500 and 750 r.p.m. were made at various throttle settings. For one speed and throttle, differences between measured flows at the four stations, which were obtained by integrating the measured velocities across the annulus, were less than 3 per cent and generally 1 per cent. Thus, taking into account the possible errors in velocity due to instrument yaw, the flow seems evenly distributed around the annulus.

The velocity profiles for one station, at one flow condition, showed variations in the region away from the walls, that is, from 1 to 8 inches from the hub, of about 1 per cent. Hence the velocity may be assumed to be uniform across the annulus, at the four measuring stations, away from the wall boundary layers.

There was a tendency for more flow to pass through the side stations than through the top or bottom. For the eighteen combinations of flow and speed examined, the highest measured flow passed through one

of the side stations fifteen times. However, the differences were so small that it can only be described as a general trend.

1.3 Wall Static Tests

Wall static tapping readings were taken at a range of rotor speeds and throttle settings, to give an approximate picture of the tunnel performance. Readings were also taken from a pitot static tube, placed one chord length upstream of the inlet guide vanes at the calculated mean flow height of 5 inches from the hub.

The axial positions of the wall static tappings are listed below -

(i) 3 inches upstream of the inlet guide vanes leading edge;
(ii) 2 inches downstream of the inlet guide vanes trailing edge;
(iii) $2\frac{1}{2}$ inches downstream of the rotor trailing edge
(iv) $1\frac{1}{2}$ inches downstream of the stator trailing edge.

To draw approximate total pressure versus flow characteristic curves, the following assumptions were made. Axial velocity at the mid blade height of the rows was assumed to be the same as measured by the inlet pitot static tube, and the static pressure at mid blade height was assumed to be the same as measured by the appropriate wall tapping. Then assuming that air deviations from the inlet guide vanes were given by Reeman's Rule, and those from the rotor and stator were given by Constant's Rule, as set out in Ref. 8, approximate absolute velocity and hence total pressure were calculated.

These curves and the approximate efficiency curves calculated from these results, served as a guide to the flows to be tested. The flows and their corresponding throttle settings are shown in the following table, Table IV.

TABLE IV

Throttle (in)	22	13	10	8	6	5.2	4.8	
ϕ_m	0.90	0.85	0.80	0.75	0.65	0.60	0.56	

The approximate stage total pressure and efficiency curves are shown in Fig. 7 with the corresponding characteristics from detailed tests. They show the agreement to be very good, especially considering the assumptions made when plotting the characteristics from the wall static measurements. The position of maximum total pressure rise is indicated very accurately.

The curves drawn in Fig. 8, showing the wall static pressure readings at different flows and rotor speeds, indicate the differences caused by Reynolds Number effects. The curve for a rotor speed of 600 r.p.m. is not shown as it coincides with that at 750 r.p.m., indicating that the effect has disappeared at those speeds. To be on the safe side, detailed

tests were made at 750 r.p.m. The stator Reynolds Number, based on vector mean velocity and blade chord length, was 1.5×10^5 to 2.2×10^5 for the flow range tested at 750 r.p.m.

2. Instrumentation and Procedure for Detailed Testing

For detailed testing downstream of the blade rows, a $\frac{1}{4}$ inch diameter, Fechheimer cylindrical yaw meter was used. The holes are 0.015 inches diameter and the side holes are spaced approximately $\pm$ 40 degrees from the total pressure hole.

The following table gives the positions of the yawmeter when used for detailed testing, distances being measured axially along the tunnel from an arbitrary datum near the inlet guide vanes. The positions of the centrelines of the blade rows are given as convenient reference points.

TABLE V

Station	Position (inches)
Centre Line - Inlet Guide Vanes	4.00
Yawmeter Position I	6.84
Centre Line - Rotor	10.09
Yawmeter Position II	13.66
Centre Line - Stator	16.28
Yawmeter - Position III	19.10

Before detailed tests were made at 750 r.p.m., tests were made at rotor speeds of 300, 500 and 750 r.p.m. to determine Reynolds Number effects in more detail than could be obtained from wall static tests alone. The tests, which were yawmeter traverses in the radial direction only, were inconclusive from the point of view of Reynolds Number effects and will not be discussed. However, from them the radial stations for more extensive tests were chosen so that the wall boundary layers and other interesting features could be shown. Radial stations chosen were 0.2 or 0.3 inches apart near the walls and 1 inch apart elsewhere.

For detailed tests at 750 r.p.m., circumferential traverses downstream of the inlet guide vanes and stator, and radial traverses downstream of the rotor were made by adopting the following procedure. Downstream of the stationary rows, the yawmeter was positioned at a radial station and the side holes balanced with the instrument in the free stream between the wakes. Yaw angle, total and side hole pressures, torque, and ambient pressure and temperature were recorded. Then the blade was traversed past the instrument, yaw angle being maintained constant, and total pressure was recorded at circumferential stations 1/180 radians apart through the wake and no more than 1/18 radians apart elsewhere. For one flow two blades were traversed past the instrument to measure any differences in the air flow caused by individual differences in the

blades. Downstream of the rotor, yaw angle and total and side hole pressures were recorded at the appropriate radial stations.

3. Calculation of Velocity

To calculate velocities downstream of the stationary rows, both yaw angle and static pressure were assumed constant in the circumferential direction. This is in accordance with the test procedure described in the previous section.

Subsequent tests showed that the yaw angle variation through the free stream was less than 0.5 degrees, giving a cosine difference of less than 1 per cent, for the angles measured. An examination of calculations and measurements taken 1½ chord lengths downstream of the low speed, two dimensional cascade, from which Ref. 4 was compiled, showed that the yaw angle variation across a blade space was, at most, 2 degrees from the free stream yaw angle. Tests on the ¼ inch cylindrical yaw meter indicated that for the total pressure range examined in the Vortex Wind Tunnel, a yaw angle of 5 degrees from balance would give an error of little more than ½ per cent, providing the flow was two dimensional. With this proviso, and allowing that the measuring station is much closer to the blade row in the Vortex Wind Tunnel, errors made by assuming yaw angle constant circumferentially should be no more than 1 per cent. In any case, the behaviour of the cylindrical yawmeter in sheared flow is unknown, especially since radial flows along it are almost certainly present, so that any yaw angles measured in a wake would be looked upon with some suspicion.

Ref. 7 notes that to a first approximation, the static pressure across a wake is constant. This assumption was made for these tests.

Another assumption is necessary to calculate velocity from the measurements taken. Velocities at one flow were calculated assuming side hole pressures to be true static. Then, these velocities were multiplied by a constant so that the flow obtained by integrating them across the annulus, checked with the flow measured by the inlet pitot static tube. This had the effect of adjusting side hole pressure to true static. The basic assumption made, to calculate velocities in this manner, was that there were no Reynolds Number effects on the yawmeter. Overall, these effects are probably small, since the flows derived from the calculated velocities checked to within 2 per cent of the corresponding flows, measured by the inlet pitot static tube. The constants used were 0.839 downstream of the inlet guide vanes and stator, and 0.866 downstream of the rotor.

Check calibration tests in a small calibration tunnel showed that there was a 10 per cent variation in the ratio of velocity, calculated from the difference between total and side hole pressures of the yawmeter, and true velocity. The Reynolds Number range was 3.5×10^3 to 11×10^3, based on instrument diameter and free stream velocity. The results of these tests were used to try and determine velocities in the Vortex Wind

Tunnel, but the attempt was unsuccessful, probably due to higher turbulence levels,

By using one yawmeter constant across the tunnel annulus, velocity is overestimated near the walls and underestimated elsewhere. However, since the areas affected by the walls are small, the underestimation near mid blade should be less than 1 per cent. The error may be larger in the wall regions.

4. Discussion of Errors Involved in Measurements

4.1 Torque

As mentioned in page 10 , the error in no load torque may be as large as ± 0.5 per cent. Because of the vibration of the needle when the tunnel wasoperating, the torque reading could not be made to better than ± 0.5 ft. lb., introducing another error of ½ per cent. Hence, assuming that the scales read the correct load, the error may be as high as ± 1 per cent. An attempt to calibrate the scales themselves proved unsuccessful. As mentioned before however, torque measurements were only used for calculating efficiency, which could be checked by another method, so that errors in torque were not really critical.

4.2 Rotor Speed

The measured rotor speed which was obtained by reading the calibrated strobodisk illuminated by a fluorescent tube, was dependent on the frequency of the domestic power supply. It is possible to detect a difference of 1 r.p.m., by the apparent movement of the strobodisk and frequent checks and adjustments were constantly made to the speed.

The variation of the frequency of the power supply was investigated using a frequency counter. It was found to be less than 1/6 per cent, apart from odd fluctuations of up to ½ per cent which lasted for only a few seconds. Hence any errors made by dividing pressures and velocities by U_m^2 and U_m respectively, to make them non dimensional, should be small.

4.3 Yaw Angle

From experience in testing the Vortex Wind Tunnel with the cylindrical yaw meter, yaw angles cannot be consistently repeated to better than 0.2 degrees. This angle is very small as far as its effect on computations are concerned, as the cosine difference in the range of angles tested is only ½ per cent, and the tangent difference, 1 per cent.

4.4 Measuring Station

The measuring station adopted, as shown in Fig. 1(a) was on the side of the tunnel furthest away from the nearest wall of the building; that is, the most favourable from the point of view of inlet conditions.

It was noted on page 10 , that there was a tendency for more flow to pass through the side stations, than through the top or bottom. At the positions A and B indicated in Fig.1(a) the inlet clears the base frame by only 6 inches. Because of their inaccessibility, inlet conditions at these two stations were not measured, but it is to be expected that the flow through them is lower than elsewhere.

Hence, overall flow, total pressure rise and efficiency may be overestimated to some extent, but this of course, has no effect on the performance of individual blades.

5. Presentation

The averages with respect to length in the circumferential direction at one radial station, of total pressure and axial velocity across a blade space are denoted by $\bar{\psi}_m$ and $\overline{V_a/U_m}$. In the case of the inlet guide vanes and stator, these values were obtained by direct computation. For the rotor, the yawmeter was assumed to have measured this average of total pressure, and when continuity had been satisfied, to have measured the same average of axial velocity.

The symbols ψ_m and ϕ_m are used for the rotor and stage total pressure rise and overall air flow. ϕ_m is measured by the inlet pitot static tube upstream of the inlet guide vanes and ψ_m is calculated from the computed values of $\bar{\psi}_m$, and is an area average of $\bar{\psi}_m$ over the annulus. ψ_m was also calculated from a flow average over the annulus, which gave values 2 per cent higher than from an area average. Since this gave peak rotor efficiencies of 97 or 98 per cent, which was much higher than expected, the area average method was preferred.

Throughout the test, when velocities and total and static pressures are mentioned, they refer to the appropriate non dimensional values, unless otherwise indicated.

PART III

DETAILED SURVEY OF RESULTS

1. Stage Performance

The stage pressure rise and efficiency curves are shown in Fig. 9, with the appropriate total pressure rise curve plotted from the data in Ref. 6.

1.1 Discussion of Methods of Predicting Compressor Performance

1.1.1 Method Due to A.R. Howell, Given in Ref. 6.

The data presented in Ref. 6, is obtained from tests on two dimensional cascades. The overall performance of the compressor was predicted by calculating the Howell performance at the rotor and stator mid blade height sections. Since the downstream air angle of all rows at the design flow of $\phi_m = 0.76$ was fixed with the setting of the blades, nominal air angles for each row were automatically determined, and the rotor and stage characteristics were then drawn from the two dimensional cascade data.

In previous tests, the agreement between the measured and predicted overall characteristics has been very good. This is in line with similar comparisons shown in Ref. 13.

In Sections 2.3 and 3.3 of Part III, the Howell data is also used as a basis for examining the performance of individual blade sections. Its primary purpose is a basis for preliminary design, and although it is apparently unsuited to detailed analysis of three dimensional compressor cascades, its predictions of air outlet angle and total pressure rise are, in most cases, quite accurate.

The main points of difference between two dimensional cascade data, and the performance of sections in the Vortex Wind Tunnel, are listed below.

(i) The design curves presented in Ref. 6 are an average of results from two dimensional cascade tests of several C series aerofoils. Fig. 29 shows that the difference between the measured and predicted deflections through the two dimensional S1 Cascade is up to 2 degrees. Howell, in Ref. 13 notes that a difference of 1 degree in deflection alone, makes a difference of 6 per cent in total pressure rise.

(ii) Flow through the compressor is assumed to be cylindrical. The discussion of Fig. 11 on pages 22 and 33 shows that it is not, as the measured flow movement is as large as 5 per cent of the blade height.

(iii) Conditions downstream of a blade row are not taken into account. An analysis on page 22 of the performance of the Vortex Wind Tunnel rotor shows that a complete stall of the rotor was postponed by a tip stall of the stator. This effect

could not have been predicted from the Howell data.

(iv) In Section 8, Part III, differences between the boundary layer migration effects in two and three dimensional cascades are discussed. In the Howell design system, these effects are lumped together into an extra drag term. Comments on pages 24 and 25 indicate that they also play some part in affecting distributions of pressure and yaw angle.

(v) No account is taken of the fluctuating flow, consisting of alternate wakes and free stream regions, which is presented to the rotor and stator from the upstream blade row. From material given in Ref. 7 concerning work on oscillating cylinders, it seems unlikely that this flow pattern results in momentary separation of the flow from the blade and its subsequent reattachment. It seems more likely that, because of the short time that low speed air in a wake is incident onto the blade, the final result is a thickening of the boundary layer on the blade, resulting in slightly higher air deviations from it.

1.1.2 Method Due to A.D.S. Carter

The Carter method of predicting the performance of cascades of aerofoils is given in Ref. 15. Curves of non dimensional incidence against non dimensional deflection, plotted in Figs. 19 and 23 include stalling incidences plotted from this data.

The optimum incidence, which gives the lift: drag ratio a maximum, is assumed to occur at the leading edge of each blade. The cascade is replaced by a row of vortices, because of the shape of the pressure distributions on the suction and pressure surfaces of each blade. Both the vortex row and the action of a blade (or vortex) on its neighbours, which depends on the blade spacing, involve adjustments to the direction of the upstream air to give optimum incidence.

Using two dimensional cascade data, derived from C1 aerofoils, but which, he claims, should also apply to C2 and C4 profiles, several useful refinements are produced. For instance, stalling incidence may be obtained. Also, critical Reynolds Number, corrections for variation in stagger angle of a cascade, and the effects of the position of maximum camber and maximum thickness are discussed in general terms. These provide useful additional knowledge for compressor design, and although performance curves from this data were not plotted, stalling incidence, as shown in Figs. 19 and 23, is predicted quite closely.

1.2 Stage Pressure Rise

The stage pressure rise curve, shown inFig. 9, gives pressures lower, except at the high flows, than those predicted from the

Howell data. The reason for this is not apparent without a detailed examination of the rotor and possibly the stator, performance. In the region of the design flow, ϕ_m = 0.76, the gradient of the design curve is higher by about 50 per cent. Referring to Fig. 5., the difference between the Howell and measured characteristics, is somewhat similar to the difference between the mid blade characteristics of Setting I and Setting III. That is, the difference is similar to that produced by altering the rotor stagger by a few degrees.

1.3 Stage Efficiency

The stage efficiency shown in Fig. 9, is flat and indicates that the efficiency is high over a wide range of flows. Since the rotor and stage efficiencies were calculated from the overall pressure rise and flow and the measured torque, they may be more than 1 per cent in error. However, Table VI, on page 27, which compares stage efficiencies calculated by two methods, suggests that the curve in Fig. 9 gives a fair picture of the efficiency characteristics, differences being not larger, in general, than 1 per cent.

2. Rotor Performance

2.1 Presentation and Calculations

The rotor predicted and measured total pressure rise characteristics and the efficiency curve, are shown in Fig. 9.

Radial distributions of deviations from the inlet guide vanes at various flows, are shown in Fig. 10. They are plotted as δ/δ_0, where δ_0 is the predicted deviation calculated from Reeman's Rule, as in Ref. 8.

Radial movement of flow is shown in Fig. 11. Only those at the four smallest throttles tested are given, as for the other three flows, the movement was too small to be plotted. The movement was calculated by integrating the measured values of $\overline{V_a}/U_m$ across the annulus at each measuring station, and plotting the corresponding integrated flow positions.

Predicted and measured curves of air outlet angle α_3, and total pressure rise at stations 1 inch apart across the annulus, are drawn in Figs. 12 to 18. The predicted values were calculated from the Howell data using values of axial velocity and yaw angle measured downstream of the inlet guide vanes, at the appropriate stations. The axial velocity $\overline{V_a}/U_m$ was used as the rotor was assumed to "see" this average of the wake and free stream velocities. Comparisons between predicted and measured values of α_3 were preferred to comparisons of α_2, as calculating α_2 from measurements downstream of the rotor involves two assumptions, both of doubtful validity, which are discussed below.

(i) The yawmeter measures a certain average of the wake and free stream velocities downstream of the rotor, What average this is, is unknown, since it depends on the damping characteristics

of the yawmeter, connecting tubes and manometer. The measuring setup is heavily overdamped which suggests that the average of total pressure which is measured by the yawmeter is closer to free stream total pressure and hence is higher than a simple average over a blade space, similar to those calculated downstream of the inlet guide vanes and stator. Because of the larger wakes near the walls, total head, and hence velocity in the region of the walls is higher than true velocity, bringing about a decrease in calculated velocity away from the walls, as compared to true velocity when continuity is satisfied. This accentuates errors caused by Reynolds Number effects, as discussed on page 14.

(ii) The wake downstream of the rotor has a certain momentum or displacement thickness. In a later section, Section 5, use is made of the similarity in blade shape between the mid blade sections on the rotor and stator to assume a momentum thickness for the rotor wake. However, similar assumptions about other blade sections are considered to be unwarranted.

In discussing values of either α_1 or α_3 it should be kept in mind that yaw angles measured by the yawmeter downstream of the rotor, are some average of the yaw angles of the wakes and free stream regions. Without making assumption (ii) above, and having some knowledge of the damping characteristics of the system which measured side hole pressures, it is impossible to estimate the variation in α_3 or what average of it, the yawmeter measures. This instrument error is only 2 or 3 degrees at most, and is almost certainly much less.

Curves of deflection ratio $\frac{\varepsilon}{\varepsilon_*}$ plotted against incidence ratio $\frac{i-i_*}{\varepsilon_*}$ for various stations along the rotor, and at various flows are shown in Fig. 19. The ratios are the same as used in Ref. 6. Deflection was calculated from the measured values of $\overline{V_a}/U_m$ and α_3 downstream of the rotor, by assuming no wakes, but since the curves are used for comparison purposes only this does not matter.

The radial distributions of $\frac{\delta}{\delta_0}$, plotted in Fig. 20 are presented in a similar manner to those for the inlet guide vanes shown in Fig, 10. Values of δ were calculated by assuming no wakes from the rotor so are also used for comparison purposes only. δ_0 was computed using Constant's Rule, in Ref. 8.

Radial distributions of total pressure $\overline{\psi}_m$ as measured by the yawmeter downstream of the rotor, and of axial velocity $\overline{V_a}/U_m$ as calculated to satisfy continuity, are given in Figs. 21 and 22.

When examining the total pressure rise and deflection through a section of the rotor, the flow was assumed axial. Although this is not so, as demonstrated in Fig. 11, the discussion on page 32, dealing with flow through the stator, shows that with the present knowledge of flow in compressors, no other assumption has any greater validity.

2.2 The Detection of Stall

For purposes of design, an empirical stall point involving the achievement of some chosen drag, signifies that the blade has stalled. An example of this is given in Ref. 6, where the stall point is taken as occurring when losses reach twice their minimum value.

When detailed traverses, such as those downstream of the stator are available, the fixing of an empirical stall point is relatively simple. Downstream of the rotor, detailed measurements cannot be made, and other means of detection must be used.

Curves drawn in Ref. 6, show that at the arbitrary stall point, the lift and hence the deflection curves, have flattened off. Thus, when overall flow is decreased, a corresponding decrease in total pressure or air deflection at a station, is an indication that the empirical stall point has been reached, or is being approached. The blade may be said to be in a "stalling condition." Whenever the term stall is used in this text, it means that the blade section is in this "stalling condition".

2.3 Discussion of Results

2.3.1. Rotor Overall Performance

The comparison between the predicted and measured total pressure rise characteristics, is similar to that between the predicted and measured stage characteristics, especially with regard to the higher gradient of the predicted curve. However, agreement is better in the region of the design flow of $\phi_m = 0.76$ and generally, Fig. 9 suggests that stator losses are larger than predicted. Also, as the flow is decreased from $\phi_m = 0.60$ to 0.56, rotor overall total pressure rise increases, while that for the stage decreases, indicating high stator losses at $\phi_m = 0.56$.

Maximum measured rotor efficiency is about 96 per cent, which, as discussed on page 14, may be in error by 1 per cent or more, because of incorrect torque measurements and overestimation of flow. However, as mentioned on page 18, the table on page 27 suggests that the errors are no larger than 1 per cent.

2.3.2 Inlet Guide Vane Deviations

The curves of δ/δ_p, plotted for the inlet guide vanes in Fig. 10, show deviations are higher, and hence deflections lower, than expected, by at least 2 degrees.

When predicting the inlet guide vane deviations from other compressors installed in the Vortex Wind Tunnel, Reeman's Rule has agreed with measurements to better than $\frac{1}{2}$ degree over the greater part of the annulus. On page 7, reference is made to possible sources of difference between predicted and measured air angles in this test. One of them was that the measured blade angles, from which the predictionswere made, do not bear

the same relation to the blade profile, as do the angles in Fig. 3. Taking into account the reliability of Reeman's Rule in previous tests, measured deflections at a given incidence, which are 2 degrees lower than those predicted from the Howell data, will be attributed to this cause. This 2 degrees difference will be called the "blade distortion effect."

The effect of theincreased inlet guide vane deviations, is to increase the incidence onto, and hence the pressure rise through the rotor, for a given flow. Thus the overall pressure rise characteristic will be raised.

2.3.3. Rotor Outlet Air Angles

Curves of measured and predicted values of α_3, (Figs. 12 to 18), show measured angles generally lower than those predicted, suggesting increased deviations from the blade.

An error was made in instrument traverses downstream of the inlet guide vanes at $\phi_m = 0.56$, and predictions at this flow are not included. It was considered unnecessary to rerun the tunnel to gain results of inlet guide vane performance, at a flow approaching surge.

The effect of the yawmeter measuring an average of the wake and free stream yaw angles, as mentioned on page 19, should be to increase the measured angle, since the yaw angle of the wakes must be higher than of the free stream regions.

Generally, considering the possible 2 degrees difference due to the "blade distortion effect" the agreement at stations 2 to 5 inches from the hub, where the difference is 2 degrees or less, is remarkably good. At stations 1, 6, 7 and 8 inches from the hub, the difference is much larger being up to 5 degrees. With decreasing flow the difference between corresponding predicted and measured curves increases, especially for those stations where the agreement was best. This comparison is similar to that between the Howell and measured curves for the S1 Cascade, shown in Fig. 29. One interesting feature is the large increase in air outlet angle as flow is decreased from $\phi_m = 0.60$ to 0.56, indicating a decrease in deviation, from that expected.

The curves of δ/δ_0 from the rotor, drawn in Fig. 20 give the effects mentioned above, especially the increased deviations in the region of the tip. Allowing for the "blade distortion effect", it seems probable that the poor tip performance is a result of boundary layer migration to that region, which is discussed in a later section on pages 36 and 39.

The deviation curves for $\phi_m = 0.60$ and 0.56, afford an interesting comparison, as the deviations at $\phi_m = 0.56$ are lower from the hub to 2 inches from the tip, and higher from there to the tip. This shows clearly the effect noted with the air outlet angles plotted in Figs. 12 to 18. Referring to Fig. 19, where the deflection ratio falls off after $\phi_m = 0.65$ and picks up

after ϕ_m = 0.60 for all stations except at 1 inch from the tip, it is apparent that at ϕ_m = 0.65 the rotor is on the point of stall, and has actually stalled at ϕ_m = 0.60. However, as the flow is further decreased the stall becomes more severe inthe tip region, and the remainder of the flow accelerates through that part of the annulus nearer the hub. The rotor tip stall and subsequent flow acceleration seems to be a result of a stator tip stall at ϕ_m = 0.60, which becomes very severe at ϕ_m = 0.56. The stator tip stall is discussed on page 25. The result of the flow acceleration is an increase in deflection and also an increase inpressure rise. Apparently the acceleration was not large enough to prevent the high deflections giving correspondingly high pressure rises.

The large radial movements of the flow at the lower throttle settings, are illustrated in Fig. 11. The effect of acceleration through the mid blade and hub regions at ϕ_m = 0.56, is shown by the axial path taken by the flow, compared to the radially outward movement at higher throttle settings.

2.3.4. Rotor Total Pressure Rise

The comparisons between measured and predicted total pressure rise along the rotor, are similar to those for the outlet air angles. The agreement is best from 2 to 5 inches from the hub, and worst in the tip region. The rotor recovery at ϕ_m = 0.56, mentioned on pages 21 and 22, is shown in Figs. 12 to 18, although Fig.18(a)suggests that the tip is completely stalled at that flow. The non agreement between the predicted and measured overall rotor total pressure rise characteristics shown in Fig. 9, is due to the low pressure rise obtained from the rotor tip. As the characteristics drawn in Fig. 5,show; at the low flows the tip region makes the greater contribution to the work output, so that the poor performance of the tip has a marked influence on the overall total head rise.

Which of the possible reasons for differences between measured and predicted performance, as discussed on page 7, has caused this, is difficult to determine. On pages 36 and 39 there is some discussion on the possibility of low energy air migrating in the rotor boundary layers to the tip region, piling up there, and so interfering with the flow in that region. However, the effect is so extensive, since rotor performance is much lower than expected for 3 inches from the tip, that the explanation probably lies in a combination of boundary layer migration and the "blade distortion effect."

The velocity distributions downstream of the rotor, shown in Fig. 22, indicate that the axial velocity across the annulus was, in general uniform. The increasing thickness of the hub and tip "boundary layers" is a phenomenon noted in previous tests described in Ref. 3, and is caused by the spreading of the

secondary flows and a general thickening of the boundary layers themselves, with decreasing flow.

2.4 Conclusions

The Howell predictions seem fairly good away from the wall regions. However, it is possible that the two effects noted on page 7, neutralise themselves in the mid blade height region to give this agreement.

If the difference due to the "blade distortion effect" is taken as 2 degrees, then the agreement is very good, considering the sources of error discussed on pages 16 and 17.

The differences between the predicted and measured overall characteristics can be explained by the poor performance of the rotor tip, which is attributed to the influence of boundary layer migration to the tip and the 2 degrees "blade distortion effect."

The effect of downstream conditions on the performance of a row, is demonstrated by the pick up of the rotor at $\phi_m = 0.56$ after it had apparently stalled at $\phi_m = 0.60$. This is caused by a stall at the stator tip at $\phi_m = 0.60$ and 0.56 which causes a flow acceleration through the rotor away from the tip region.

The rotor efficiency is high over the whole operating range and, in spite of some reservations about the accuracy of the results, seems to conform to other measurements.

The Carter stalling incidence, plotted in Fig. 19 is quite close to the incidence at which the deflection decreases from its peak, so that it gives a fair estimate of the "region of stall."

3. Stator Performance

3.1 Presentation and Calculations

Comparisons between predicted and measured air outlet angles from the stator are shown in Figs. 12 to 18. The predicted angles were calculated from the air angles measured by the yawmeter downstream of the rotor, using the Howell data. The stator was assumed to "see" the same average of yaw angle as measured by the yawmeter, so that these predictions are subject to the same errors of yaw angle as have been discussed on page 19.

Curves of incidence ratio $i-i''/\varepsilon_*$ against deflection ratio $\varepsilon/\varepsilon_*$, are plotted in Fig. 23, the values being obtained from yaw angle measurements downstream of the rotor and the stator. The curves are similar to those in Fig. 19, except that air outlet angle from the stator was measured directly, and no assumptions were made about the wakes, as was the case with Fig. 19.

Radial distributions of axial velocity $\bar{V}_a/U_m$, total pressure $\bar{\psi}_m$ and deviations δ/δ_D are shown in Figs. 24, 25 and 26.

Radial distributions of loss downstream of the stator at various flows, and loss at each station downstream of the stator for varying flow, are shown in Figs. 27 and 28. The losses were taken as the difference between free stream total pressure and the

average total pressure across a blade space. A method of measuring losses due to A. Betz is discussed in Ref. 7, and the first term of the Betz expression is the difference between the average and free stream total pressures. The second term is a correction, the magnitude of which depends on the variation in static pressure through the wake. Thus the correction term becomes smaller the further the measuring station is moved downstream of the blade row. On pages 28 and 29 a comparison between the losses at the stator mid blade height and the losses through the S1 Cascade is discussed, the comparison being shown in Fig. 29. Adding the correction term to the stator losses made a difference of less than 10 per cent, that is, less than 1 per cent in measured total head, which is considered the limit of accuracy of the yawmeter, and therefore too small to be significant.

3.2 Discussion of Other Work

Both the Howell and Carter methods of predicting cascade performance have been discussed on pages 16 and 17. In Ref. 10, Carter refers to drag traverses downstream of a two dimensional cascade. The curves showing drag distributions rise to a peak near the wall and then fall off to almost zero at the wall itself. No mention is made of the method of measurement, which is a drawback when comparing these curves with the results in Figs. 27 and 28. Drag distributions similar to those for the two dimensional cascade are given for a radial cascade of untwisted blades.

The effect of secondary flows on the air outlet angle from a cascade is also discussed in Ref. 10. Because of the various sources of error discussed on page 19, which are present when measuring air outlet angle from the rotor, discussion of the influence of secondary flows on air angle will be confined to the stator.

3.3 Discussion of Results

3.3.1 Stator Outlet Air Angle

The differences between predicted and measured air outlet angle from the stator, shown in Figs, 12 to 18, are with one exception, 2 degrees or less. At the station 8 inches from the hub the difference is as large as 5 degrees. Thus the agreement is generally very good since, as was discussed on page 21, 2 degrees difference might be expected from the "blade distortion effect".

The poor agreement at 8 inches from the hub is possibly due to a vortex from the rotor tip. Work in Ref. 11, which is discussed in detail in Section 8.3.3 shows flow separation on a cascade caused by a vortex from another cascade upstream. Although these corner vortices are present both at the hub and the tip, the tip vortice from the rotor has a higher circumferential component of velocity than the one at the hub and should therefore, because of its higher total energy, exist for a longer time and hence distance, down the tunnel. This explains why the agreement is poorer at the stator tip than at the stator hub.

At stations 1 and 6 inches from the hub, there is a sharp increase in outlet angle, that is, in deviation, as the flow is decreased from ϕ_m = 0.60 to 0.56. Exactly the opposite effect occurs at the station 3 inches from the hub. The reason for this may be local stalling along the blade as the flow is decreased. Because of the irregular surface of the blades it is possible that one section may stall at a higher flow than an adjacent section, producing local accelerations which result in higher deflections. This is a similar effect to that for the rotor discussed on page 22. Although Fig. 23 suggests that the stator is working at a lower incidence than the stalling incidence predicted from the Carter data, yet the difference between it and the maximum positive stator incidence is only about 2 degrees. This 2 degrees can easily be accounted for by errors in yaw angle measurements downstream of the rotor and in the "blade distortion effect."

The curves in Figs. 12 to 18 indicate that the agreement is generally best at ϕ_m = 0.65 and 0.75 and becomes worse with increasing flow although the difference is still within 2 degrees.

The curves in Figs. 19 and 23 suggest that the stator is working in a lower incidence range than the rotor, since it is most likely that differences between predicted and measured air angles due to the "blade distortion effect" are approximately the same on rotor and stator. Thus at the high flows ϕ_m = 0.90 0.85, and especially at stations near the tip, the stator is working at high negative incidence. This may account, in part, for the comparatively poorer agreement between predicted and measured air outlet angles in the high flow range.

The curve of incidence ratio against deflection ratio at 8 inches from the hub, in Fig. 23, suggests a stall at the lowest flow. This is supported by Fig. 28 which shows a sharp increase in losses at the stations 7 and 8 inches from the hub, at ϕ_m = 0.56. The effect of this stator tip stall on rotor performance has already been discussed on page 22. The other curves in Fig. 23 show no interesting features except that there is some recovery in deflection at ϕ_m = 0.56, which is probably a result of flow acceleration similar to that through the rotor. The diagrams in Fig. 11 suggest some radial flow movement towards the mid blade height region at that flow.

The radial distributions of δ/δ_0, plotted in Fig. 26, show the same form as the curves of outlet angle plotted by Carter in Ref. 10, as they have similar peaks near the walls and a depression near the centre of the passage. The effect of the stall at 7 and 8 inches from the hub at ϕ_m = 0.56, is to decrease the deviations in the tip region below those at ϕ_m = 0.60. However, any attempt to discuss these phenomena in detail is

rendered suspect by the probable errors in measured yaw angles near the wall. The lower deviations in the hub region at $\phi_m = 0.56$ compared to $\phi_m = 0.60$, are most likely to be a result of the flow acceleration mentioned on page and shown in Fig. 11.

3.3.2 Distributions of Flow and Total Pressure Downstream Stator

The irregularities in these curves, shown in Figs. 24 and 25, are largely attributable to irregularities in the blades themselves, although the pronounced lip in the curves near the hub is a manifestation of a vortex or pair of vortices in that region. These are further discussed on pages 38 and 39. Generally, both sets of curves follow the corresponding rotor curves fairly closely. However, the diagrams of flow movement in Fig. 11, indicate that boundary layer growth at the stator hub, causes a radially outward movement of the flow through the stator.

3.3.3 Losses Through the Stator

The radial distributions of loss in Fig. 27, show features different from those in Ref. 10. Generally, the peaks in Fig. 27 are at the station nearest the wall, although the curves at $\phi_m = 0.65$, 0.60 and 0.56 suggest some decrease in loss at that station. The large loss peak near the hub, compared with that at the tip, is attributed to the radial transport of low energy air to the hub. This is further dealt with on page 42.

At the three highest flows, there is a subsiduary loss peak near the hub, similar to a loss distribution curve in Ref. 10, which is plotted downstream of a cascade with an M shaped velocity distribution incident onto it. Although the peaks are small and may be the result of measurement errors, it is most likely that they are caused by twin vortices in the hub region. These are further explained on page 38.

The stator losses were used in a check on stage efficiency. The rotor and stage efficiencies, shown in Fig. 9, were calculated from the work output of the compressor, which is the product of total pressure rise and flow, and the work input from the measured torque. In gas turbine practice, the work output of the machine is obtained from the stage temperature rise. However at the low rotor speeds, encountered in the Vortex Wind Tunnel, the temperature rise is too small to measure. The rotor efficiency calculated from the measured torque and rotor pressure rise and flow, was multiplied by the stator efficiency obtained from the stator losses to give Stage Efficiency I in Table VI below. Stage Efficiency II was obtained from the stage pressure rise and flow.

TABLE VI

Flow	0.90	0.85	0.80	0.75	0.65	0.60	0.56	
Rotor Efficiency%	92.5	93.0	96.1	96.6	94.5	93.8	91.1	
Stator Efficiency%	91.3	93.2	94.0	94.7	95.4	95.4	92.5	
Stage Efficiency I %	84.4	86.7	90.4	90.5	90.2	89.5	84.3	
Stage Efficiency II%	76.9	86.8	88.0	90.5	91.3	89.3	83.5	

The table shows good agreement between the two stage efficiencies. Since the Betz correction term has the effect of reducting the losses and thus increasing efficiency, the stage efficiencies obtained from the measured torque are probably low. This depends on whether the torque errors for the rotor and stage efficiencies are the same. The measured torques agree to $\frac{1}{2}$ ft. lb., that is, $\frac{1}{2}$ per cent, so that the differences in the errors is very small.

3.4 Conclusions

The agreement between stator performance and the two dimensional cascade data is very good, taking into account the possible differences discussed on pages 16 and 17, and the "blade distortion effect". The comparatively poor agreement at the station 8 inches from the hub, is attributed to a vortex from the rotor tip.

At the lower throttle settings, the flow moves radially from the blade extremities and concentrates through the mid blade height region. This effect is most marked in the flow movement away from the hub. This is attributed to hub boundary layer growth and boundary layer migration to the hub region, as the flow is decreased.

The comparison between Figs. 19 and 23, suggests that the stator either works in a mainly negative incidence range, or in a lower incidence range than the rotor.

4. Row Matching

As mentioned immediately above, Figs. 19 and 23 suggest that the stator works in a lower incidence range than does the rotor. It is a reasonable assumption that the incidence onto the rotor, measured with reference to the measured blade angles, bears the same relation (that is larger or smaller) to the incidence mentioned in Ref. 8 and elsewhere, as does the stator incidence. This being so, the stator does work in a lower incidence range than the rotor.

In the original design of the free vortex blades for the Vortex Wind Tunnel, the deflection at mid blade height on the rotor and stator at the design flow, was made 0.837 of the nominal deflection from the Howell data. This gave a design incidence on rotor and stator of about -4 degrees. As the flow is varied from design, the change of incidence with flow, is more for the rotor than for the stator, giving the rotor a wider operating

incidence range. Thus the stator was designed to work at negative incidence over most of the flow range. Table II on page 8 indicates that the rotor and stator are at negative incidence at design conditions, so that the performance of the cast blades is in line with the original design.

5. Comparison of Results with the S1 Cascade Tests

5.1 Presentation and Calculations

Comparisons between the incidence versus deflection curves for the S1 Cascade and the Vortex Wind Tunnel rotor and stator at mid blade height are shown in Fig. 29. The Howell curve for the S1 Cascade is also included. Curves of drag coefficient, C_D plotted against incidence, for the S1 Cascade and the stator at mid blade height are also presented. The coefficient of drag was computed by the method due to A. Betz, discussed on page 24 .

The rotor deflections were calculated from measurements downstream of the rotor, by assuming the momentum thicknesses of the rotor and stator wakes at mid blade height to be the same. The assumption that the displacement thicknesses were the same, made no significant difference to the calculated deflections.

The results of the S1 Cascade tests are given in Ref. 4, but the actual numbers used to plot the graphs were taken from the calculations file of the S1 Cascade tests.

5.2 Discussion of Results

5.2.1 Discussion of Deflections

Although the curves of the S1 Cascade, and the rotor and stator mid blade height deflections do not coincide, their gradients are very similar. The "blade distortion effect" has been assumed to give deflections, 2 degrees smaller for a given incidence, than those predicted from two dimensional cascade data. In this case the deflections are higher by about 2 degrees for both rotor and stator.

The only explanation that can be advanced for this is that the growth of wall boundary layers through the diffusing vanes, causes a flow acceleration, especially through the mid blade height region. This causes an effect similar to that noted for the rotor hub and mid blade height regions, on page 22 , resulting in increased deflections. This should not have been present in the low speed S1 Cascade tests, as boundary layer suction just upstream of the cascade was employed to give nearly two dimensional flow through it.

5.2.2 Discussion of Losses

The agreement between the stator mid blade height and S1 Cascade losses is good. The difference is, at most 25 per cent of the profile drag which is usually taken as 50 per cent of the losses at a station. The losses, as shown by Table VI on page 27 , are as small as 4 to 5 per cent of the total head, so that the differences of 25 per cent in the profile drag coefficient, represent less than

1 per cent of the measured total head, which is the limit of accuracy of the yawmeter when measuring through wakes. Thus the difference is negligible.

However, as the stator operating range is within the positive and negative stalling limits, comparisons cannot be carried too far.

5.3 Summary

The performance of the rotor and stator at mid blade height seems to be close to that of the S1 Cascade. Considering the points of difference between two and three dimensional cascades, discussed on page 20 the agreement is very good. The "blade distortion effect" cannot be considered a contributing factor as it should result in lower, not higher deflections at a given incidence.

The greater deflections from the rotor and stator are difficult to explain, and the reason offered; that the growth of wall boundary layers and the resulting flow accelerations cause the increased deflections; is not convincing.

The most significant feature of the comparisons is that the deflection curves from rotor, stator, and S1 Cascade are parallel to one another, showing that any difference is constant for all flow conditions.

6. Comparison of Results with Previous Tests

6.1 Summary of Results from Previous Tests

Detailed descriptions of former tests on the cast and machined free vortex blade sets, are given in Ref. 3. When the tests were being conducted, the core of the tunnel was open to atmosphere, and air leaked into the tunnel upstream and downstream of the rotor disk, at the rotor leading edge and $\frac{1}{8}$ inch from the trailing edge.

Poor overall performance was achieved, the maximum efficiency obtained with both blade sets being between 70 and 80 per cent, and the maximum pressure rise being less than 0.6.

A comparison between the stage efficiency and pressure rise characteristics of the current tests and the earlier tests of the compressor fitted with machined blades, is shown in Fig. 30. In the results obtained during the previous tests, the machined blade set had a slightly better performance than did the cast blades. For this reason, and also because it is thought that the machined blades were more carefully set, the machined blade results have been used for this comparison.

The total head contours shown in Figs. 32 to 45 are discussed in more detail on pages 38 and 39. The contour drawn downstream of the stator, from the previous series of tests (Fig. 31), is compared with Fig. 36 from the current tests, since the flows at which each was obtained, are nearly the same. The compressor was fitted with a machined rotor and cast stator when the results for Fig. 31 were taken.

6.2 Discussion of Differences Between Current and Previous Tests

The remarkable improvement of 10 per cent in efficiency and 25 per cent in total pressure rise, achieved in the current tests is illustrated in Fig. 30.

The reason for the improvement is suggested by comparing Figs. 31 and 36. The very thick hub boundary layer shown in Fig. 31, which extends to more than 2 inches from the hub, indicates that the hub region of the stator, and probably of the rotor also, produces very little work output. This thick boundary layer is attributed to the air leak, since it is difficult to find any other factor or combination of factors which would produce this result. Any effects of poor blade setting would be too small to result in such a large scale and persistent effect, since the thick boundary layer was observed at all flows in the previous tests.

As well as rendering the rotor and stator hub regions unserviceable, the leak also appears to result in the forcing of the flow through the remainder of the annulus. Although any accelerations of the flow through sections of the diffusing rows need not be deleterious, as mentioned on page 22, the effect of the choking of the flow near the hub has been to worsen the overall row performance, probably because of unsatisfactory incidence conditions elsewhere along the blade height.

One beneficial result of the air leak has been to widen the flow range of the compressor. If the flow has been accelerated through the region away from the hub, then this has presumably postponed stall at the tip, which Fig. 5 shows is the first section of the blade to stall, and has resulted in the compressor working at a lower flow.

7. Radial Equilibrium Studies

7.1 Presentation and Calculations

Curves showing the degree of radial equilibrium attained downstream of the rotor and stator, are given in Figs. 46 and 47. The simple radial equilibrium condition derived in Ref. 8, is that $\partial(\Delta p_s)/\rho.\partial r = V_w^2/r$ This relation applies only to free stream regions since friction forces, and any radial flows in the wakes are ignored.

The relation was simplified for computation by integrating both sides with respect to r giving

$$\Delta p_s/\tfrac{1}{2}\rho U_m^2 = 2\int_{r_1}^{r_2} (V_w/U_m)^2 . dr/r$$

Integrations are made over finite increments of r which effectively alters the relation to

$$\Delta p_s/\tfrac{1}{2}\rho U_m^2 = 2\sum_{r_1}^{r_2} (V_w/U_m)^2 . \Delta r/r$$

For the rotor, the static pressure rise $\Delta p_s/\tfrac{1}{2}\rho U_m^2$, and $(V_w/U_m)^2$ were computed from the values measured by the yawmeter downstream of the rotor. In the case of the stator, the free stream values were used.

To plot results, the "radial equilibrium function"

$$\left[2\sum_{r_1}^{r_2} (V_w/U_m)^2 . \Delta r/r - \Delta p_s/\tfrac{1}{2}\rho U_m^2\right]$$

was introduced, and, was plotted against distance from the hub for each flow.

Since the radial equilibrium function downstream of the rotor is plotted from measurements of wake and free stream velocities and pressures,

it may be termed a "bulk" radial equilibrium function. The values used downstream of the stator, on the other hand, are velocities and pressures at a circumferential station, so that the function downstream of the stator may be termed a "stream-line" function.

7.2 Discussion of Radial Equilibrium Condition

In using two dimensional cascade data for the design of axial flow machines, the attainment of radial equilibrium upstream of a blade row, and its retainment through the row are assumed. This assumption is also made in some "actuator disk" design methods, referred to in Ref. 9.

Carter in Ref. 10 mentions that in a test on a cascade, radial equilibrium was attained at 1/3 chord lengths downstream of the row. As the method of recognising radial equilibrium is not given, the value of this statement is somewhat reduced.

Ainley and Jeffs in Ref. 12, found that radial equilibrium was attained 1/3 chord lengths downstream of a stator in a multistage compressor. Although the simple radial equilibrium test did not apply in Ref. 12, the fact that the velocity distributions at 1/3 and 1½ chord lengths downstream of the row were the same, was taken to indicate that radial equilibrium had been attained.

As tests were made at only one station downstream of the rotor and stator of the Vortex Wind Tunnel, the check method of two traverses used by Ainley and Jeffs, could not be employed. However, since the outer wall of the tunnel annulus is provided with an instrument slot this could be attempted in the future, using other instruments than the cylindrical yawmeter.

7.3 Discussion of Results

On pages 34 and 35 there is a discussion concerning the presence of vortices in the free stream and wakes downstream of a blade row. These vortices are always formed in turning flow such as through a stator. The complete equation of forces in the radial direction as given on page is,

$$-1/\rho \cdot \partial(\Delta p_3)/\partial r = V_r \cdot \partial V_r/\partial r + V_u \cdot \partial V_r/r \cdot \partial C_\theta + V_a \cdot \partial V_r/\partial z - V_u^2/r - F_r$$

The symbols are explained on page 1 .

At a given point in the annulus, the vortices must introduce V_r, $\partial V_r/\partial r$, $\partial V_r/\partial C_\theta$ and $\partial V_r/\partial z$ terms in the above equation, so that at the point, the flow cannot be in radial equilibrium. For the total flow however, these terms will cancel themselves out, and the total flow may be in radial equilibrium. If the total flow is in radial equilibrium, then the velocity distribution will remain constant as noted by Ainlie and Jeffs, although the simple radial equilibrium test, which was probably calculated by them at a point, as with the stator of the Vortex Wind Tunnel, did not apply.

Radial flows are known to occur (page 37) in wakes. From the point of view of "bulk" radial equilibrium, any radial flows in the wakes must result in a movement of the flow in the free stream, in the opposite

direction, with the flow incompressible. However, these flows are small and so should give only negligible movements in the free stream.

Investigations were made on the stator of the Vortex Wind Tunnel to see if the Bernoulli Theorem applied. The total pressure, as measured at a radial station downstream of the rotor, was compared with the free stream total pressure at the corresponding station downstream of the stator. The differences varied from 0 to 10 per cent for the various stations and flows. The differences were random, and comparing total pressures at corresponding flow stations, as in Fig. 11, made no significant difference. Since any instrument error would show a systematic difference one explanation for the random difference is that the main stream vortices bend the stream lines from the axial direction A figure in Ref. 16, which is further discussed on page 35, shows quite clearly this effect. Since the main purpose of investigating radial equilibrium is to determine the applicability of two dimensional cascade data to axial compressors, it is clear that for practical purposes radial equilibrium was not maintained through the stator. Furthermore, although the flow may be in "bulk" radial equilibrium, yet the simple radial equilibrium test at a point should show that flow is not in "streamline" radial equilibrium.

The curves of radial equilibrium function downstream of the stator (Fig. 47) show out of balance pressure gradients of the order of .01 to .05 per inch. The local velocity head varies from about 0.5 to 1 as the flow increases from ϕ_m = 0.56 to 0.90, neglecting the regions adjacent to wall, that is from 0 to 1 and 8 to 9 inches from the hub. Those parts of the curves, such as between 1.5 and 4 inches from the hub at ϕ_m = 0.90, and the curve at ϕ_m = 0.56, are considered significant, as the out of balance pressure gradient is greater than 5% of the local velocity head. Although this is arbitrarily considered a significant pressure gradient it is still very small. The other curves do not show any large scale effects, the steep gradients being more localised. Thus the flow, particularly in the mid passage region and with the exception of that at ϕ_m = 0.90 and 0.56, is, according to the simple test, in radial equilibrium.

It is noticeable that in general the gradients become smaller as the overall flow, and the local velocity head decreases, meaning that at the measuring station the flow at all conditions is out of equilibrium by about the same amount.

Downstream of the rotor the curves are not so regular as those downstream of the stator, and local gradients are, in most cases steeper. At mid passage however, the curves are quite flat, with the exception of the curve at ϕ_m = 0.65. As noted on page 22, the rotor has stalled, and this may give rise to the large out of balance pressures, because of the unstable conditions along the blade. These are shown in Fig. 49, where the static pressure distributions is very irregular compared to those at the other flows.

One reason for the rotor curves showing larger out of balance pressures than those for the stator may be that the static pressure

direction, with the flow incompressible. However, these flows are small and so should give only negligible movements in the free stream.

Investigations were made on the stator of the Vortex Wind Tunnel to see if the Bernoulli Theorem applied. The total pressure, as measured at a radial station downstream of the rotor, was compared with the free stream total pressure at the corresponding station downstream of the stator. The differences varied from 0 to 10 per cent for the various stations and flows. The differences were random, and comparing total pressures at corresponding flow stations, as in Fig. 11, made no significant difference. Since any instrument error would show a systematic difference one explanation for the random difference is that the main stream vortices bend the stream lines from the axial direction A figure in Ref. 16, which is further discussed on page 35, shows quite clearly this effect. Since the main purpose of investigating radial equilibrium is to determine the applicability of two dimensional cascade data to axial compressors, it is clear that for practical purposes radial equilibrium was not maintained through the stator. Furthermore, although the flow may be in "bulk" radial equilibrium, yet the simple radial equilibrium test at a point should show that flow is not in "streamline" radial equilibrium.

The curves of radial equilibrium function downstream of the stator (Fig. 47) show out of balance pressure gradients of the order of .01 to .05 per inch. The local velocity head varies from about 0.5 to 1 as the flow increases from ϕ_m = 0.56 to 0.90, neglecting the regions adjacent to wall, that is from 0 to 1 and 8 to 9 inches from the hub. Those parts of the curves, such as between 1.5 and 4 inches from the hub at ϕ_m = 0.90, and the curve at ϕ_m = 0.56, are considered significant, as the out of balance pressure gradient is greater than 5% of the local velocity head. Although this is arbitrarily considered a significant pressure gradient it is still very small. The other curves do not show any large scale effects, the steep gradients being more localised. Thus the flow, particularly in the mid passage region and with the exception of that at ϕ_m = 0.90 and 0.56, is, according to the simple test, in radial equilibrium.

It is noticeable that in general the gradients become smaller as the overall flow, and the local velocity head decreases, meaning that at the measuring station the flow at all conditions is out of equilibrium by about the same amount.

Downstream of the rotor the curves are not so regular as those downstream of the stator, and local gradients are, in most cases steeper. At mid passage however, the curves are quite flat, with the exception of the curve at ϕ_m = 0.65. As noted on page 22, the rotor has stalled, and this may give rise to the large out of balance pressures, because of the unstable conditions along the blade. These are shown in Fig. 49, where the static pressure distributions is very irregular compared to those at the other flows.

One reason for the rotor curves showing larger out of balance pressures than those for the stator may be that the static pressure

gradients downstream of the rotor are from the tip to the hub, that is in the opposite direction to those relative to the rotor. This effect, which is further discussed on page 39 should give rise to a reversal of flow in the wakes downstream of the rotor, and a redistribution of fluid which has accumulated near the tip, thus delaying the attainment of radial equilibrium.

7.4 Conclusions

The out of balance pressure gradients, given in Figs. 46 and 47 are, even at their steepest, small compared with the local velocity head, and should give rise to only small radial redistributions of flow as the fluid moves downstream from the measuring station. The flow should be in radial equilibrium both "bulk" and "streamline", a short distance, say $\frac{1}{2}$ inch, downstream of the measuring station.

Both Fig. 11, and the total head checks on the stator mentioned on page 32 indicate that large radial movements have taken place before the measuring station has been reached.

It is considered that the simple radial equilibrium test, when applied at a point, should give a true indication of whether the flow is in radial equilibrium or not, from the point of view of the practical applications of this knowledge. Although the velocity distributions at several stations downstream of a row may show no change, yet the presence of vortices should result in radial movement of streamlines, and subsequent non cylindrical flow.

8. Secondary Flows.

8.1 Note on the Term "Secondary Flows"

The term "Secondary Flows" is used to cover flows occurring in a different plane to the bulk flow. For example, when a fluid passes through the bend of a pipe, the flow follows the shape of the bend, but vortices are generated in the fluid in a plane perpendicular to the axis of the pipe. These vortices fall within the general group of secondary flows.

Since the energy of these vortices cannot be recovered, they constitute a loss, and an understanding of their generation with a view to either controlling them, or at least, taking account of their presence in the preliminary design of a turbomachine is of considerable value.

8.2 Presentation and Calculations

Contours of total pressure downstream of the stator and inlet guide vanes, are shown in Figs. 32 to 45. The centrelines of the wakes are represented by the broken line, and are plotted as the peaks of the total pressure curves measured circumferentially through the wakes at each radial station. The upper sides of the wakes shown are from the suction surface of the stators, and the pressure surface of the inlet guide vanes.

Radial distributions of static pressure downstream of the inlet guide vanes, rotor and stator are shown in Figs. 48, 49 and 50. The static pressure downstream of the inlet guide vanes and stator was calculated from the free stream total pressure and velocity. The measurements as averaged by the yawmeter, were used downstream of the rotor.

8,3 Review of Other Work

8.3.1 Work of A.D.S. Carter

Three dimensional flow in two dimensional cascades, compressors and turbines is dealt with by A.D.S. Carter in Ref. 10.

The large scale secondary flows, which will be referred to here as main stream vortices are explained by assuming that the flow through a cascade is similar to the flow through a series of curved channels. Referring to Fig. 51(a), the static pressure at A & B on the pressure surface of the blade are higher than the pressures at C and D on the suction side of the blade. Furthermore, because of the lower pressure gradient between the blades at the wall, due to the wall boundary layers, the pressure at B is less than the pressure at A and the pressure at C is greater than the pressure at D.

Therefore $P_A > P_B > P_C > P_D$

These pressure gradients give rise to the large vortices shown in Fig. 51(a).

Downstream of the cascade, small vortices, in the nature of "ball bearings" are assumed to exist between two main stream vortices from adjacent passages. These are shown in Fig. 51(b). This vortex sheet, being unstable, rolls up into one vortex which appears as a core of high loss in contours of total head, presented in Ref. 10. This trailing vortex is shown in Fig. 51(c), its direction of rotation being opposite to the adjacent main stream vortices. The direction of rotation was observed by placing small windmills into these "corner" or "rolled up" vortices.

Carter notes than when an M shaped velocity distribution is incident onto a cascade, twin "rolled up" vortices are formed downstream of it. The M shaped velocity distribution gives rise to two sets of three main stream vortices, per passage, and the "ball bearing" vortices roll up into twin vortices, showing as twin loss peaks downstream of the cascade. A sketch taken directly from Ref. 10 is used to illustrate this effect in Fig. 52(a).

Carter also states that there is no basic difference between two and three dimensional cascades. Annular cascades, as in turbo-machines, are discussed on the basis of this assumption.

The effects of end clearance and the moving wall are also mentioned. In stationary rows the effect of end leakage is assumed to be the augmenting of the main stream vortices, as in Fig. 52(b), as fluid moves through the end clearance from the pressure to the suction surface of the blade. The magnitude of the flow is certain to be dependent on the relative sizes of the adjacent wall and blade boundary layers.

In Ref. 10, a total pressure contour is shown drawn downstream of an annular cascade with a moving inner wall, the relative motion being similar to that in a compressor. The contour suggests that a separate flow regime has been set up in the form of an additional

main stream vortex. The regions of high loss have been moved very close to the wall and show twin loss peaks in the region of the moving wall.

The explanation that the trailing vortices are the result of the rolling up of the "ball bearing vortices" is difficult to accept, especially in view of the observations made in Ref. 11 (pages 36 and 37) and also because the ball bearing vortices have not been seen in any of the references examined. The direction of rotation of the trailing vortex is opposite to that noted elsewhere (page 40).

The assumption that there is no basic difference between two and three dimensional cascades seems totally erroneous as the radial movement of fluid in boundary layers and wakes gives rise to some important effects, as discussed in Ref. 11 and on pages 36 and 37.

However, the distributions of loss and the total head contours presented make this reference extremely valuable for comparison purposes, as this type of information is available in only a few publications.

8.3.2 Work of W.D. Armstrong (Ref. 16)

To study secondary flow in cascades, Armstrong used swansdown and smoke traces for visualisation studies, and total pressure traverses downstream of the cascade. An ingenious method used was the tracing of artificially heated filaments of air, which showed the actual movements of the streamlines.

The total head contours which were plotted at the trailing edge of the row, and one chord length downstream, at a blade Reynolds Number of 3.9×10^5 (axial velocity of 130 ft./sec.), showed that movements of a streamline were as large as $\frac{1}{2}$ inches, the blade chord length being 6 inches and the aspect ratio 3. This effect was referred to on page 32. The movement of the streamlines shows the turning effect of the main stream vortices. The paths followed by the heated filaments of air, indicated similar turning of the flow.

When the air was heated in the corner between the wall and the blade it became dispersed very rapidly, apparently due to the presence of a rolled up vortex, as noted by Carter.

8.3.3 Work at the Lewis Flight Propulsion Laboratory

Johnsen and Bullock, in Ref. 11, give a survey of work undertaken at the Lewis Flight Propulsion Laboratory, Cleveland, U.S.A., and this is the most comprehensive work on secondary flows available. It contains work published elsewhere, which, with the exception of Ref. 17, is referred to in this text, under Ref. 11. The observations made coincide closely, in most cases, with those made in the Vortex Wind Tunnel.

Chapter 3 of Volume I, includes a quasi-theoretical attempt to analyse the formation of secondary flows in cascades. Chapter 15 of Volume III gives details of extensive tests made on cascades, many

being taken from Ref. 17 which showed detailed visualisation studies.

In Volume I, the equation of forces in the radial direction

$$-\partial(\Delta P_s)/\partial r = V_r.\partial V_r/\partial r + V_u.\partial V_r/r.\partial\theta + V_a.\partial V_r/\partial z - V_u^2/r - F_r$$

is examined, and the assumption is made that static pressures and their gradients in wakes and boundary layers are nearly the same as those of the adjacent free streams. Assuming also, that in stator boundary layers and wakes V_a and V_u are smaller than the free stream values, and that F_r remains small, the derivatives of V_r and hence V_r itself become significant.

On rotors, V_u is larger than in the adjacent free stream, so that if the above assumptions still hold good, the sign of the derivatives of V_r is reversed.

The assumption that static pressures in boundary layers and wakes are nearly the same as in the adjacent free stream is reasonable, as noted in Ref..7. The assumptions that V_a and V_u are smaller in wakes, are all right from the definition of a boundary layer. However, the assumption that F_r is small must depend on factors such as the Reynolds Number of the flow, and whether the vanes are accelerating or diffusing. In separation bubbles, separated regions at the trailing edge and thick wakes, F_r will be much smaller than if the wakes are thin, and so it is in these regions that radial boundary layer flows may be expected to occur. This is supported by photographs of paint traces on blades which are discussed on page 37 .

Once the idea of flows within boundary layers and wakes is introduced, the possibility arises that regions of high loss, such as those near the walls are caused, at least in part, by the transport of low energy fluid from elsewhere. This is easy to understand in the case of stators, as low energy air from the blade pressure side moves down the wall through the boundary layer, and collects in the corner between the suction surface and the adjacent wall. This is discussed on page 37. . Observations in Vol. III show that the movements in rotor boundary layers are rather more complicated.

Reference is made in Volume I to tests on an axial flow compressor where, at a radial station, the efficiency of the stage was higher than that of the rotor. If the flow is wholly cylindrical, then the efficiency of the stator is more than 100 per cent. The logical reason for this, apart from measuring error, is that low energy air has been moved from the radial station on the stator, so that losses do not appear at that station.

In Volume III observations of secondary flows in two and three dimensional cascades are shown, including the cases of tip leakage and the moving wall. The migration of fluid in the wall boundary layers, from the pressure to the suction of the channel, and the consequent rolling up of this fluid into a trailing vortex similar

to that noted by Carter, and in the manner shown by vortex A of Fig. 53 (a), is demonstrated. The size and vorticity of the vortex increased with the air deflection. The direction of rotation of the vortex,is, however, opposite to that shown by Carter, being in the same direction as the adjacent main stream vortex.

Contours of loss of kinetic energy, drawn downstream of an annular stator, show twin vortices in the region of the hub, rotating in the direction shown by vortices in Fig. 53(a). The two loss regions are similar to the twin loss peaks noted by Carter in Ref. 10 and reproduced in Fig. 27. The relatively high loss near the hub as compared to the tip, is attributed to boundary layer movement giving a similar effect to that mentioned on the previous page where the stage efficiency at a radial station, was higher than the rotor efficiency at the same radial station.

The movement of fluid in blade boundary layers, is shown by photographs of paths taken by paint smeared on stator blades. The paint traces moved radially inward from the tip to the hub along two paths, one near mid blade height and the other at the blade trailing edge. The path near mid blade height is most likely to be through the separation bubble, since the friction forces there and in the separated region at the trailing edge, should be lower than elsewhere on the blade.

Tests on a two dimensional cascade with end clearances of 0.4 and 1.7 per cent of the span, show migration of air from the wall and blade boundary layers on the pressure side, through the end clearance to the suction side. This air formed the inner of twin vortices, similar to Vortex A of Fig. 53(a). The end clearances in the Vortex Wind Tunnel are given in Table III, page 9 , and are of the same order, being within the range 2/3 to 2 per cent of the span.

The effect of a trailing vortex from one row on the downstream row, is shown by photographs of smoke traces which indicate separation occurring on the downstream row, where it was struck by the vortex.

8.4 Discussion of Secondary Flows in the Vortex Wind Tunnel

8.4.1 Conditions in the Vortex Wind Tunnel

For a clear understanding of boundary layer movement in the Vortex Wind Tunnel, it is necessary to examine blade surface pressures, especially those on the rotor. In 1958 measurements of blade surface pressures were made on rotor and stator blades of the machined free vortex set. No tapped blades of the cast set are available. Also the tests were conducted with the air leak at the rotor hub, present. Thus, the test conditions differ from those under which the current tests were conducted. However, since general trends only are being looked for, this should not prove any drawback.

The tendency was for the radial surface pressure distribution to decrease towards the shell on the rotor, and towards the hub on the stator. The gradients decreased for radial lines closer to the trailing edge. However, pressure peaks and troughs were noticeable and these must be of prime importance because of their influence on the $\frac{\partial(\Delta B)}{\partial r}$ term in the force equation in the radial direction. It is to be expected that pressure peaks and troughs will be more frequent on the surface of the cast blade set because of their irregular surfaces. The curves of static pressure, downstream of the blade rows shown in Figs. 48, 49 and 50 show that the gradients are very definitely from the tip to the hub downstream of the rotor, while downstream of the stationary rows the gradients, while being generally in the same direction, are not nearly so clearly defined.

8.4.2 Secondary Flows Induced by Stator and Rotor

Two interesting phenomena shown in Figs. 32 to 36, suggest the presence of twin vortices near the hub.

(i) The wake centreline near the hub is distorted in a manner which can be satisfactorily explained by the presence of twin vortices, the inner near the wall rotating in the clockwise direction, and the outer in the anticlockwise direction. This is similar to the effect noted in Volume III of Ref. 11, and discussed on page 37. The distortion of the wake centreline due to twin vortices is demonstrated in Fig. 53(c).

(ii) A core of high loss, smaller than that near the hub, seems to exist further away from the wall. In Fig. 36 a small loss core was actually measured, although this may be instrument error. However, the second loss peak near the hub shown in some of the curves in Fig. 27 supports this.

Although yawmeter measurements near the wall are certainly in error to some extent, yet the centreline distortion is so marked, and agrees so well with Johnsen and Bullock that the phenomenon cannot be dismissed as due to the method of instrumentation.

At the stator tip there is no sign of twin vortices, and the vortex present, seems to have little effect in distorting the wake centreline.

The contours in Figs, 32 to 38 show that the local strength of the vortices decreases with decreasing flow, that is, with increasing lift and pressure difference across the passage between the blades. This is apparently opposite to the effect discussed in Ref. 11 and noted on page 37. The contours at ϕ_m = 0.60 and 0.56 show little sign of twin vortices near

the hub. There may be no conflict however, between the observations by Johnsen and Bullock and those in the Vortex Wind Tunnel, as, on the total pressure contours, the vortices having high local vorticity show up most clearly. The vortices at ϕ_m = 0.60 and 0.56 which are large, may have higher overall vorticity although they are not so localised and therefore, not so easy to see.

A comparison between the contours downstream of the stator and the corresponding curves of $\overline{V_a/U_m}$ and $\overline{\psi}_m$ (Figs. 24 and 25) shows that a knee in the radial distribution curves near the hub, coincides with the join between the wall boundary layer and the adjacent blade wake. In this context, the wall boundary layer includes the hub vortices. The position is similar at the tip, and the knee in the curves of $\overline{V_a/U_m}$ and $\overline{\psi}_m$, in the case of the stator, is a good guide to the extent, in the radial direction, of the secondary flows in wall boundary layer and wake.

Downstream of the rotor the only curves available are the distributions of $\overline{V_a/U_m}$ and $\overline{\psi}_m$ (Figs. 21 & 22). Assuming that the static pressure gradients on the stator, which run from the tip to the hub, caused the concentration of secondary flows near the hub, it seems reasonable to expect a similar concentration at the rotor tip. However, this is not indicated by Figs. 21 and 22, where the knee in the curve near the tip, is much closer to the wall than is the case near the hub. This may be caused by the high energy of vortices from the rotor tip which are shed with a velocity component in the circumferential direction, U_r. This must give a deceptively high total head reading on the yawmeter. Also, the static pressure gradient downstream of the rotor, which runs from the tip to the hub should result in the redistributing of low energy air in the wakes, after it had collected in the tip region while passing through the rotor itself.

The effect of the moving wall at the rotor tip and for some part of the hub, as in Fig. 2, makes a detailed discussion of secondary flow formation in the rotor impossible with the lack of suitable measurements, and this will not be attempted.

8,4,3, Secondary Flows Induced by Inlet Guide Vanes

The contours of total head downstream of the inlet guide vanes are shown in Figs. 39 to 45. The static pressure distributions in Fig. 48 show that the gradients tend to run from the tip to the hub, as on the stator. On the inlet guide vanes there is no separation bubble, there are thin wakes and boundary layers, and only a small separated region near the trailing edge. Thus any radial boundary layer and wake flows are restricted because of lack of suitable paths, and high friction forces, as compared to the stator. This possibility has already been mentioned on page 36 .

The contours show wake centreline distortion, both at the hub and tip, consistent with twin vortices in those regions. The cause of this is likely to be the restricting of radial boundary layer flows, so that the inlet guide vanes are similar in this respect to a two dimensional cascade.

The thinning of the wake at about 1 inch from the hub, which is also present in the contours downstream of the stator, may be caused by the energising of the wake by the edge of a fast vortex, or may indicate the presence of a pressure peak causing wake fluid to move away from that region.

8.5 Suggested Picture of Secondary Flow Formation

8.5.1 Different Secondary Flow Formations

To obtain a clear picture of secondary flow formation a subsiduary experiment was undertaken. A small water channel, shown in Fig. 54(a) was used. It is fitted with a gate which is flush with the side walls. The height of the gate was adjusted to give a much greater depth of water on the upstream side of the gate than the downstream side. The pressure gradients in the upstream part of the water are similar to a bend in a pipe, and to the flow through an aerofoil cascade, as the water must turn to pass under the gate. Two large mainstream vortices, similar to those noted by Armstrong and Carter, could be seen and are shown in the photograph in Fig. 54(b). Their distance from the gate varied with water surface disturbances, but when they moved an inch or more away from the gate, ink fed into the corner between the gate and the wall showed the presence of small vortices in the corners. One can faintly be seen in Fig. 54(c) indicated by the arrow A.

The direction of rotation of the corner vortex was the same as of the main stream vortex; that is, opposite to the direction of rotation noted by Carter, but the same as noted by Johnsen and Bullock.

Since the tests on the cast free vortex blade set have been completed, perspex windows have been fitted in the outer annulus walls of the Vortex Wind Tunnel. Tests at very low rotor speeds using smoke were attempted, and these tests, although inconclusive, suggested that twin vortices rotating in the manner suggested by the total head contours, exist through, and downstream of, the stator hub region.

A summary of the somewhat conflicting data on secondary flow formations is now given.

In the Carter two dimensional cascade tests, and in the water channel, there was only one vortex in the corner. Loss contours shown in Ref. 17, exhibit wake centreline

distortion similar to that in the Vortex Wind Tunnel contours, which suggest the presence of twin vortices. This idea is reinforced somewhat by the smoke trace tests mentioned immediately above. Smoke tests shown in Refs. 17 and 11 show a vortex close to the wall formed by air moving in the wall boundary layer, from the pressure to the suction side of the blade space and there, rolling up. The direction of spin of this vortex was opposite to that noted by Carter, but the same as the corner vortex in the water channel.

An attempt will now be made to sort this into a coherent picture of secondary flow formation.

8.5.2 Secondary Flow Formation

As a fluid moves through a two dimensional cascade, the pressure gradient across the blade space causes the formation of main stream vortices similar to those shown in Fig. 51(a). This pressure gradient also causes fluid in the wall boundary layers to move from the pressure to the suction side of the channel as shown in Ref. 17. When it reaches the suction surface, there is no spanwise pressure gradient to move it along the blade and it rolls up into a corner vortex, as shown by the path taken by fluidAin Fig. 53(a). The direction of rotation of this vortex is the same as the main stream vortex, and is also the same as the corner vortex shown in Ref. 17.

The reason why the direction of rotation of the corner vortex noted by Carter, is opposite to that in the water channel, is thought to be because the vane used, extended into the main stream vortex. This would give it a direction of rotation opposite to that of the main stream vortex.

When, as in the case of an annular cascade, a spanwise pressure gradient is superimposed on the normal cross channel gradient, fluid will move through the pressure surface boundary layer, separation bubble, and trailing edge region, meet the fluid which moved down the wall and roll up in the manner of Vortex B in Fig. 53(a). The relative sizes of these vortices depends, of course, on the magnitude of the pressure gradients, the size of the separation bubble and the thickness of the boundary layers.

If there is blade end clearance then there is likely to be reinforcement of vortex A.

Downstream of the blade row, high pressure air from that part of the wake from the pressure surface, is adjacent to low pressure air from the suction surface. The movement of air in the wake should then be as shown in Fig. 53(b), with

a reinforcement of both vortices in the case of an annular cascade, and the formation of vortex B in a two dimensional cascade or inlet guide vane row. The formation of vortex B is due to the tendency of the fluid to distribute energy evenly, as is the case when laminar flow becomes turbulent.

At the tip of the Vortex Wind Tunnel stator, it seems likely that no vortex similar to vortex B of Fig. 53(a) has been formed. Since the pressure gradient across the annulus is from the tip, any air moving into this region from the high to the low pressure side of the wake, will form either a very weak vortex B or willall be bled away towards the hub. The reason why vortex A at the stator tip is so weak compared to the corresponding vortex at the inlet guide vane tip is probably due to a bleeding away of air from it under the influence of the spanwise pressure gradient

Thus twin corner vortices should be formed downstream of all two dimensional cascades, and at the wall of an annular diffusing cascade when the wall is the lower end of a spanwise pressure gradient. At the other wall of an annular cascade the vortices, if two are present, are weak, as air will be bled away from them under the influence of spanwise pressure gradients. Because of the thin boundary layers and wakes and the absence of a separation bubble, accelerating cascades perform in a similar manner to two dimensional cascades,

The presence of main stream vortices, rotating in the manner shown in Fig. 51(a) is undisputed, although they have not been seen or measured in the Vortex Wind Tunnel.

8.6 Conclusions on Secondary Flows

The picture of secondary flows presented in the previous section fits all the available data, apart from that due to Carter, which is the earliest work of those examined.

The blade surface pressure gradients discussed, show only general trends, and it seems obvious that pressure peaks and troughs on the blades must play a significant part in the magnitude and direction of boundary layer flows.

Plans for the use of visualisation tests in the Vortex Wind Tunnel, and the examination of boundary layers and wakes with small arrowhead yawmeters, are in hand. These measurements coupled with the normal cylindrical yawmeter traverses and blade surface pressure readings, should enable the picture of secondary flows to be clarified.

9. General Conclusions

It seems clear that cast compressor blades should give satisfactory performances. The difference between the blade profiles and design,

and the measured blade angles not being those referred to in Fig. 3, are drawbacks when comparing the cast blade performance with two dimensional cascade data. However, any blade distortion has not resulted in any serious mismatching of the rows nor seriously reduced the pressure rise and efficiency which might have been attained had the blades been of design shape.

The performance of the compressor rows is close to that predicted from the Howell data, deflections being with a few exceptions, lower by 2 degrees or less.

The air leak at the rotor hub is the obvious cause of the poor performance achieved in previous tests. Errors in blade setting would produce only small differences.

The agreement with the S1 Cascade results is quite good, the deflection against incidence curves for the rotor and stator at mid blade height and the S1 Cascade, being within 2 degrees, and the curves are parallel. However, the cascade results are lower than those measured in the Vortex Wind Tunnel and the explanation given is rather inadequate.

The flow downstream of both the rotor and stator is nearly in radial equilibrium at the measuring stations. The simple radial equilibrium test as set out in Ref. 8, should, when applied at a point, as in the free stream downstream of the stator, give a true indication of whether, for practical purposes, the flow is in radial equilibrium.

The explanation of the formation of secondary flows, based on flows in boundary layers and wakes, adequately covers the data available, although it is clear that the knowledge available is inadequate.

REFERENCES

1. P.V. CROOKS AND W. HOWARD — "Preliminary China Clay Tests on Rotary Cascade Blade Surfaces". Department of Supply. A.R.L., Note M.E. 196, December 1954

2. A.W. WRIGHT AND E. SZOMANSKI — "Calibration of the Vortex Wind Tunnel". Department of Supply. A.R.L. Tech. Memo. M.E. 165 October 1956

3. D.A. FRITH, P. PUNYANITYA AND A.R. OLIVER — "Initial Testing of C4 Blades in the Vortex Wind Tunnel". Department of Supply. A.R.L., Note M.E. 230, December 1958

4. F.G. BLIGHT AND W. HOWARD — "Tests on Four Aerofoil Cascades". Part I, Deflection, Drag and Velocity Distribution". Department of Supply. A.R.L. Report E.74 July 1952

5. R.C. PANKHURST AND D.W. HOLDER — "Wind Tunnel Technique". Pitman 1952.

6. A.R. HOWELL — "Fluid Dynamics of Axial Compressors". Proc. Inst. Mech. Eng. Vol. 153, 1945.

7. H. SCHLICHTING — "Boundary Layer Theory". Pergamom Press, 1955.

8. F.G. BLIGHT — "An introduction to the Aerodynamic Theory of Compressors and Turbines". C.S.I.R. Division of Aeronautics, Report E 56, May 1947

9. J.H. HORLOCK — "The Compressible Flow Through Cascade Actuator Disks" The Aeronautical Quarterly, May 1958

10. A.D.S. CARTER — "Three Dimensional Flow Theories for Axial Compressors and Turbines" Proc. Inst. Mech. Eng. Vol. 159.

11. IRVING A JOHNSEN and ROBERT O. BULLOCK — "Aerodynamic Design of Axial Flow Compressors" Volume I and III N.A.C.A., RM, E56B03 and E56B03b.

12. D.G. AINLEY AND R.A. JEFFS — "Analysis of the air Flow Through Four Stages of Half Vortex Blading in an Axial Compressor". A.R.C. Reports and Memoranda No. 2383 1946.

REFERENCES (Contd.)

13. A.R. HOWELL and R.P. BONHAM — "Overall and Stage Characteristics of Axial Flow Compressors" Proc. Inst. Mech. Eng. Vol. 163

14. A.R.OLIVER, W. HOWARD and P.V. CROOKS — "Tests of a Model of One Stage of the New Compressor of the Variable Pressure Wind Tunnel". Department of Supply. A.R.L. Note, M.E. 228, October 1958.

15. A.D.S. CARTER — "The Low Speed Performance of Related Aerofoils in Cascade" N.G.T.E. Report R 55.

16. W.D. ARMSTRONG — "An Experimental Investigation of Secondary Flow Occurring in a Compressor Cascade". The Aeronautical Quarterly. August 1957.

17. HOWARD Z. HERZIG, ARTHUR G. HANSEN and GEORGE R. COSTELLO — "A Visualisation Study of Secondary Flows in Cascades" N.A.C.A. Report 1163, 1954.

Fig. 1

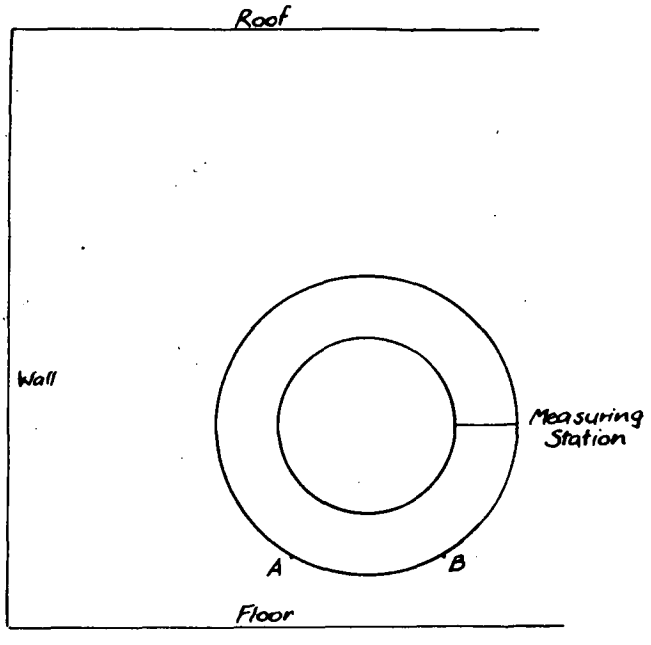

(a) Tunnel Location

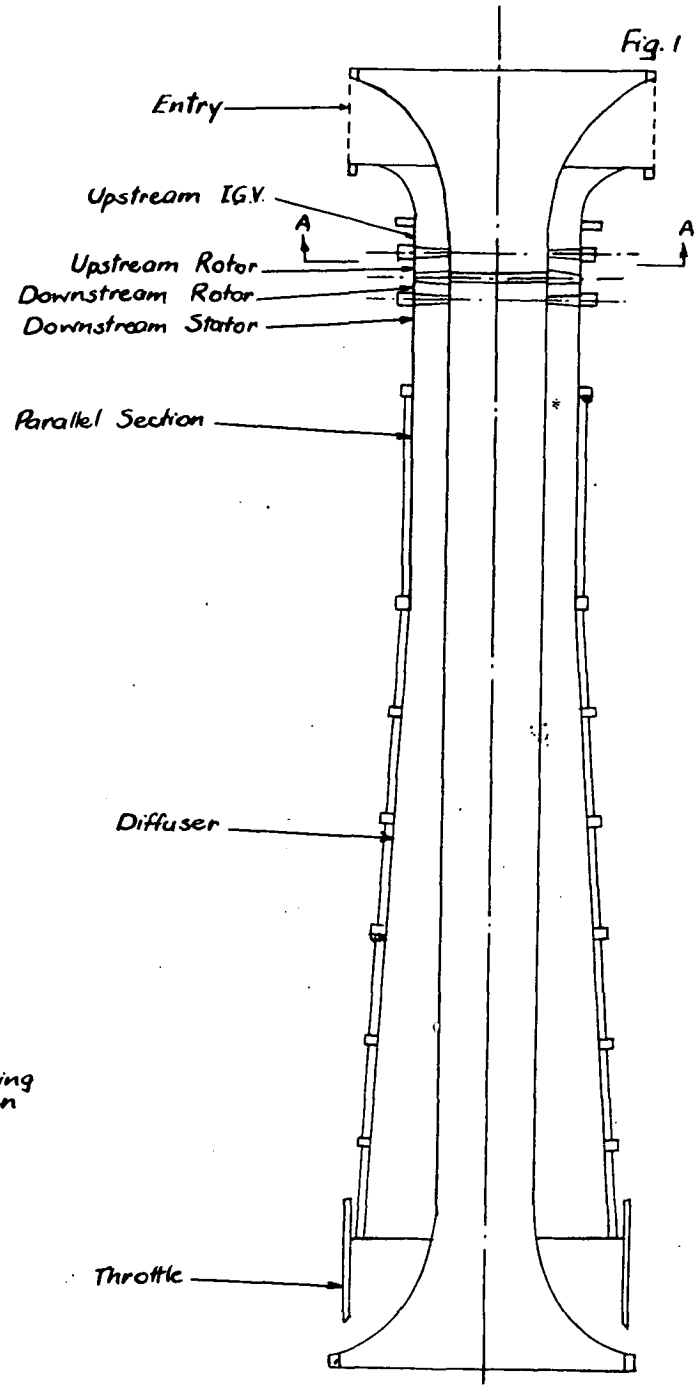

(b) Tunnel Stations

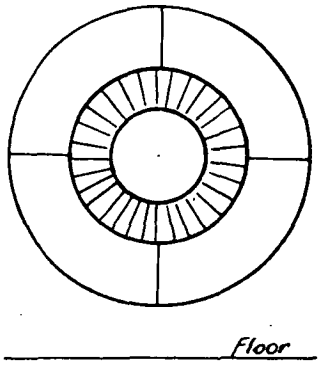

Section AA

Vortex Wind Tunnel

Location and Stations

Fig. 2

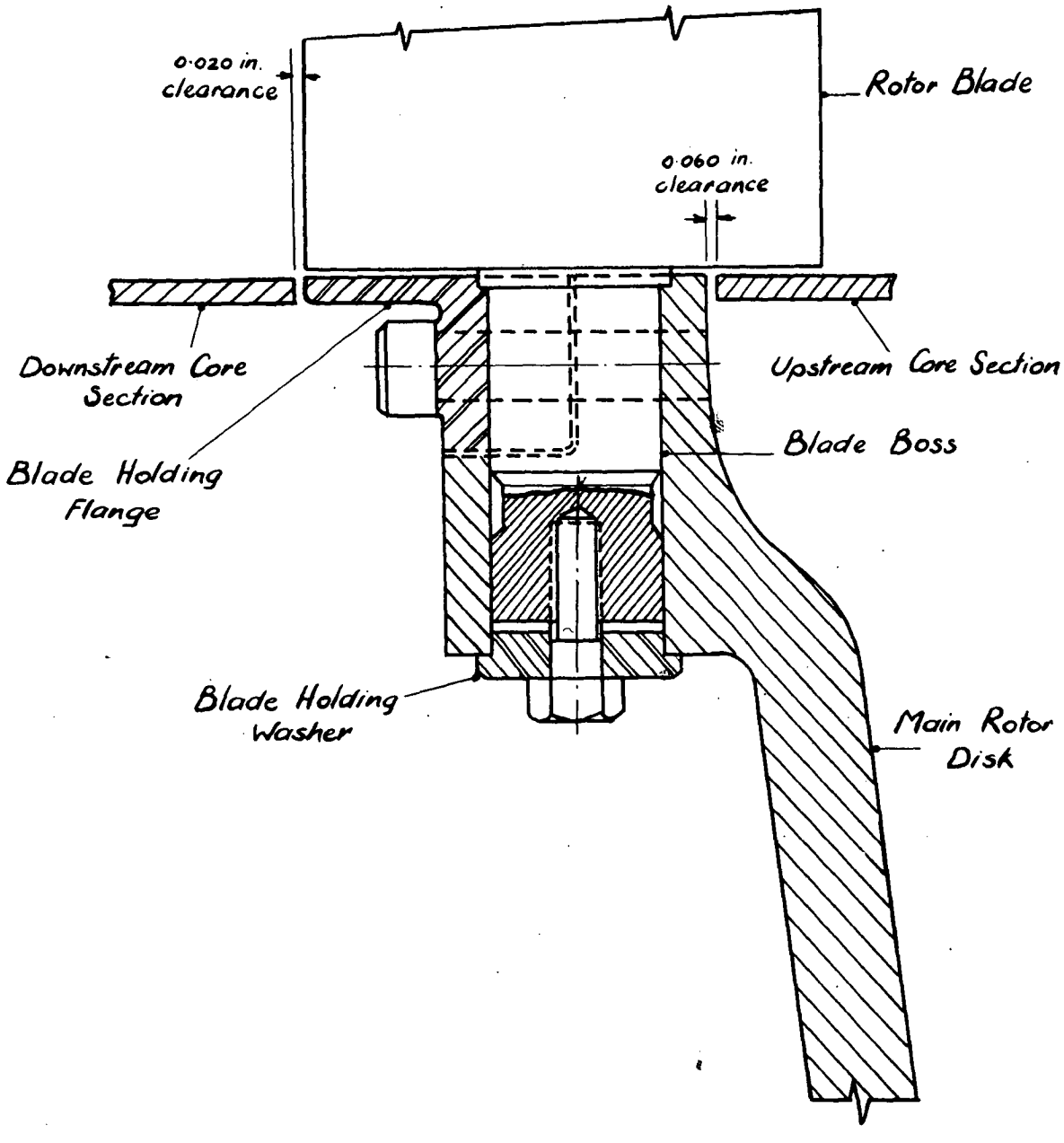

Sketch Showing Blade Holding System

Scale : Full

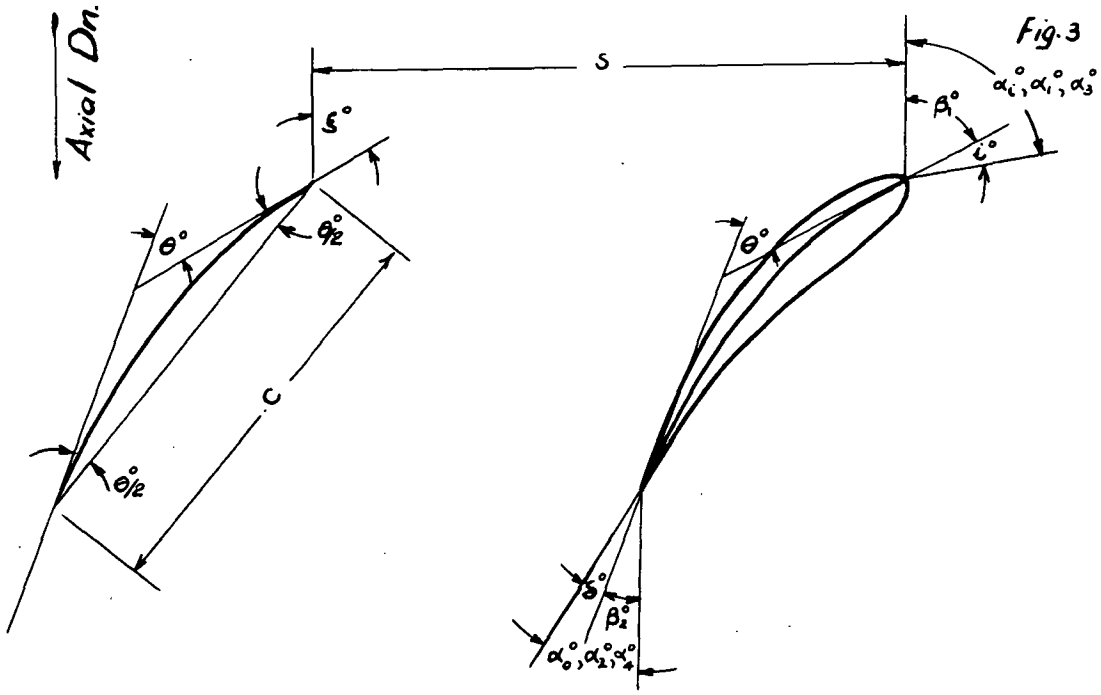

(a) Sketch Showing Blade Geometry of Circular Arc Aerofoils and Cascades (from Ref. 8)

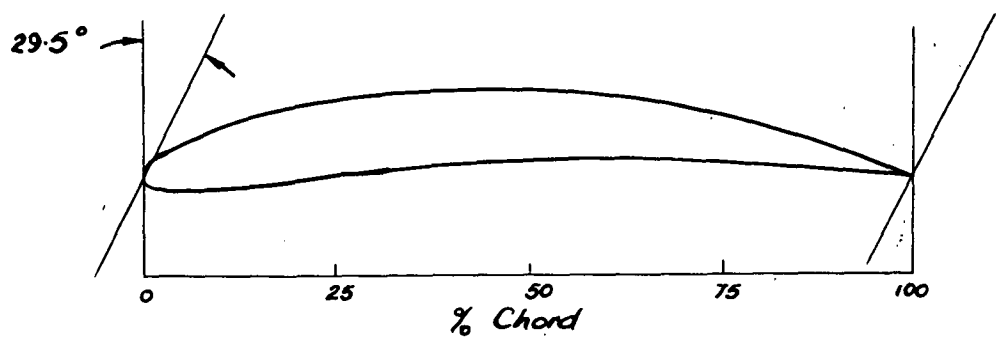

Station	% Chord	0·00	1·25	2·50	5·00	7·50	10·0	15·0	20·0	30·0	40·0	50·0	60·0	70·0	80·0	90·0	95·0	100·0
Upper	% Chord	0·00	2·33	3·27	4·73	5·83	6·77	8·17	9·30	10·80	11·43	11·40	10·67	9·27	7·13	4·30	2·57	0·00
Lower	% Chord	0·00	$\bar{1}$·13	$\bar{1}$·50	$\bar{1}$·80	$\bar{1}$·77	$\bar{1}$·57	$\bar{1}$·10	$\bar{0}$·60	0·70	1·70	2·27	2·57	2·40	1·90	0·93	0·33	0·00

s/c = 1·000

ξ = 29·50°

T.E. Radius = 0·6% Chord

(b) SI Cascade Geometry

General and SI Cascade Geometry

Fig. 4

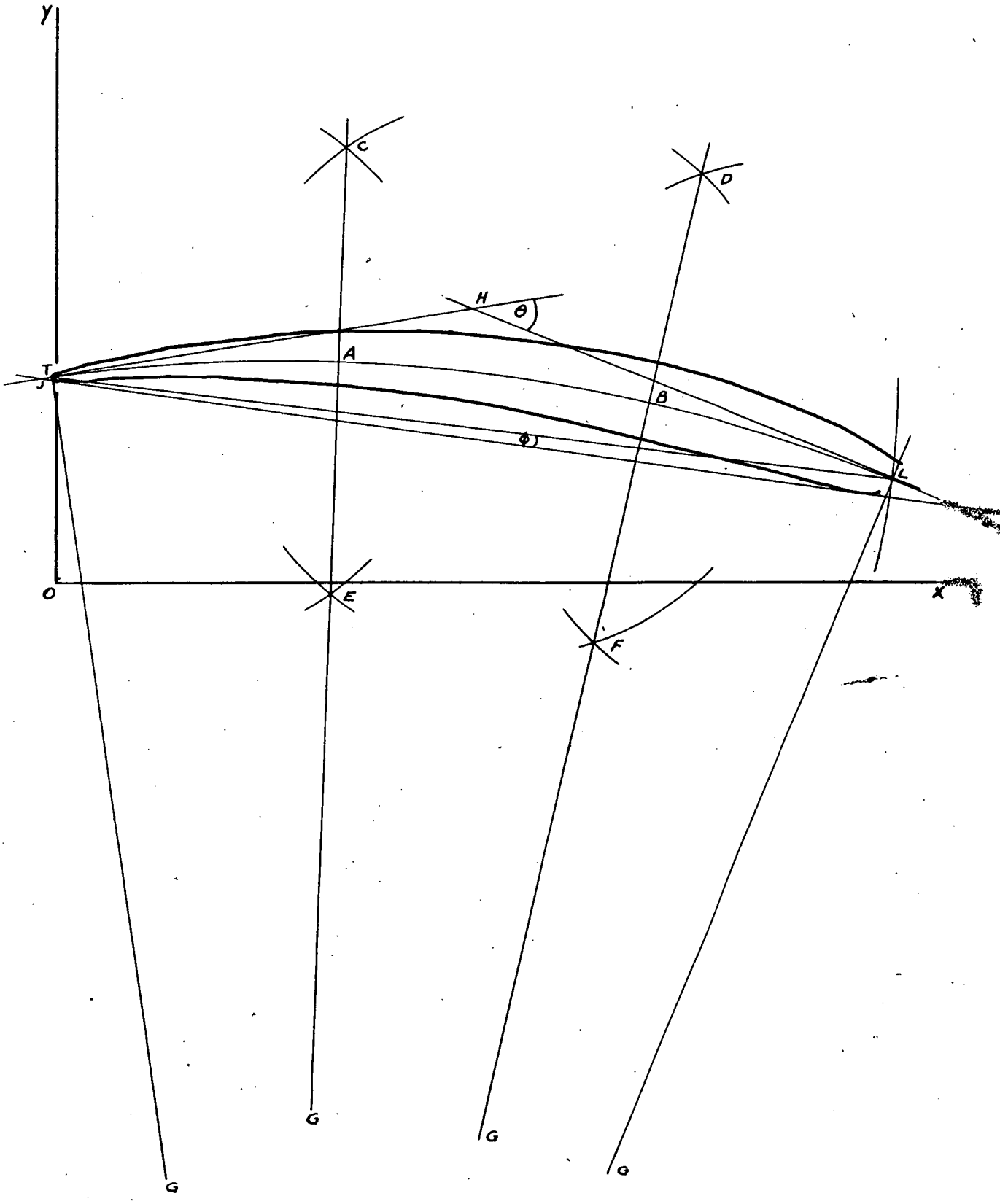

Graphical Method of Determining Angles
from
Measured Blade Sections

Section Shown is Rotor at Mid Blade Height

Fig.5

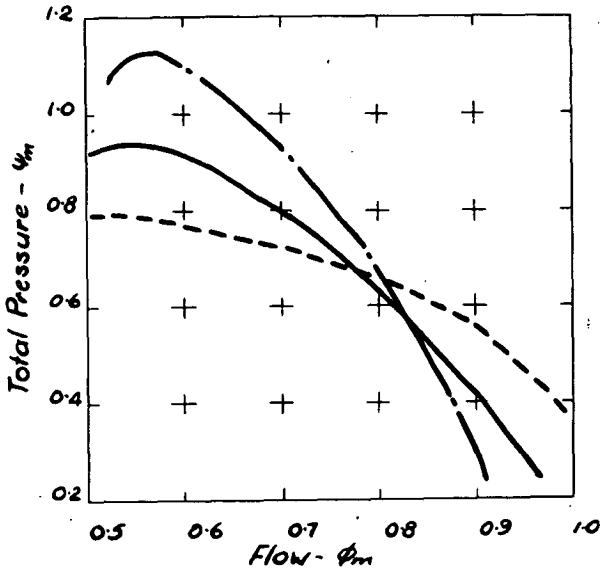

Setting I

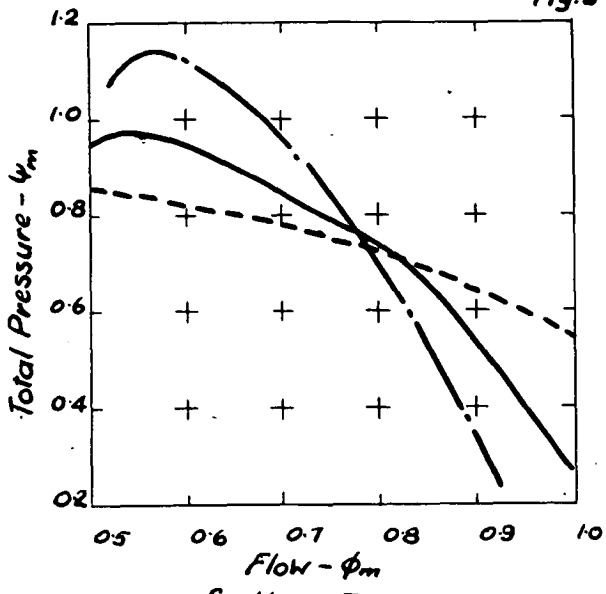

Setting II

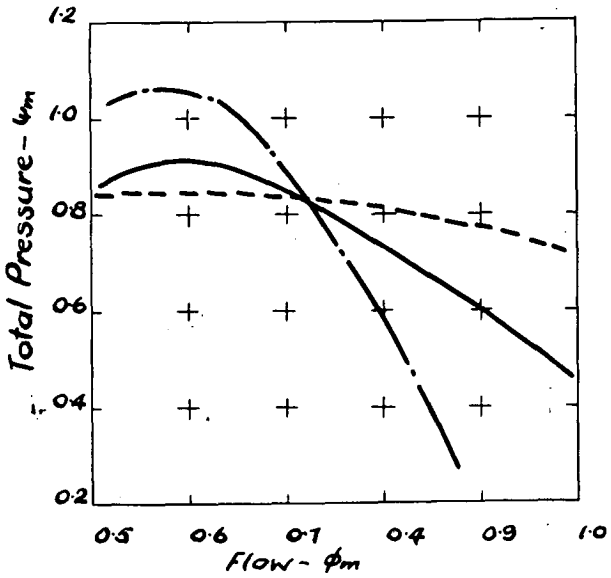

Setting III

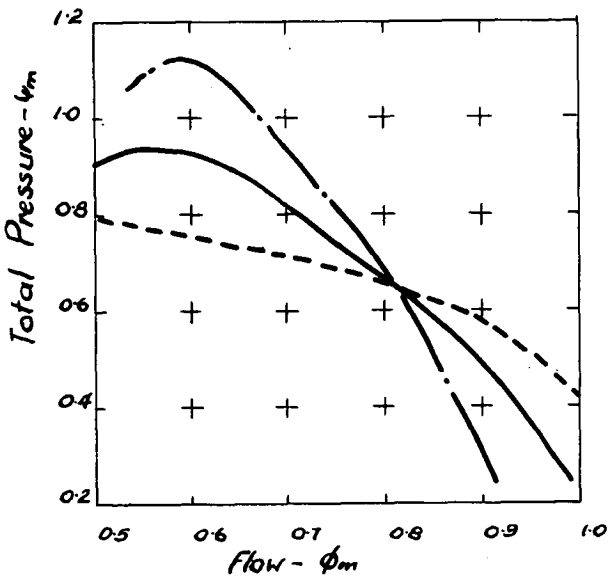

Original Design Setting

Rotor Performance Curves for Three Cast Blade Settings and the Original Design

Symbols :- --- Hub
— Mid Blade Height
—·— 1" from Tip

Fig. 6

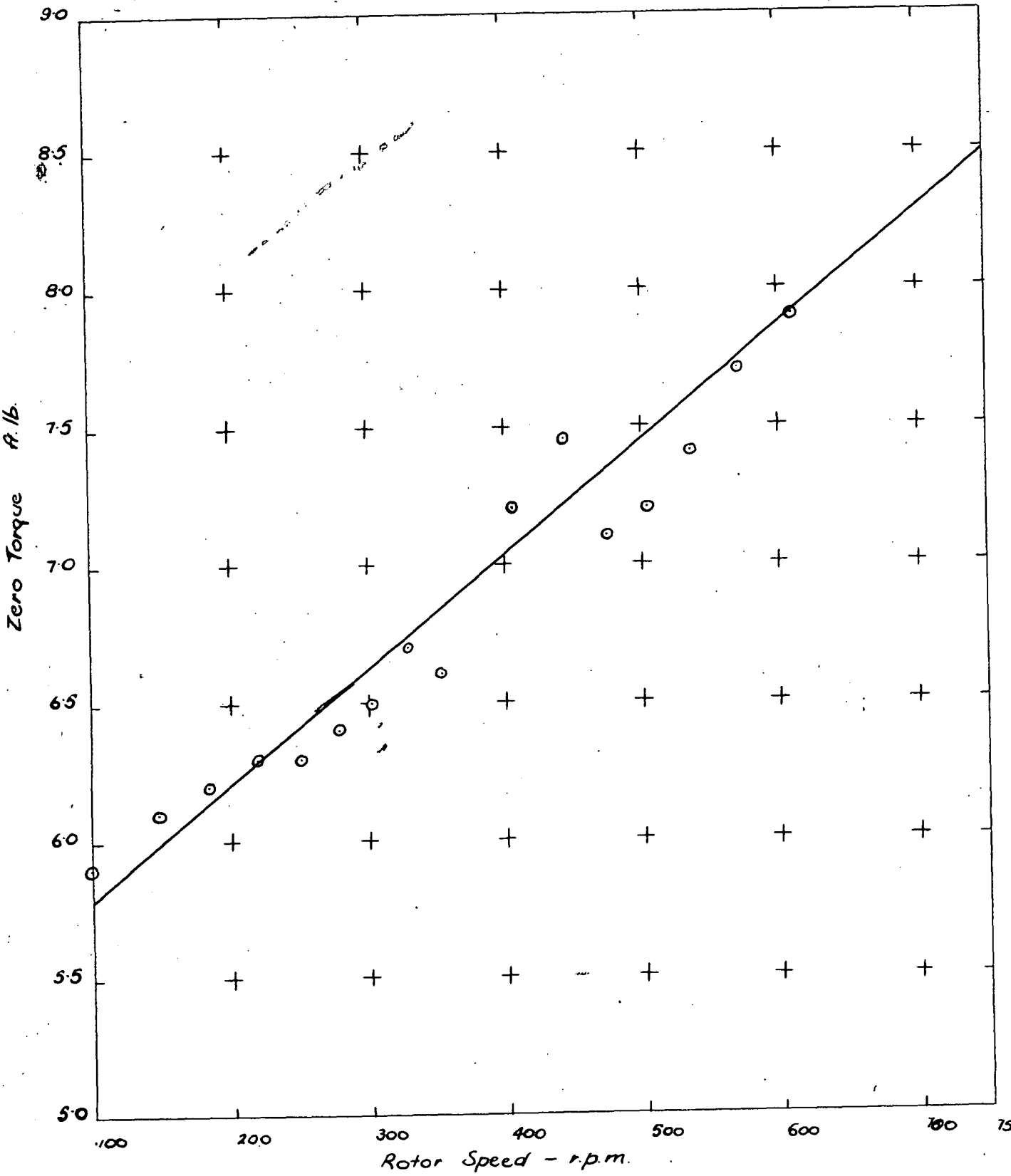

No Load Torque Calibration Curve

Fig. 7

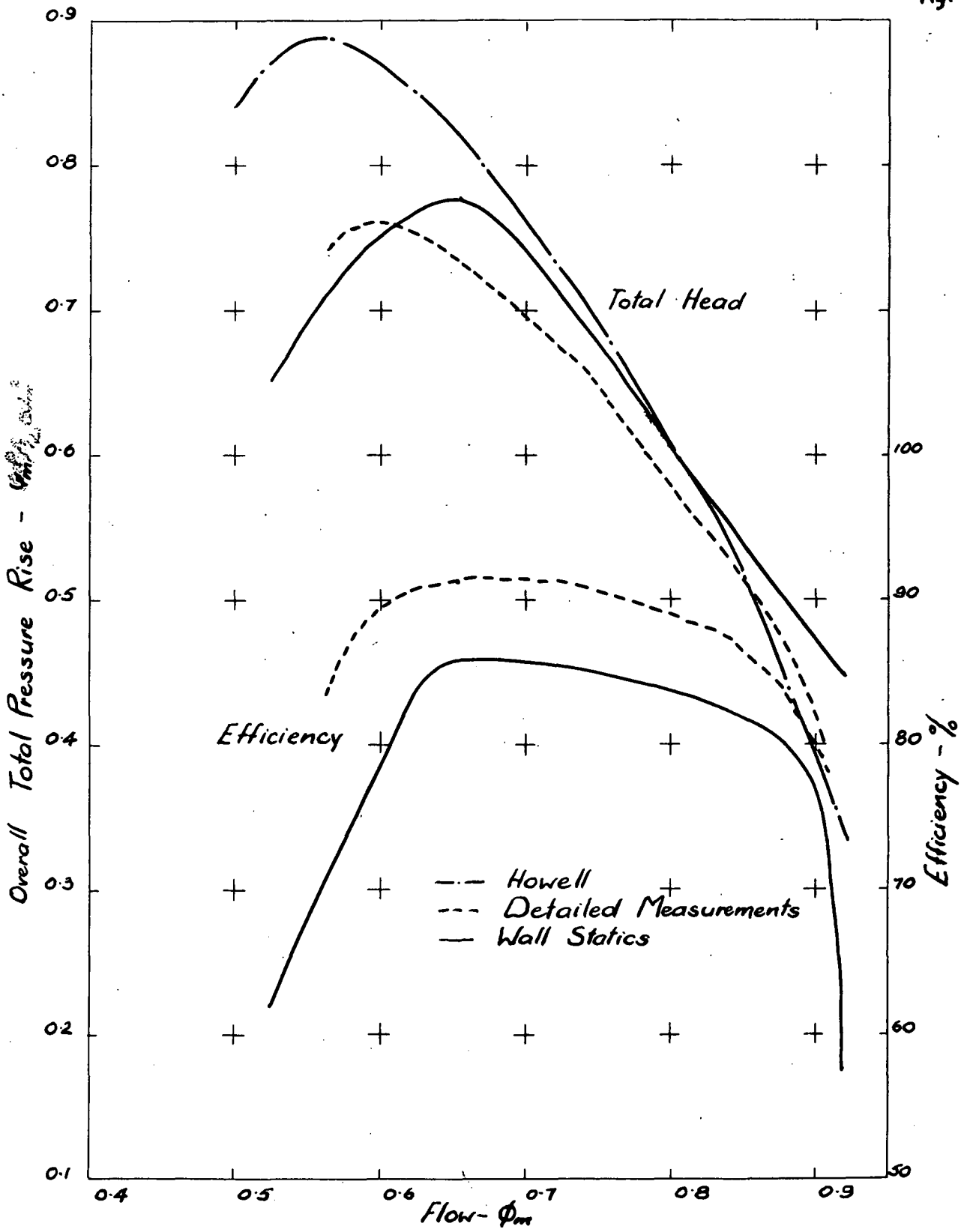

Comparison Between Total Head and Efficiency from Detailed and Wall Static Tests

Fig. 8

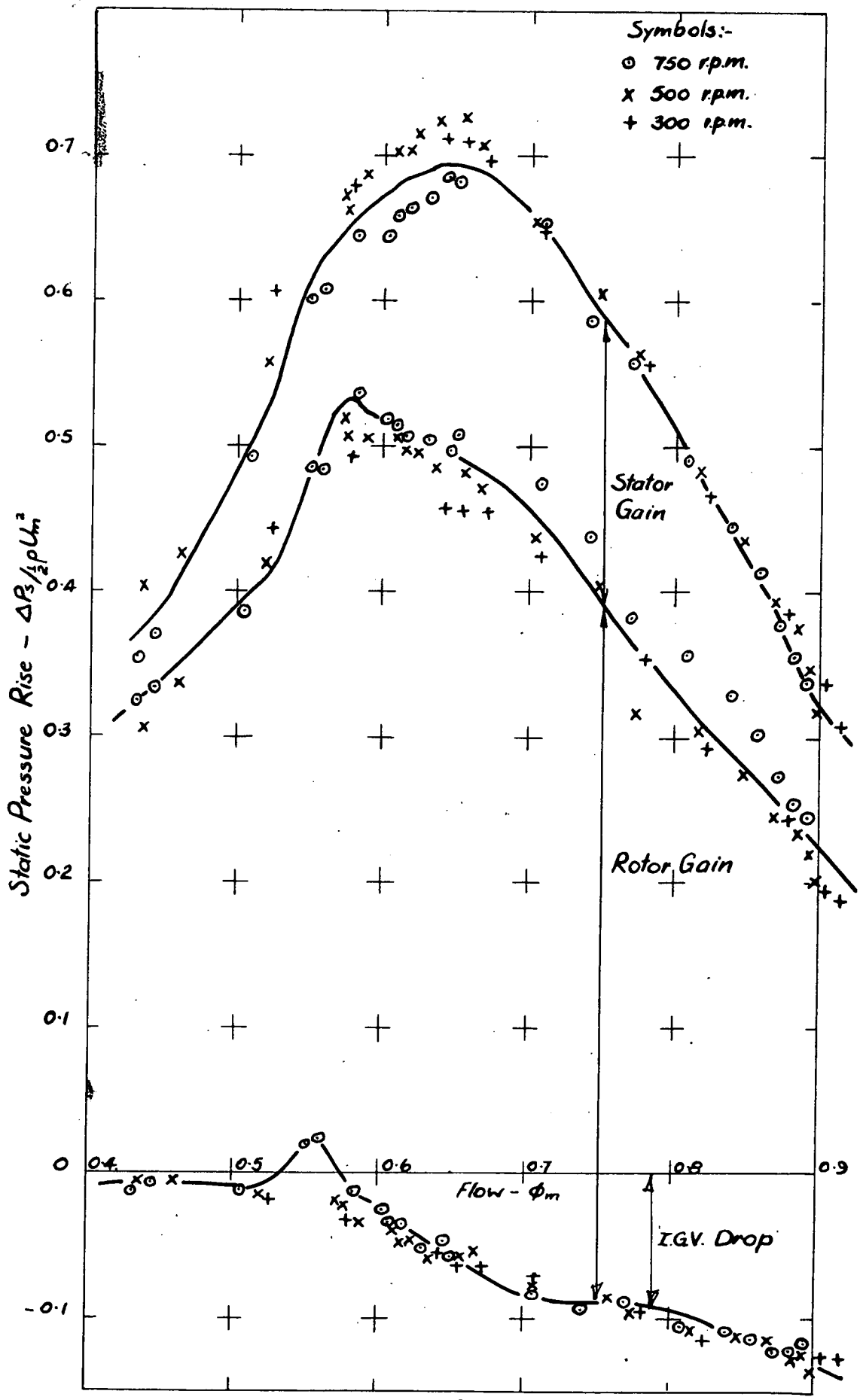

Wall Static Pressures
300, 500 and 750 r.p.m.

Fig. 9

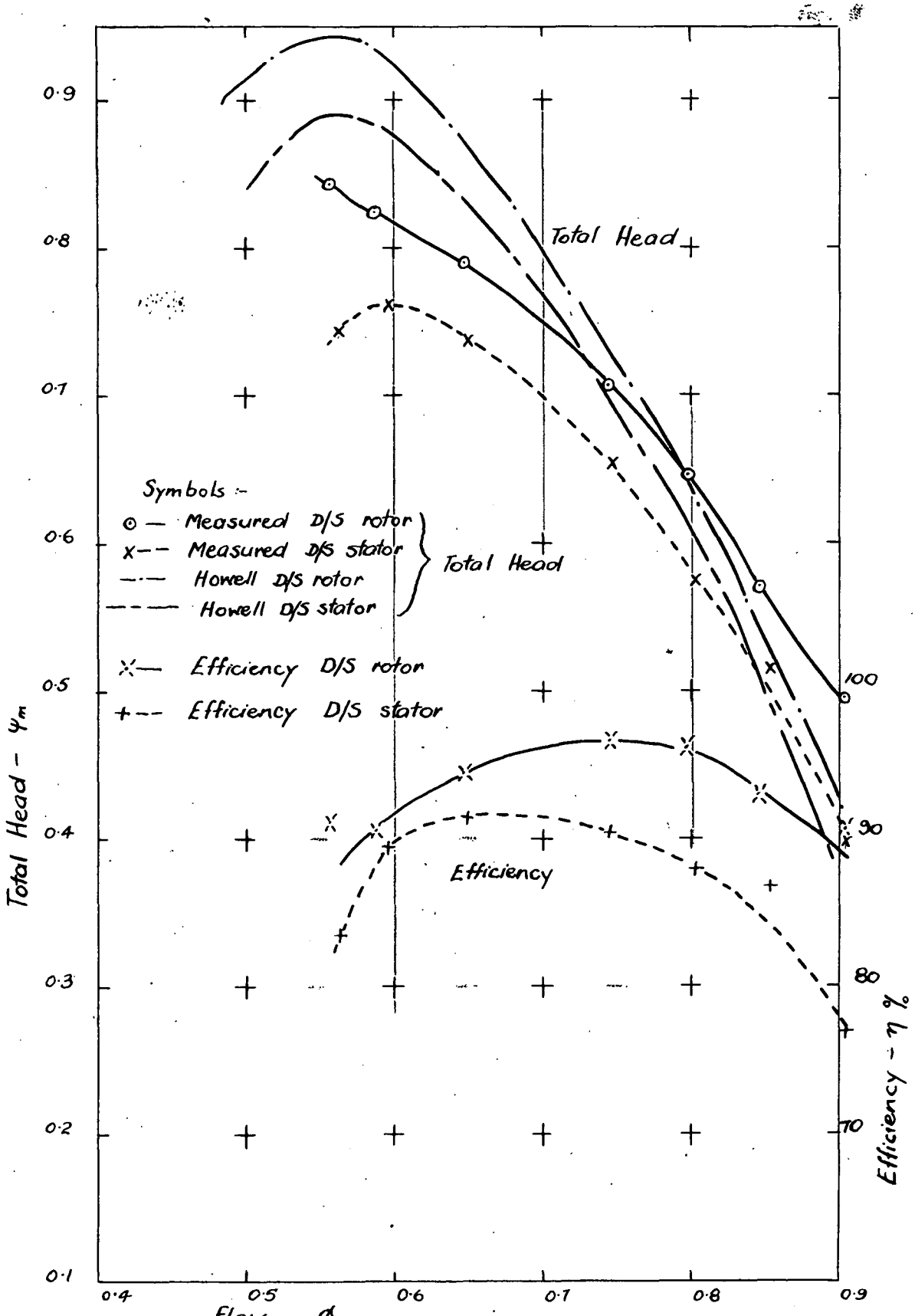

Rotor and Overall Characteristics

750 r.p.m.

Fig.10

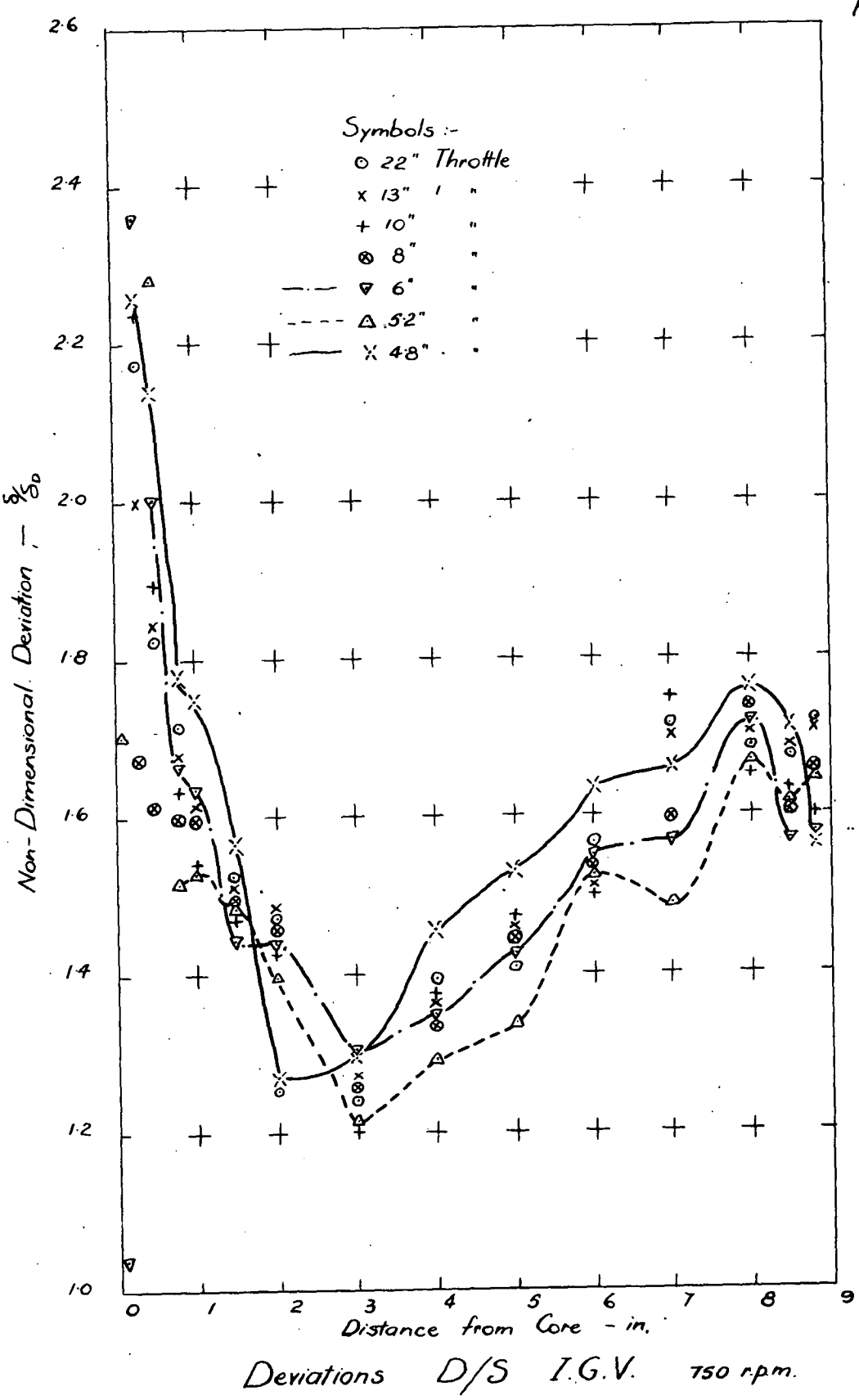

Deviations D/S I.G.V. 750 r.p.m.

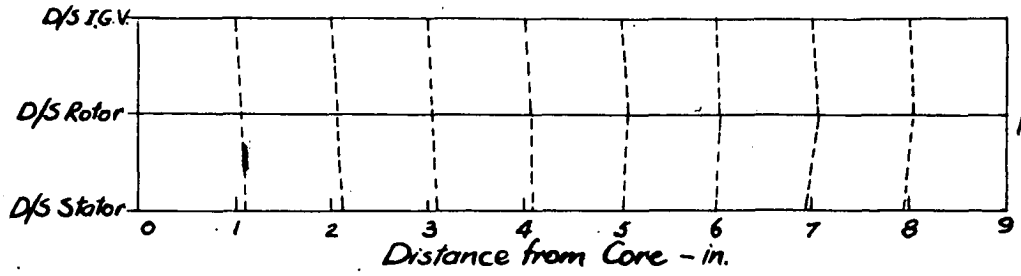

Fig. 11

Bulk Radial Movement of Flow

8" Throttle

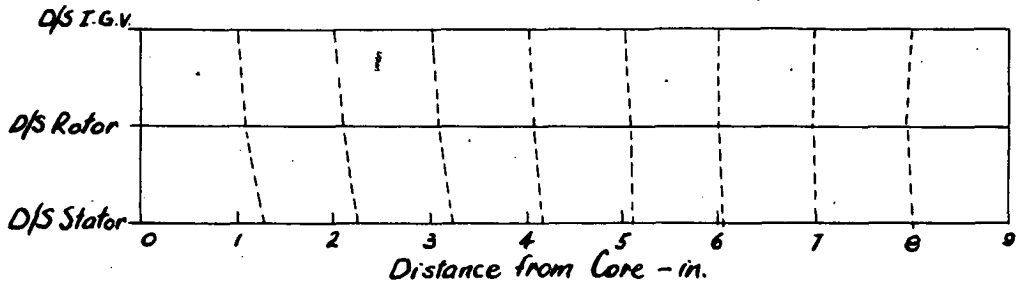

Bulk Radial Movement of Flow

6" Throttle

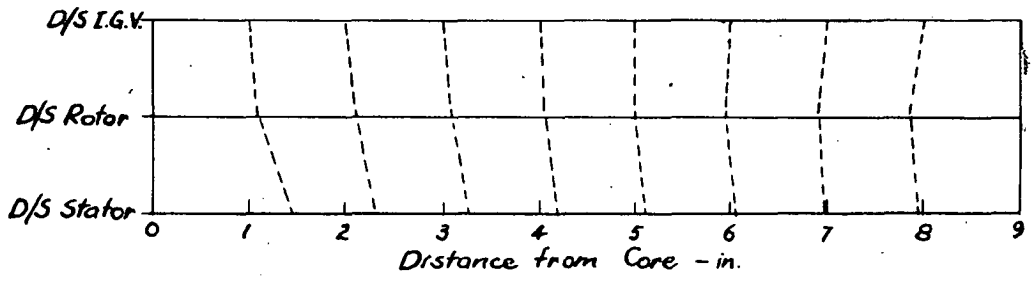

Bulk Radial Movement of Flow

5·2" Throttle

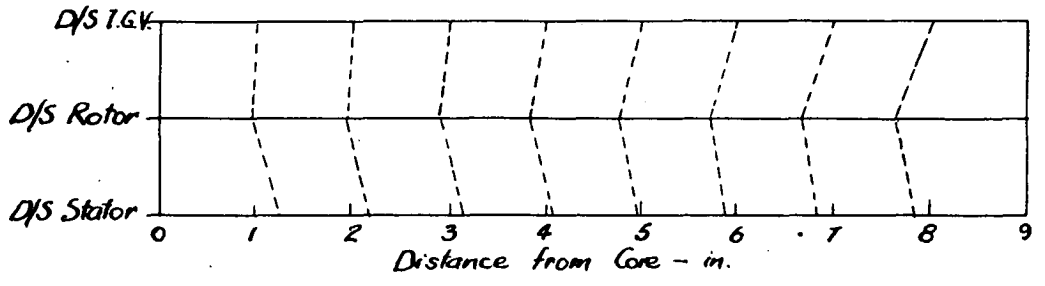

Bulk Radial Movement of Flow

4·8" Throttle

Movement of Bulk Flow Through Rotor and Stator

Fig. 12

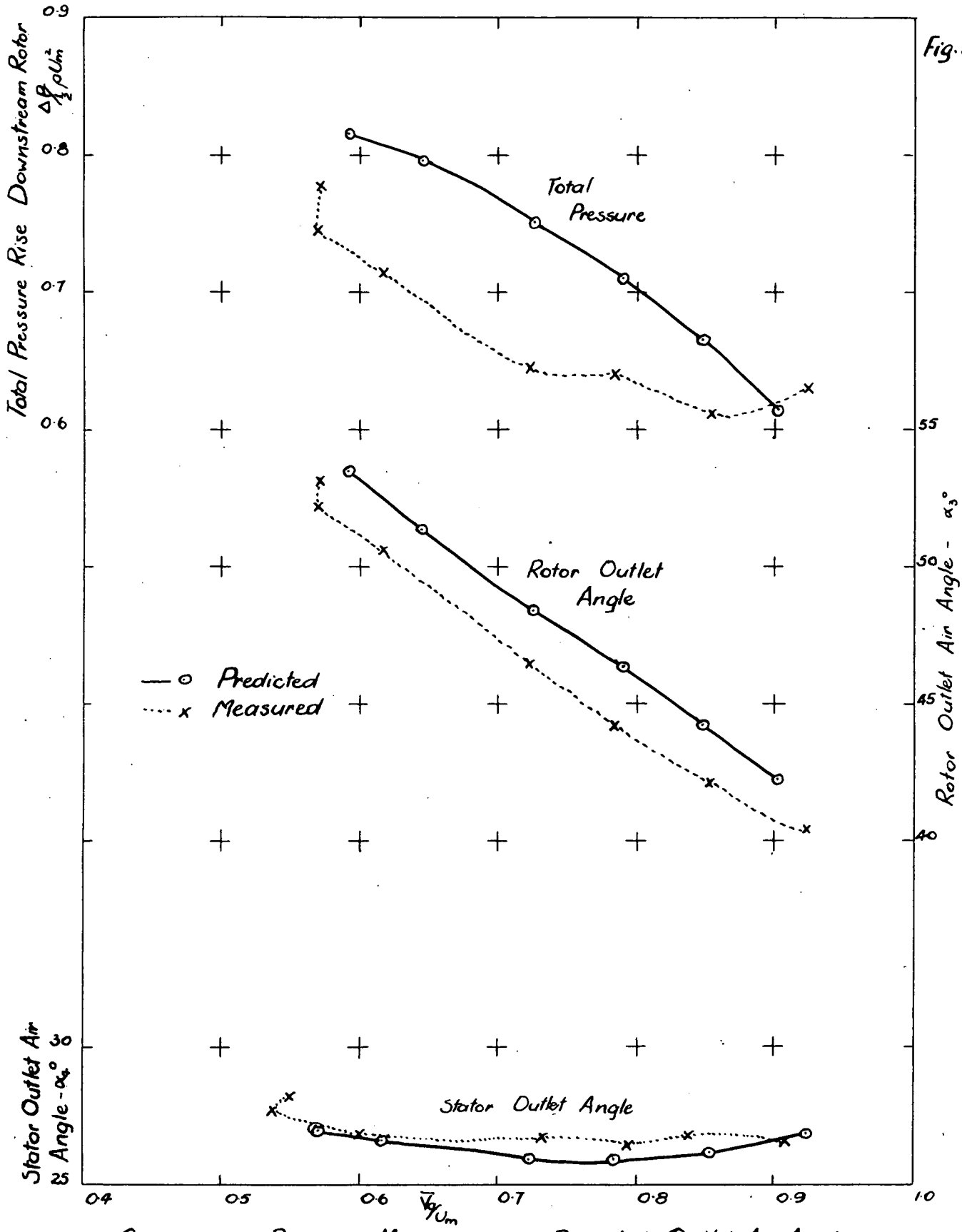

Comparison Between Measured and Predicted Outlet Air Angle and Total Pressure Downstream Rotor and Air Angle Downstream Stator 1" from Core

Fig. 13

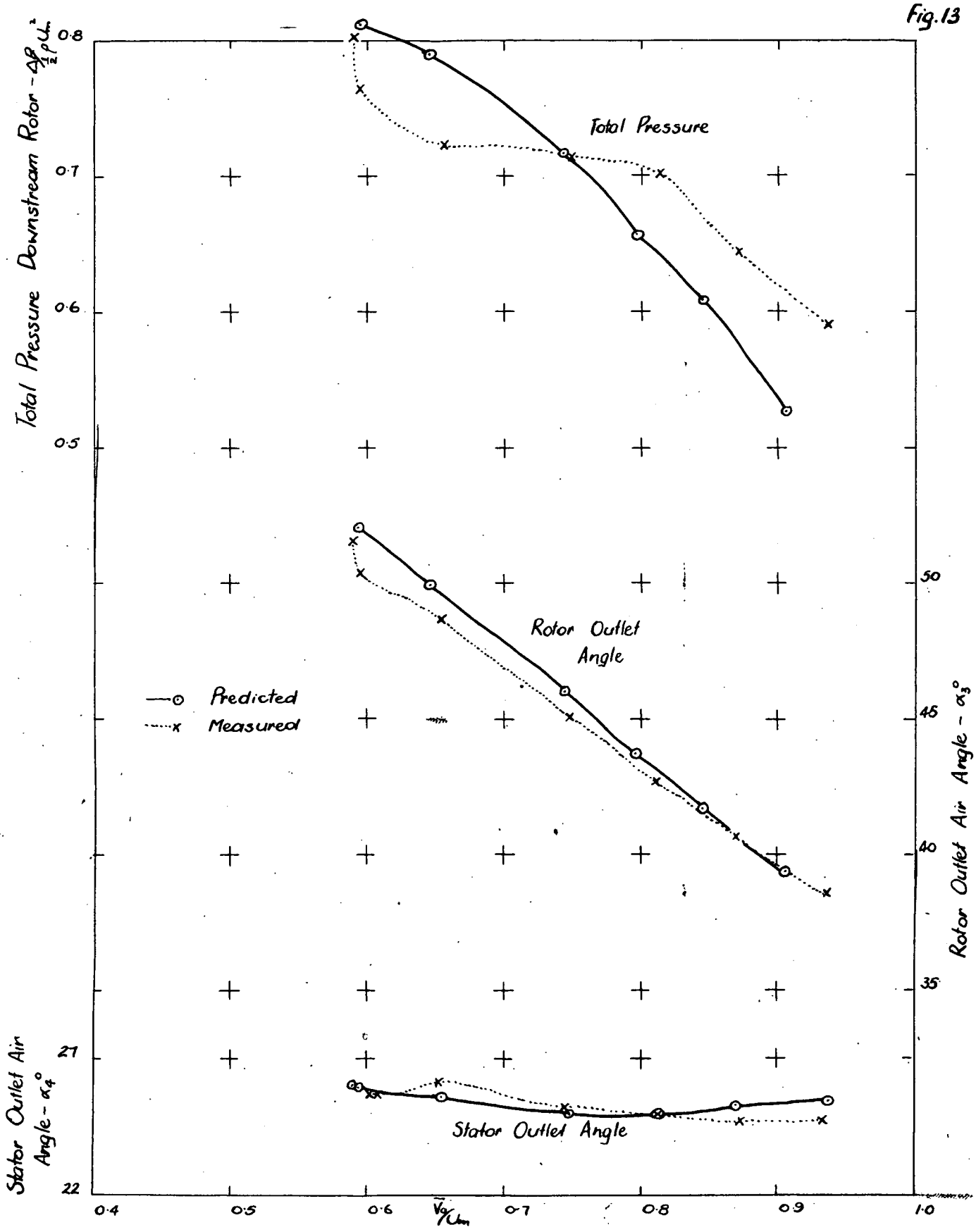

Comparison Between Measured and Predicted Outlet Air Angle and Total Pressure Downstream Rotor and Air Angle Downstream Stator 2" from Core

Fig.14

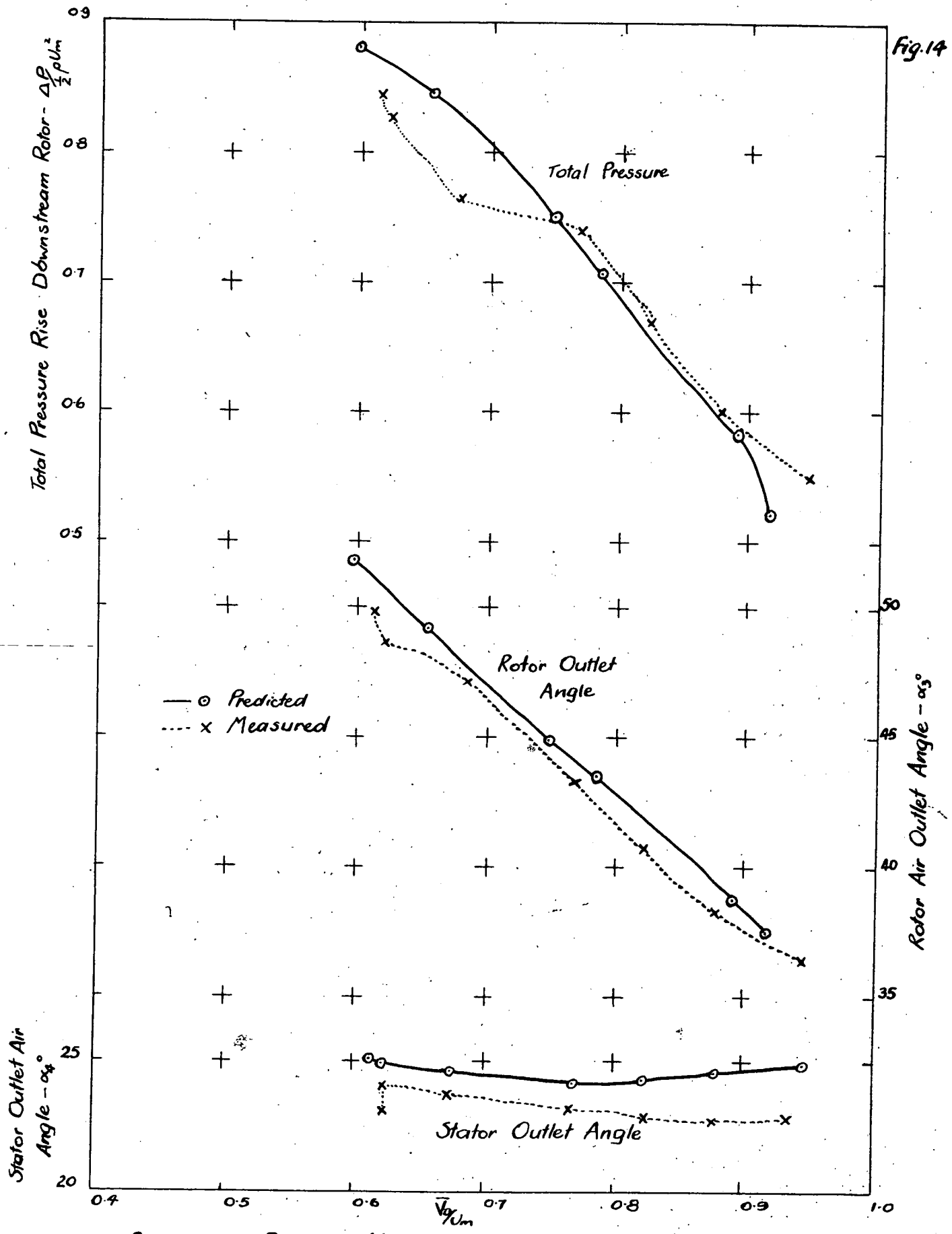

Comparison Between Measured and Predicted Outlet Air Angle and Total Pressure Downstream Rotor, and Air Angle Downstream Stator 3" from Core

Fig. 15

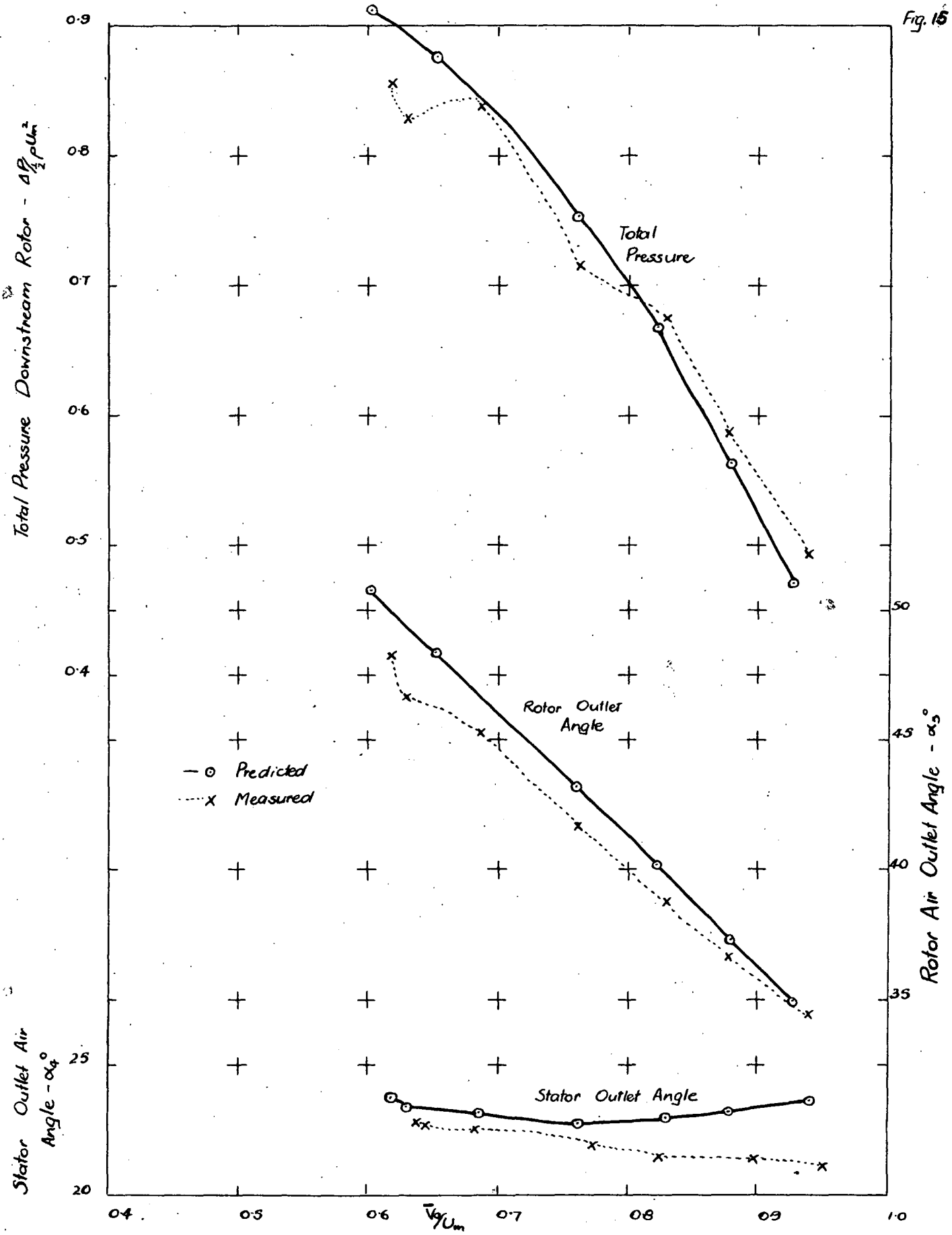

Comparison Between Rotor Outlet Air Angle and Total Pressure and Stator Outlet Air Angle, Measured and Predicted 4" from Core

Fig. 16

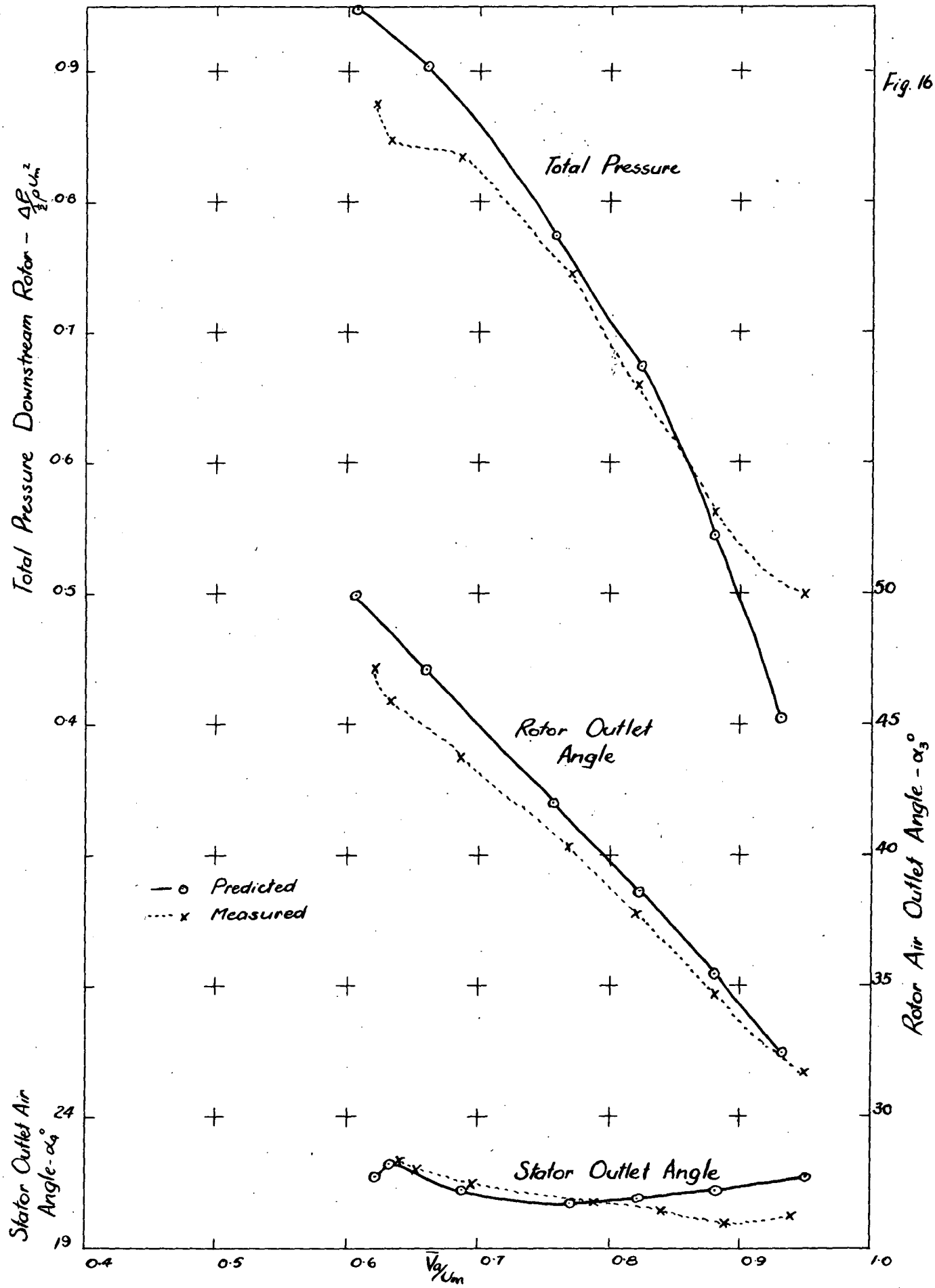

Comparison Between Measured and Predicted Air Angle and Total Pressure Downstream Rotor and Air Angle Downstream Stator 5" from Core

Fig. 11

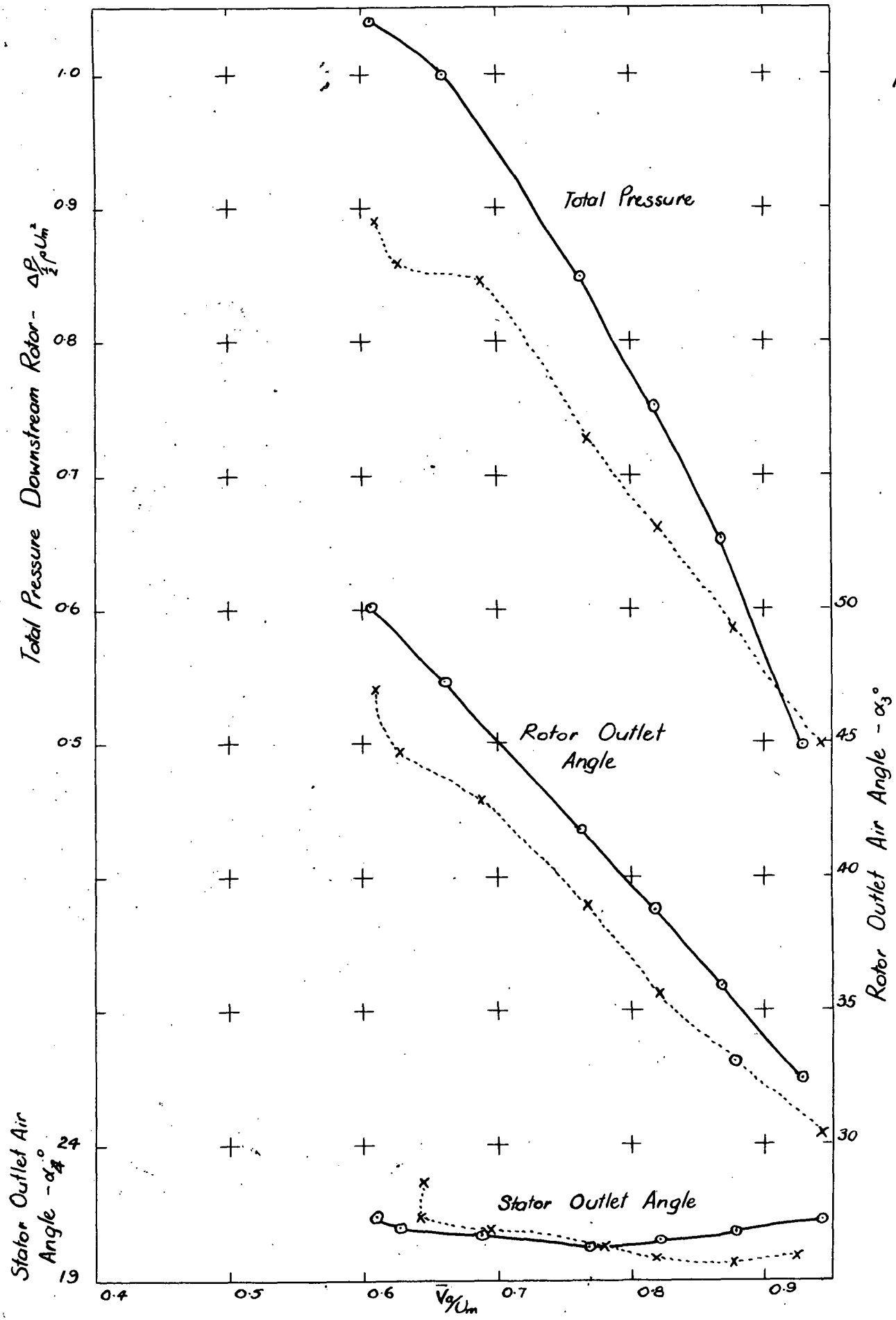

Comparison Between Measured and Predicted Air Angle and Total Pressure Downstream Rotor and Air Angle Downstream Stator 6" from Core

Fig.18

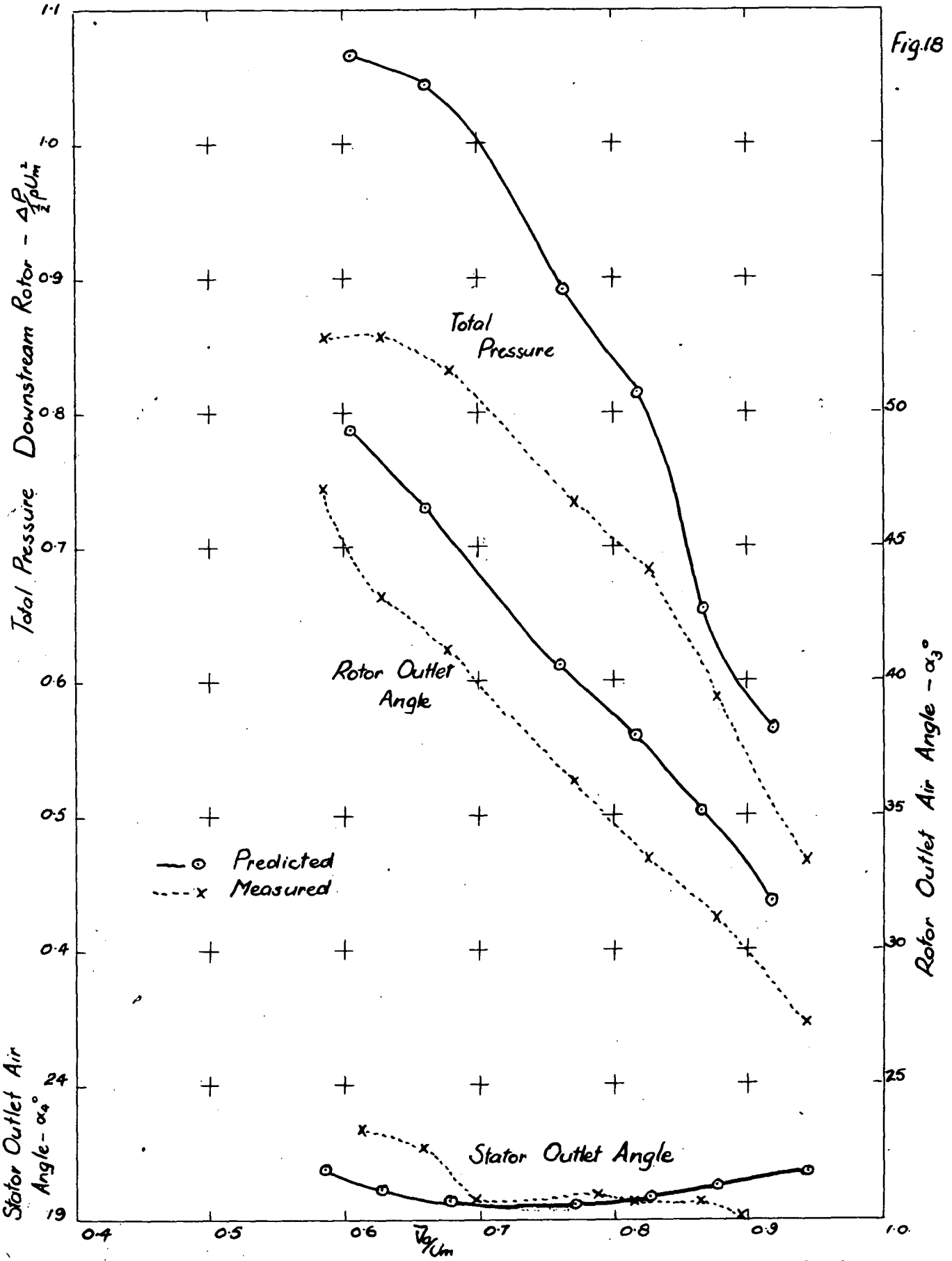

Comparison Between Predicted and Measured Air Angle and Total Pressure Downstream Rotor and Air Angle Downstream Stator 7" from Core

Fig. 18(c)

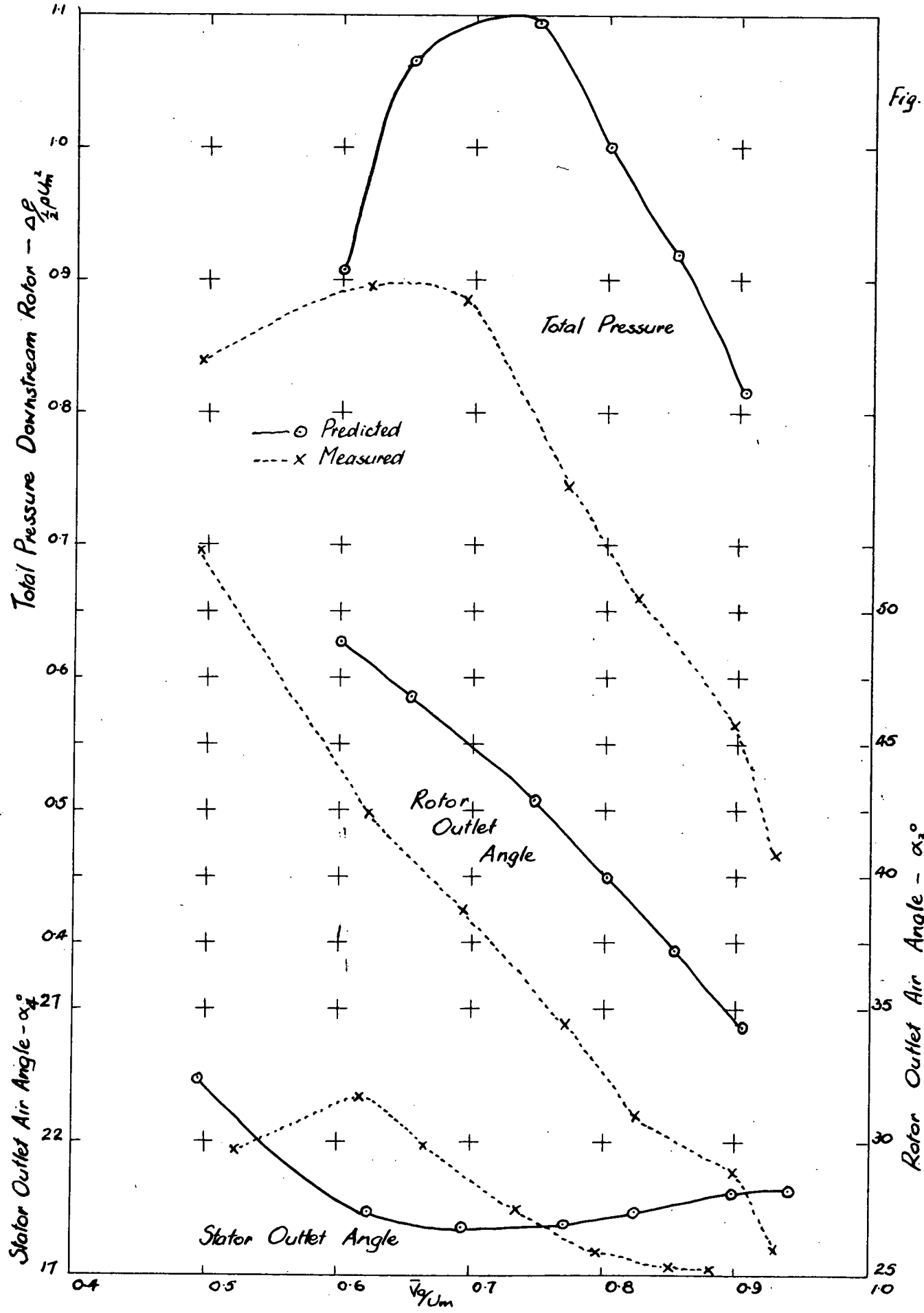

Comparison Between Predicted and Measured Air Angle and Total Pressure Downstream Rotor and Air Angle Downstream Stator

8" from Core

Fig. 19

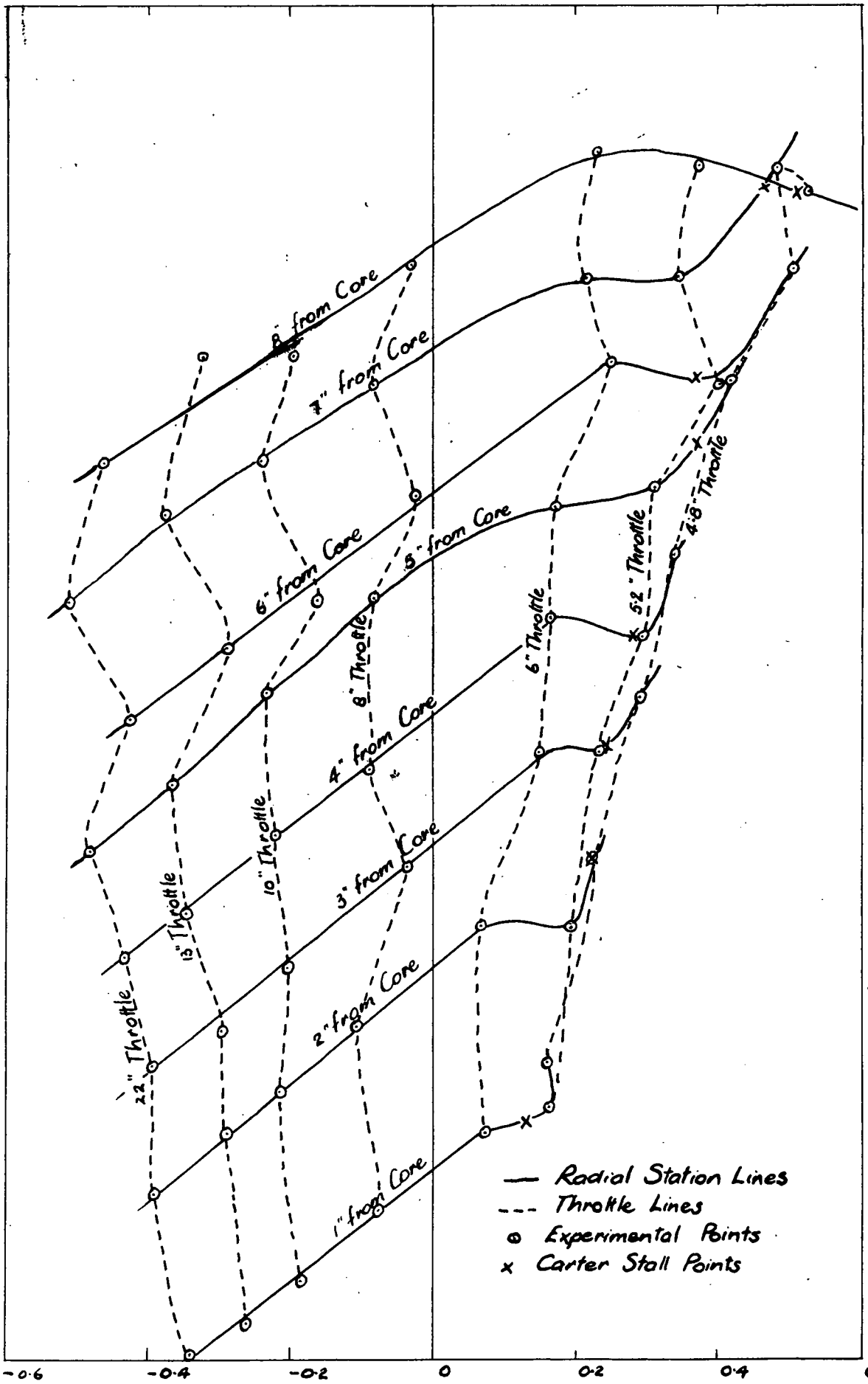

Curves of Non-Dimensional Deflection Against Non-Dimensional Incidence Downstream Rotor

Fig 20

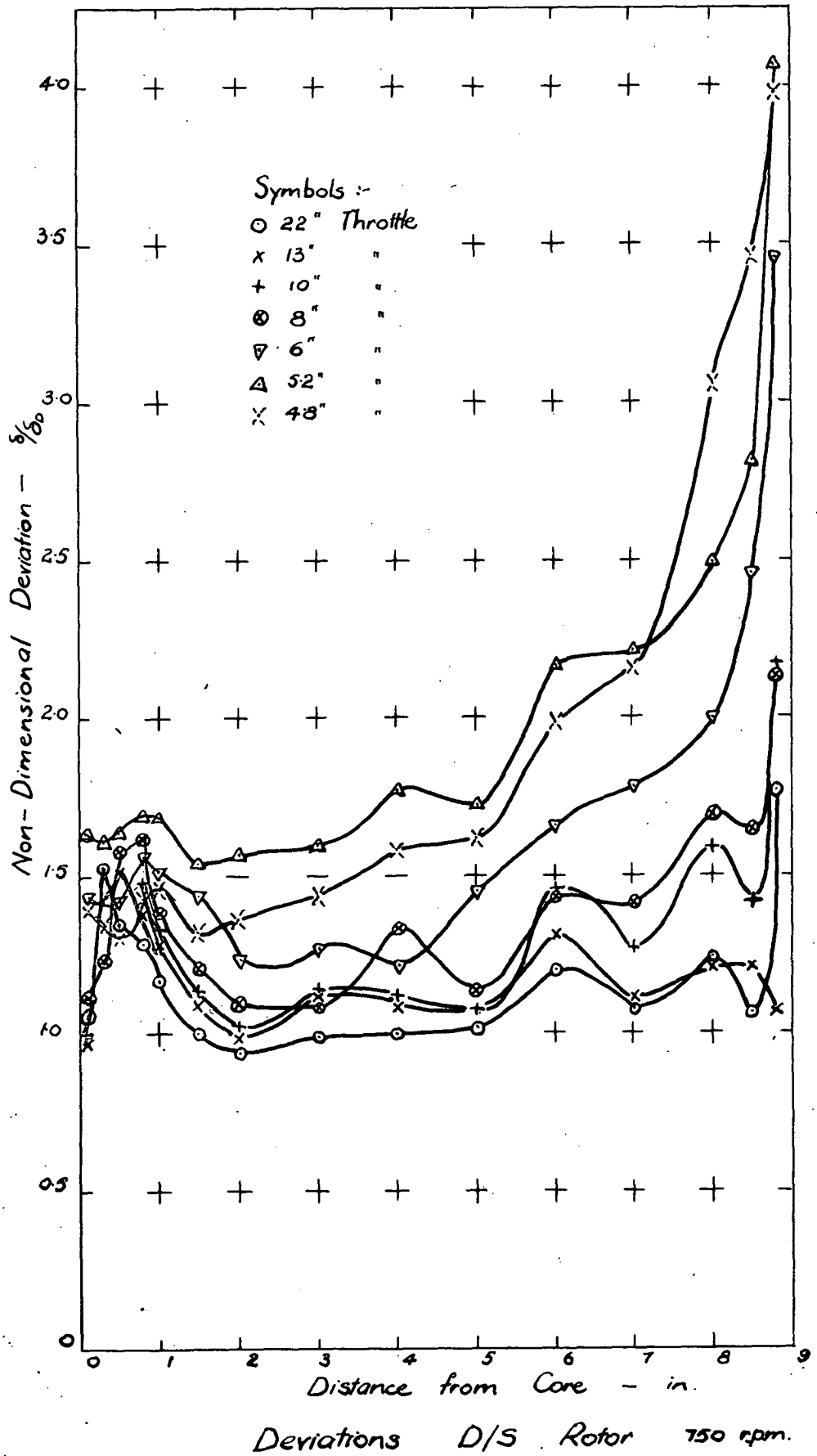

Deviations D/S Rotor 750 r.p.m.

Fig. 21

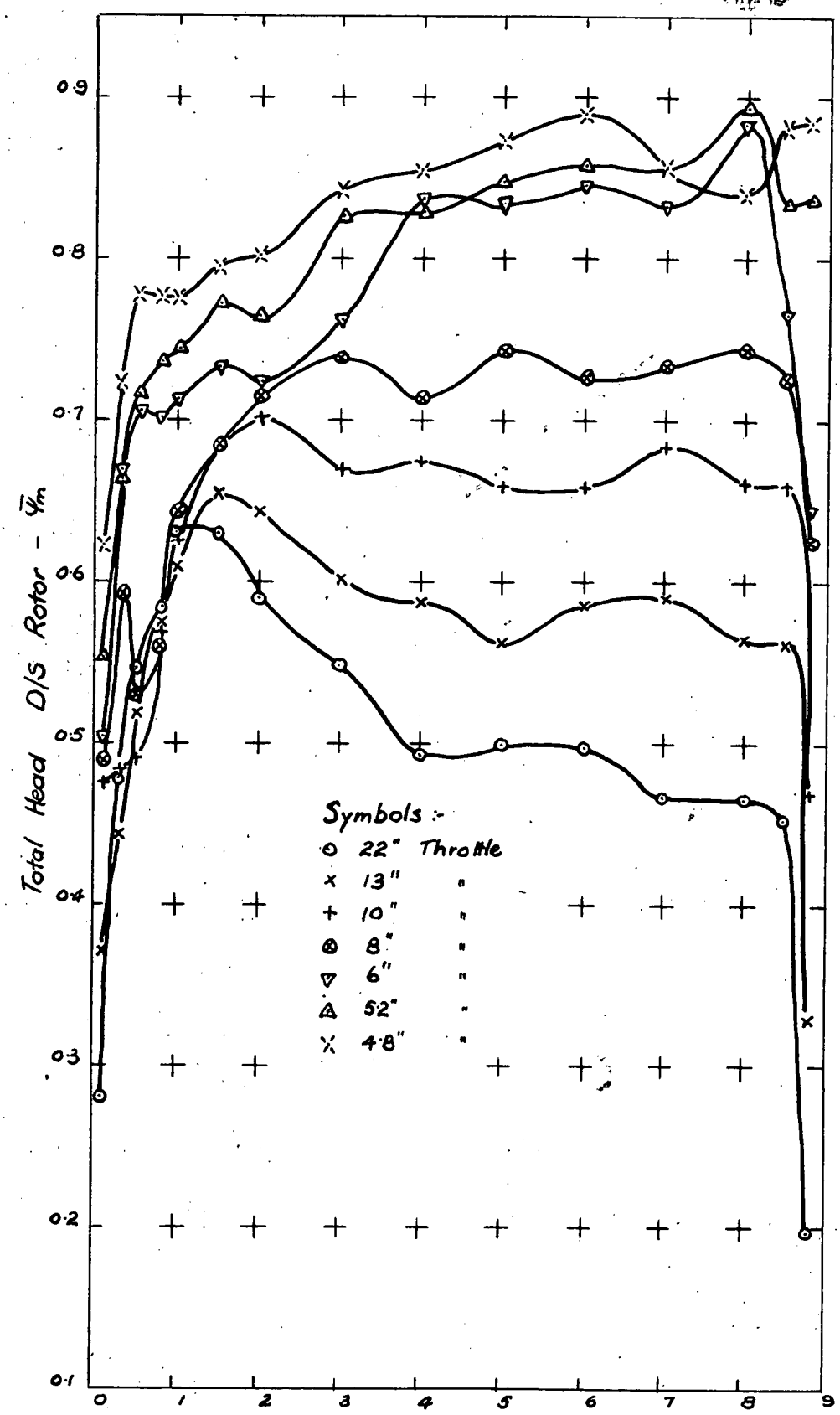

Total Head D/S Rotor 150 rpm.

Fig. 22

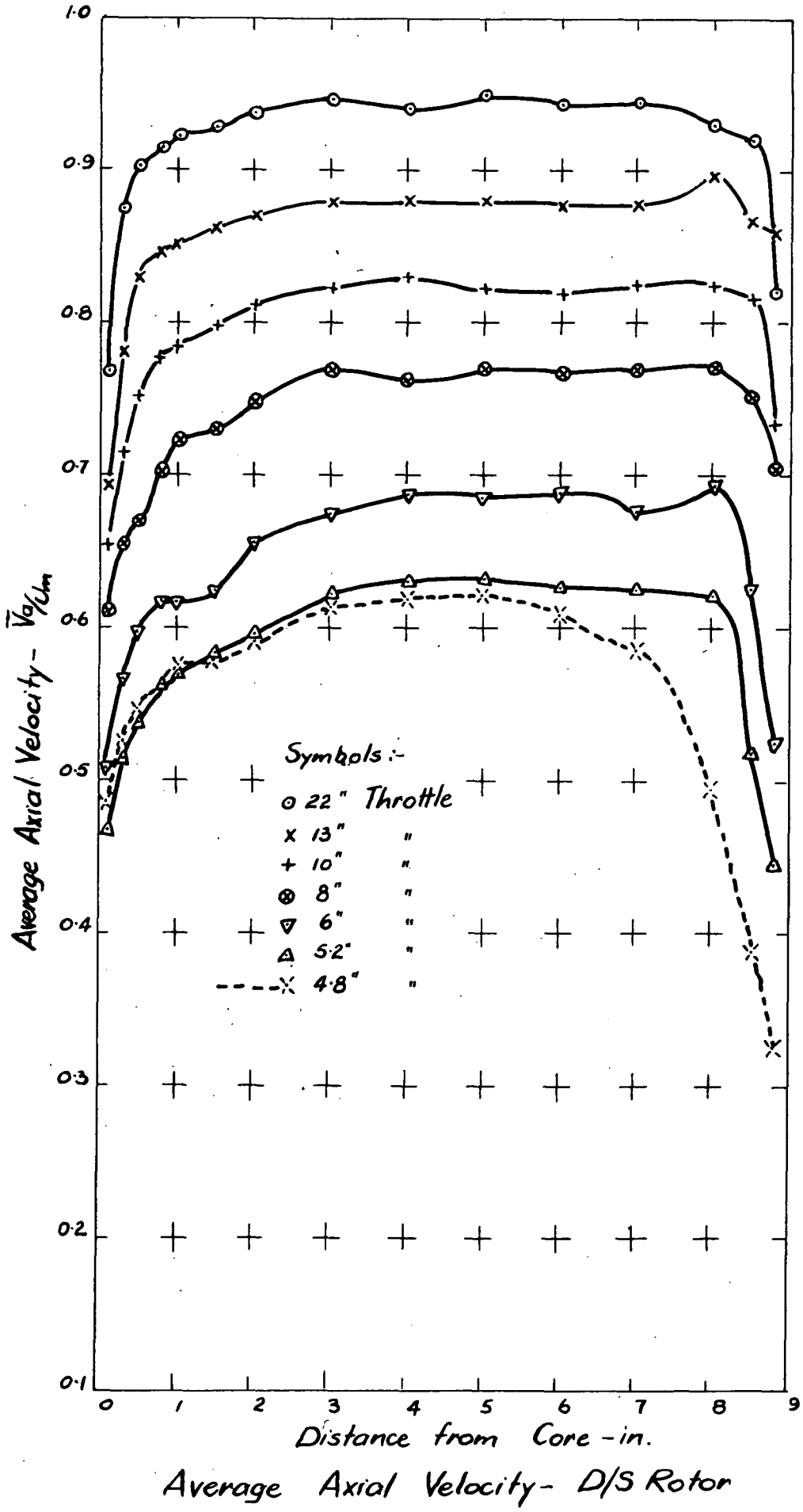

Average Axial Velocity - D/S Rotor

Fig.23

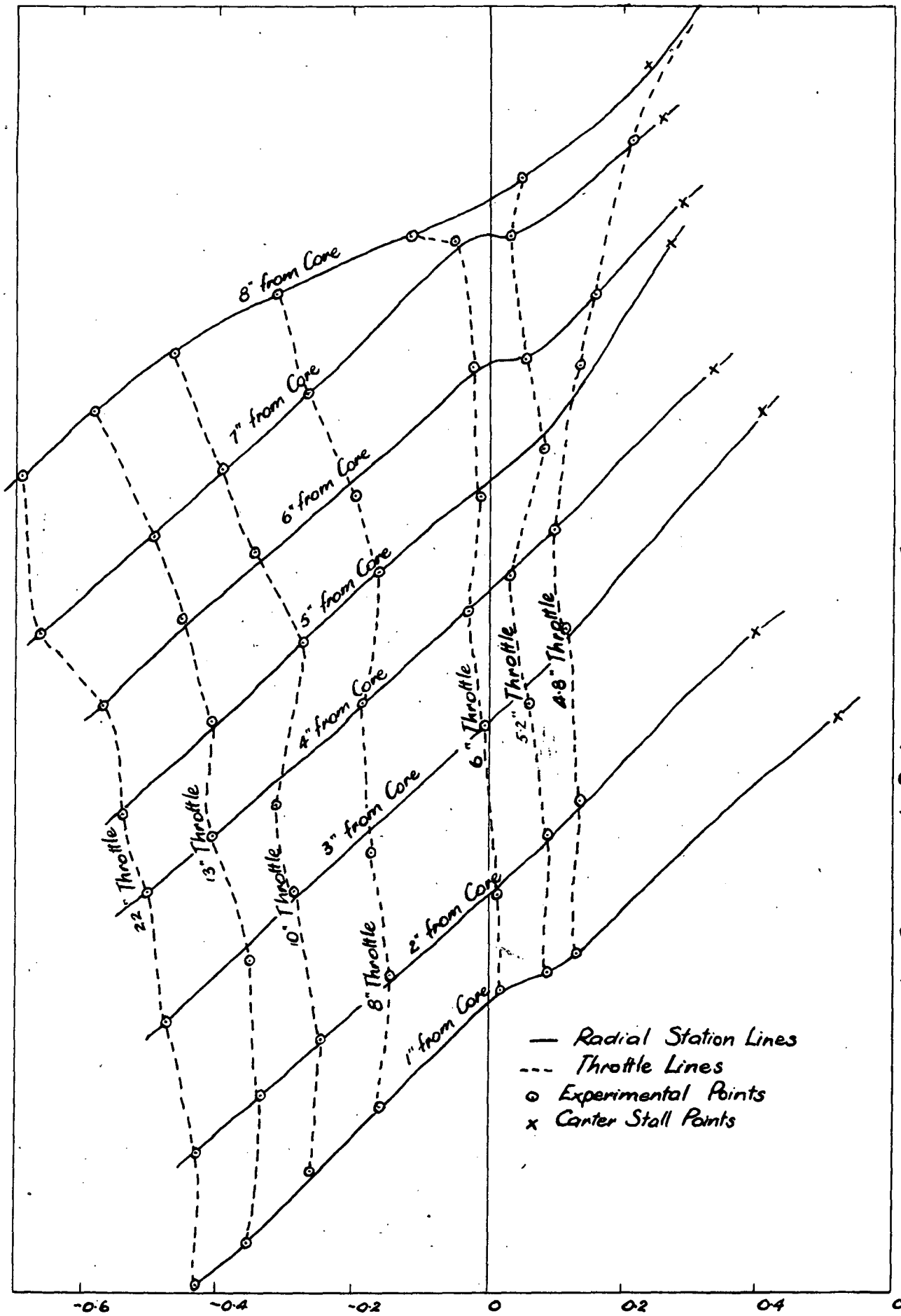

Curves of Non-Dimensional Deflection Against Non-Dimensional Incidence Downstream Stator

Fig 24

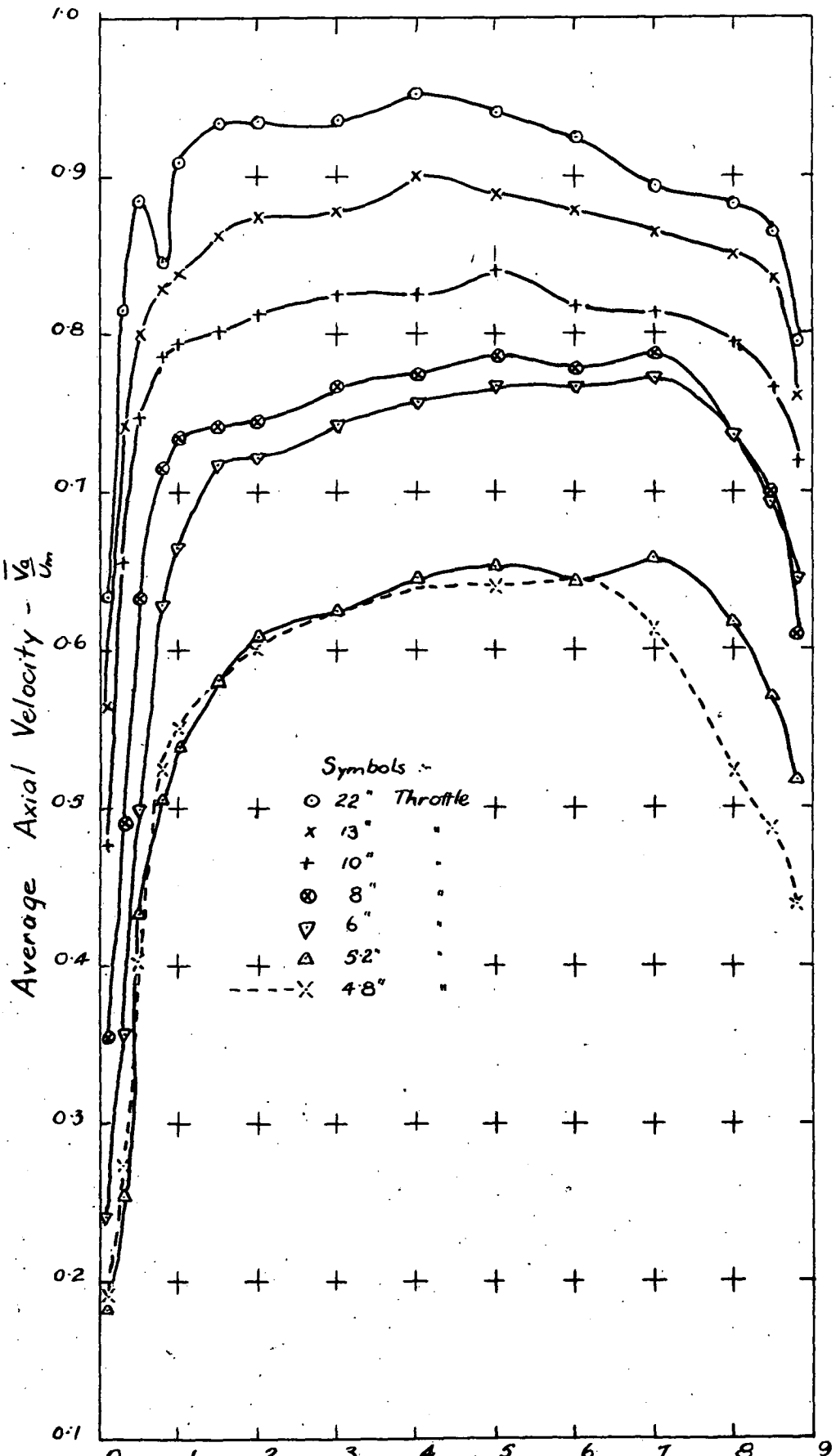

Averaged Axial Velocity D/S Stator

750 rpm.

Fig 25

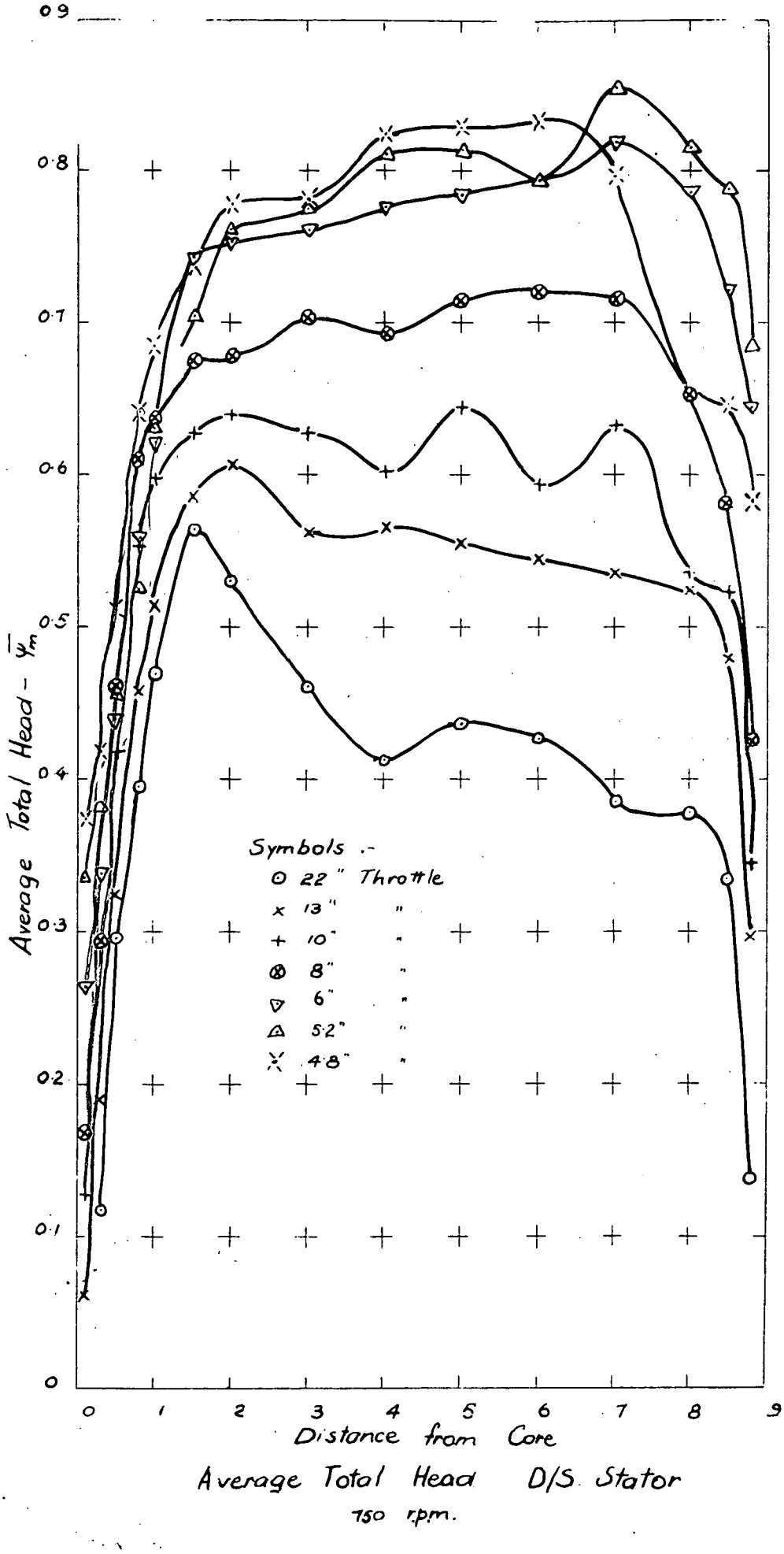

Average Total Head D/S Stator

750 r.p.m.

Fig. 26

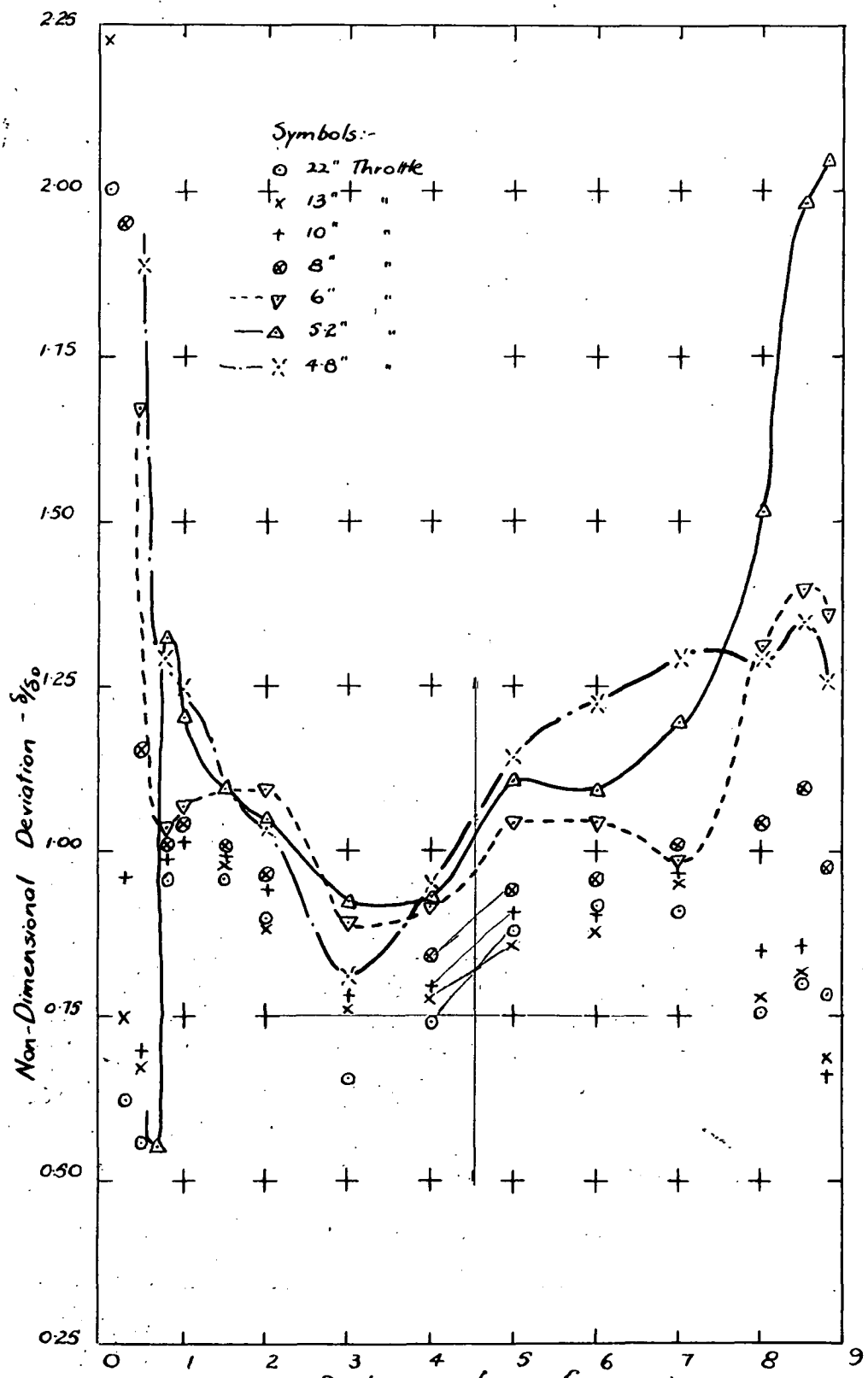

Deviations D/S Stator

750 r.p.m.

Fig. 27

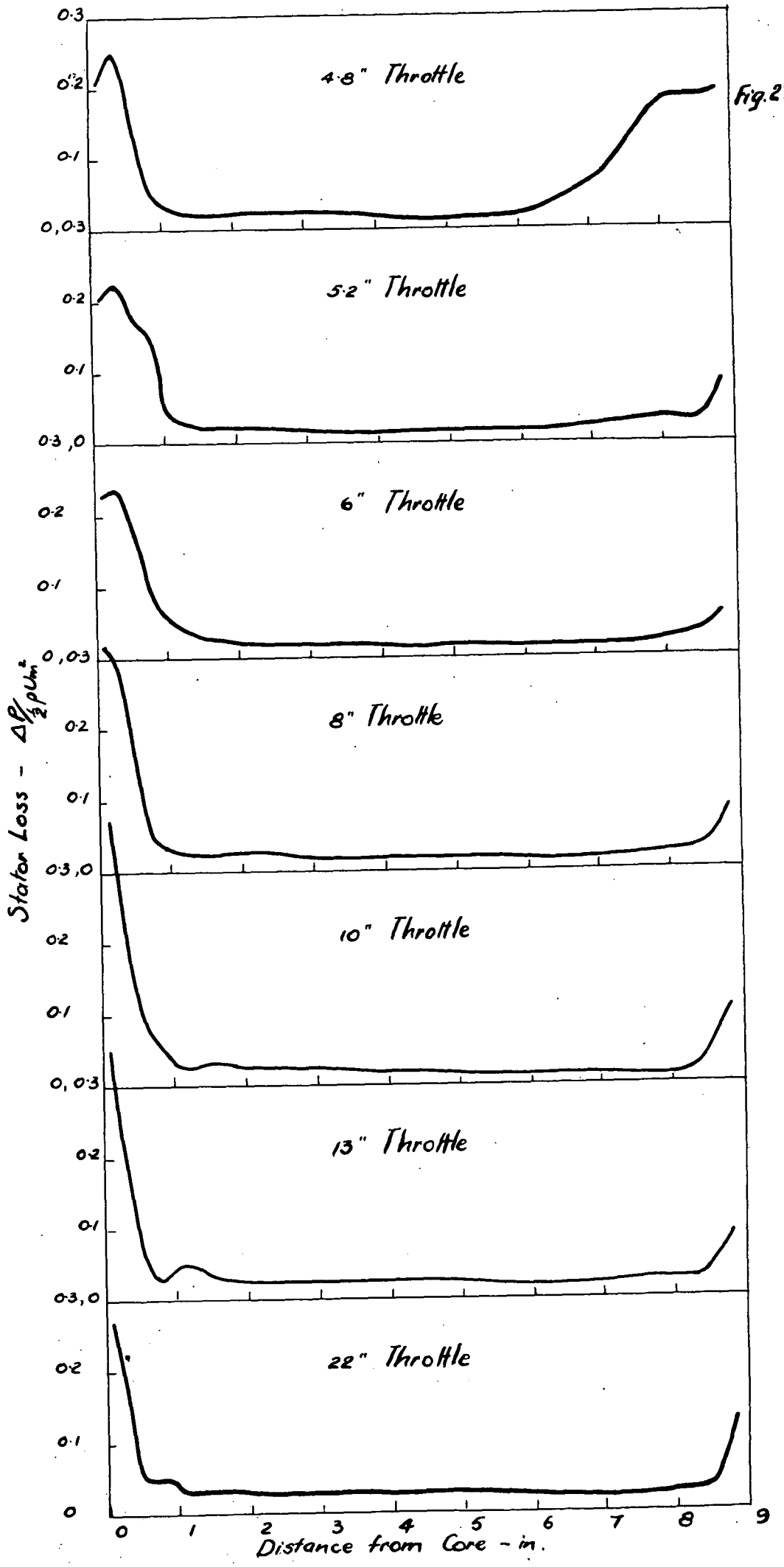

Curves of Radial Distribution of Stator Loss at Various Flows

Fig.28

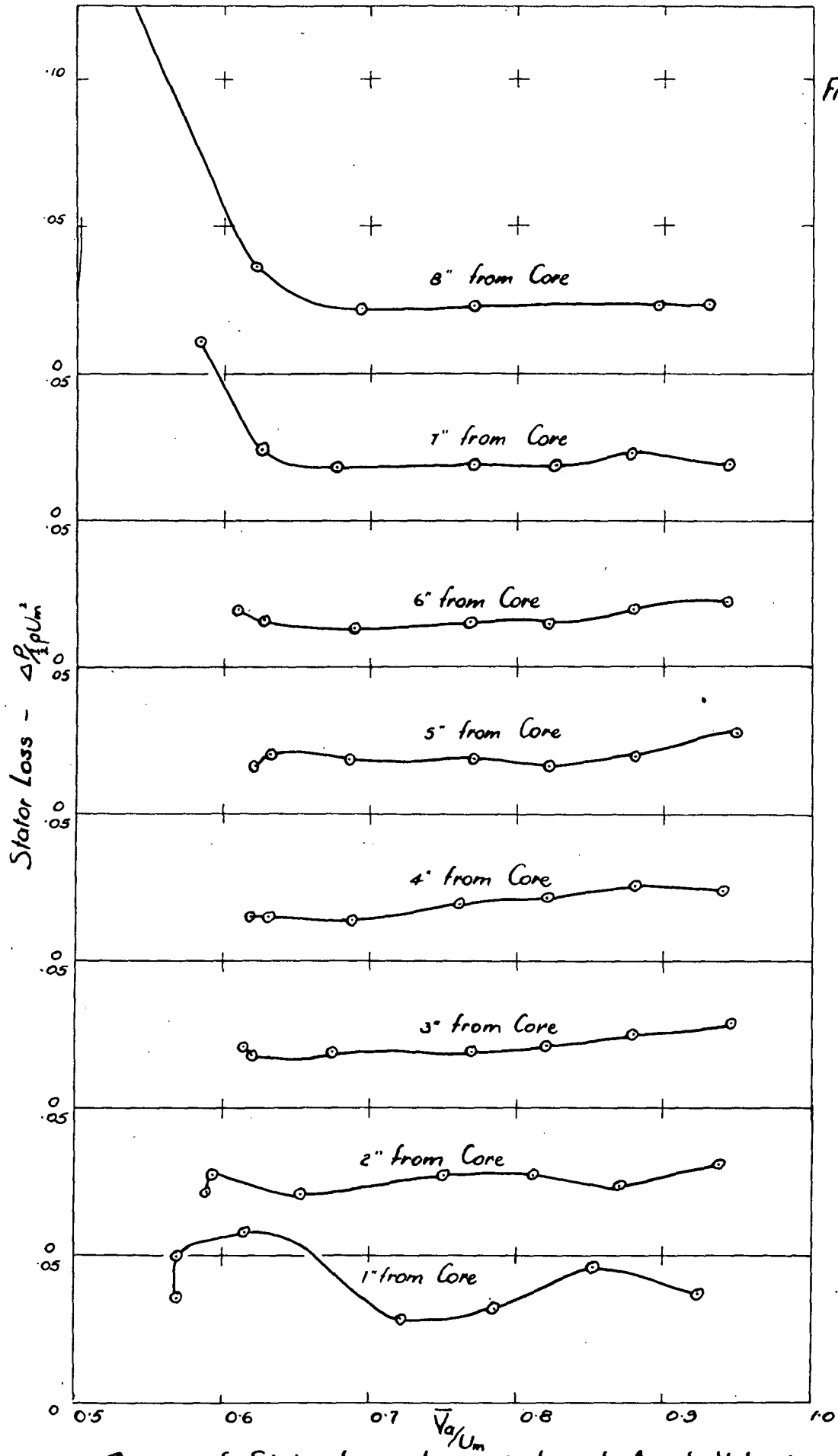

Curves of Stator Loss Against Local Axial Velocity for Various Radial Stations

Fig.29

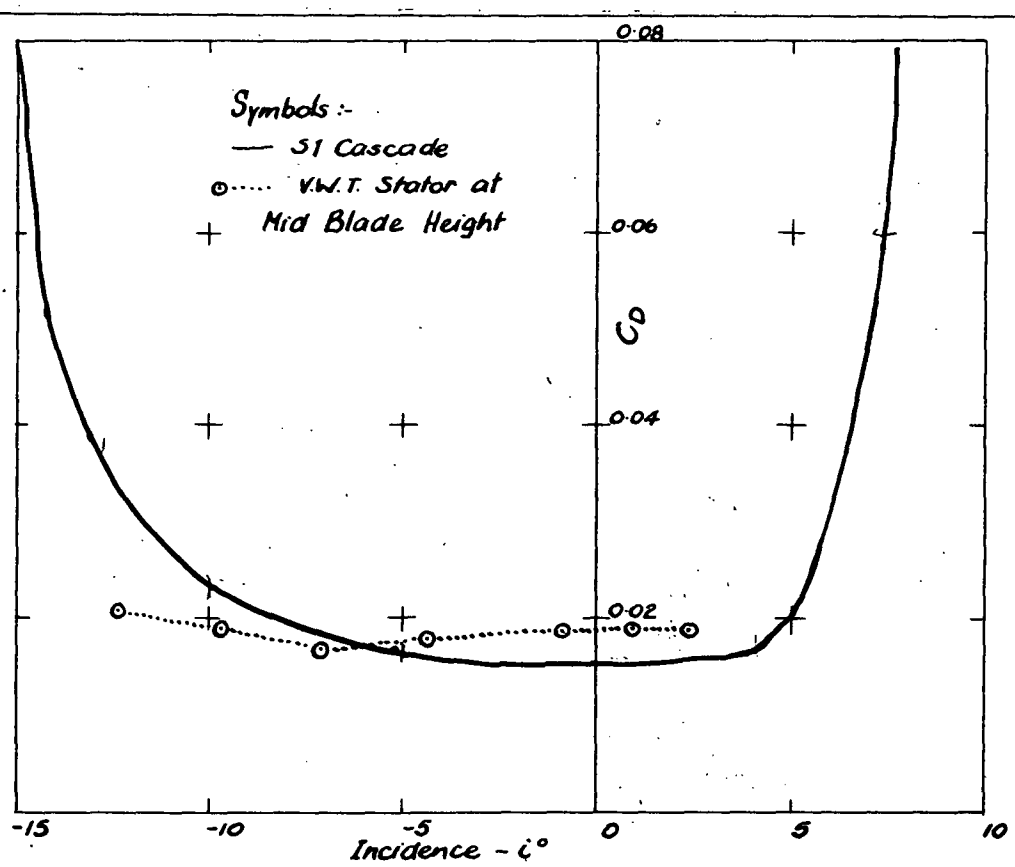

Curves of Drag Coefficient vs. Incidence for S1 Cascade and V.W.T. Stator

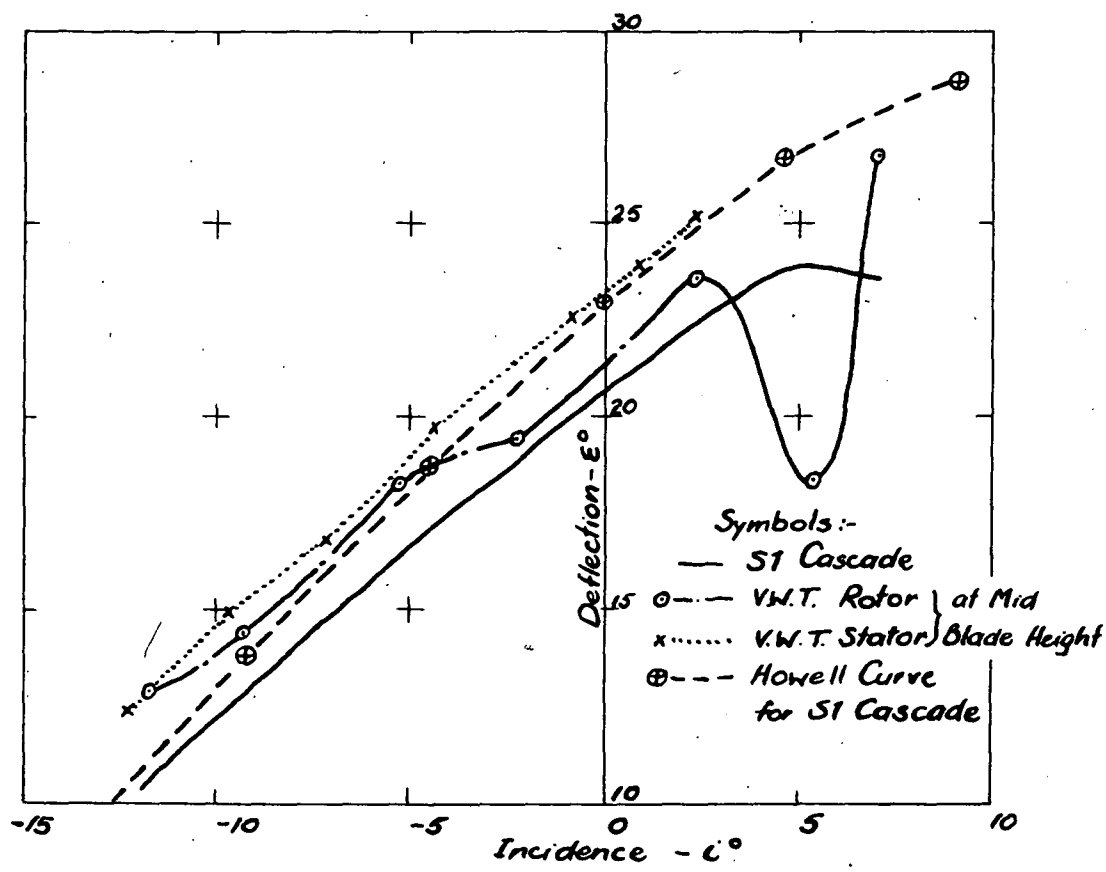

Curves of Air Deflection vs. Incidence for S1 Cascade and V.W.T. Rotor and Stator

Comparisons Between S1 Cascade and V.W.T. Rotor and Stator Measurements

Fig.30.

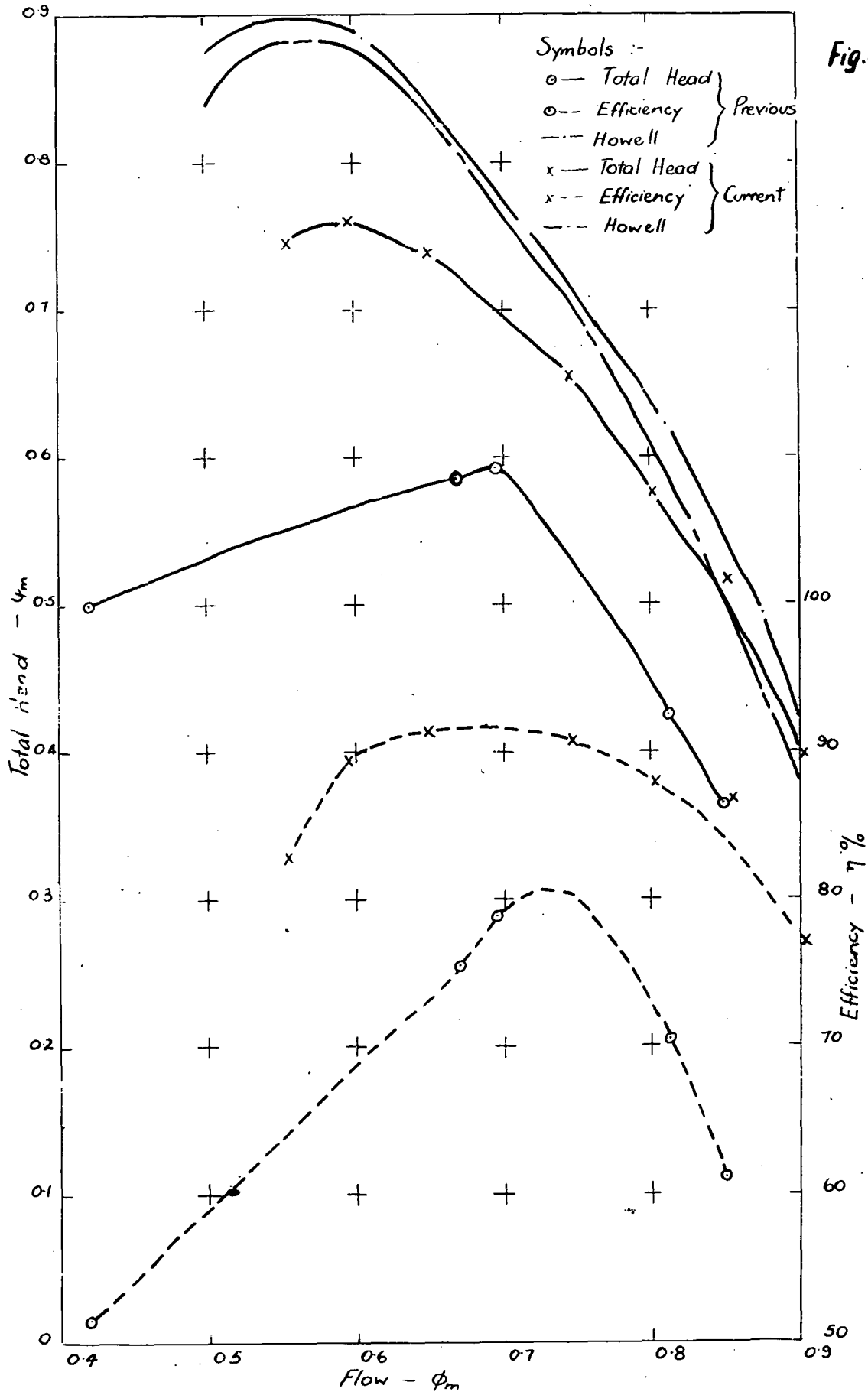

Comparison of Characteristics - Current and Previous Tests

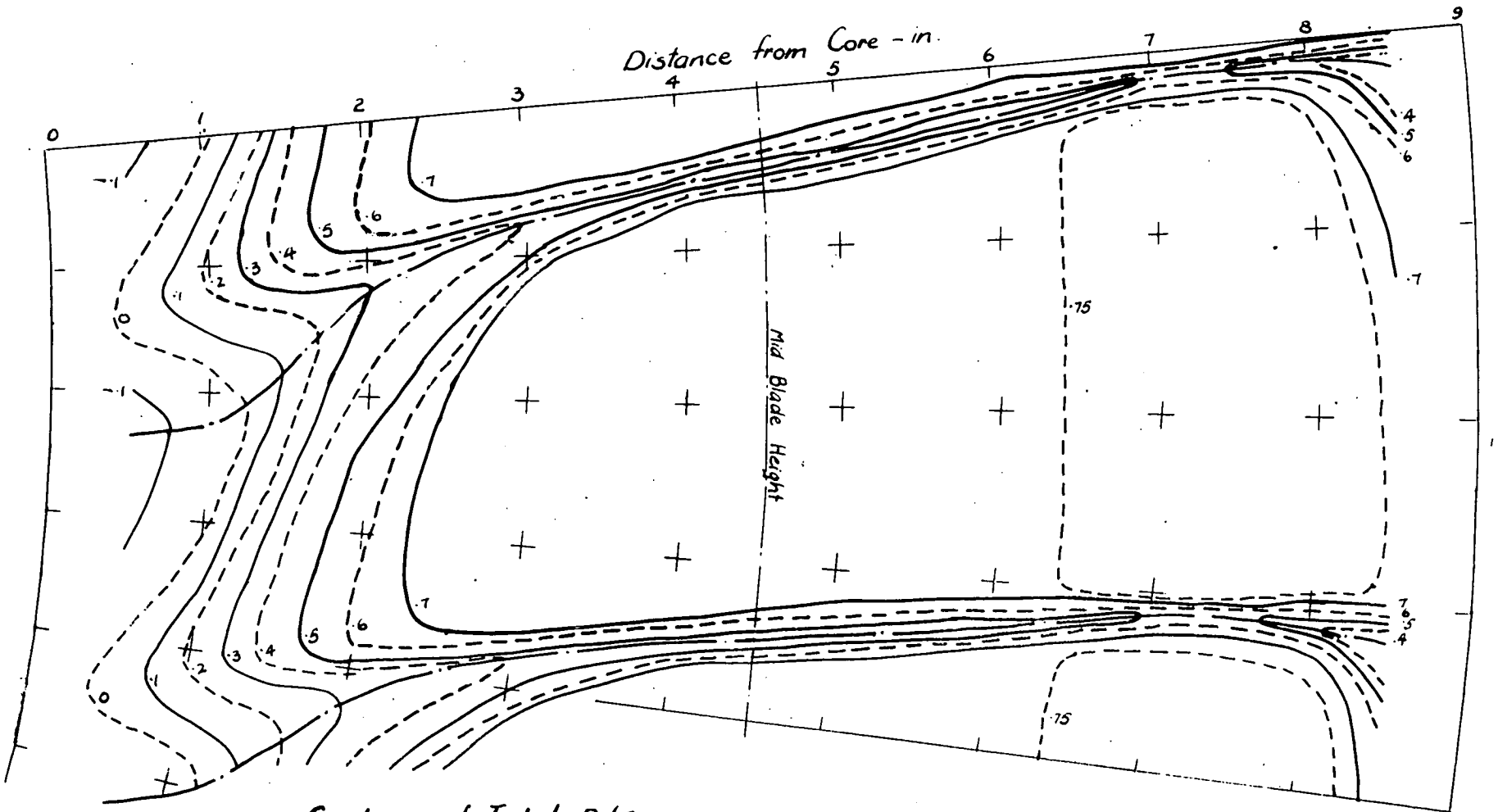

Contour of Total D/S Stator - Previous Tests With Air Leak

8° Throttle, 500 r.p.m., V_a/U_m = 0.68, Machined Rotor, Cast Stator

Fig. 31

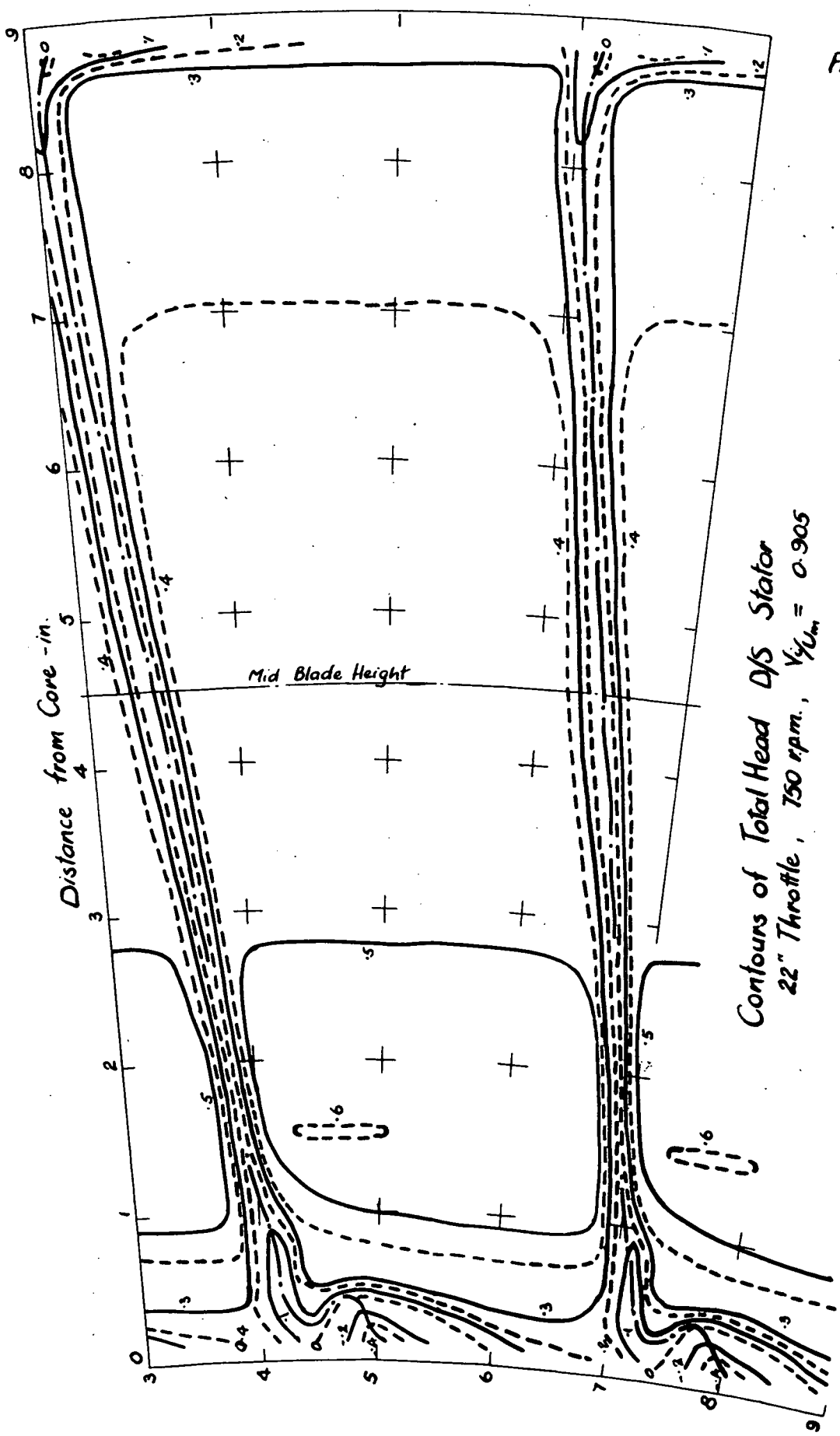
Distance from Core - in.
Mid Blade Height
Contours of Total Head D/S Stator
22" Throttle, 750 r.p.m., Y/U_m = 0.905

Fig. 32

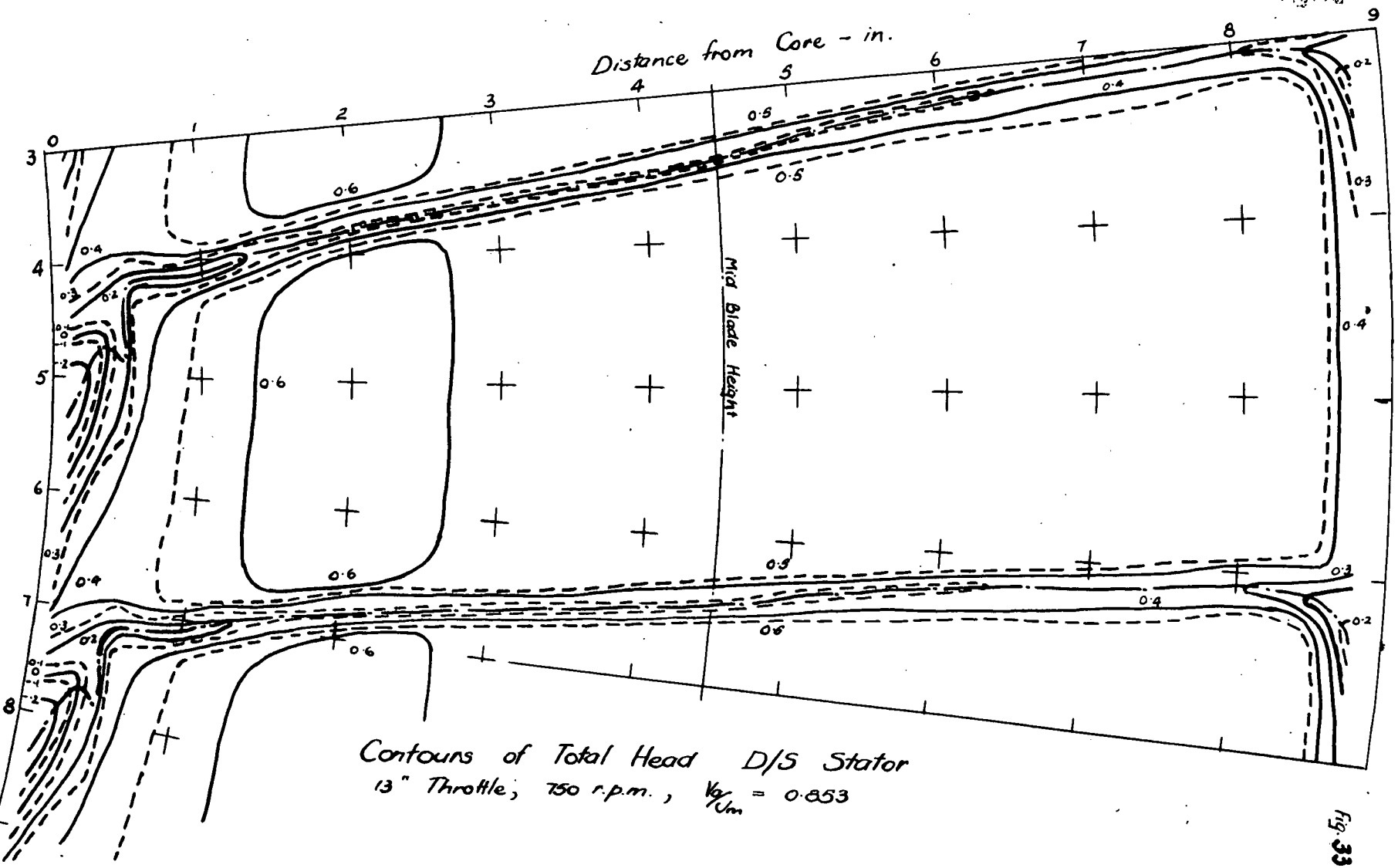

Contours of Total Head D/S Stator

13" Throttle; 750 r.p.m., V_a/U_m = 0·853

Fig. 33

Fig. 34

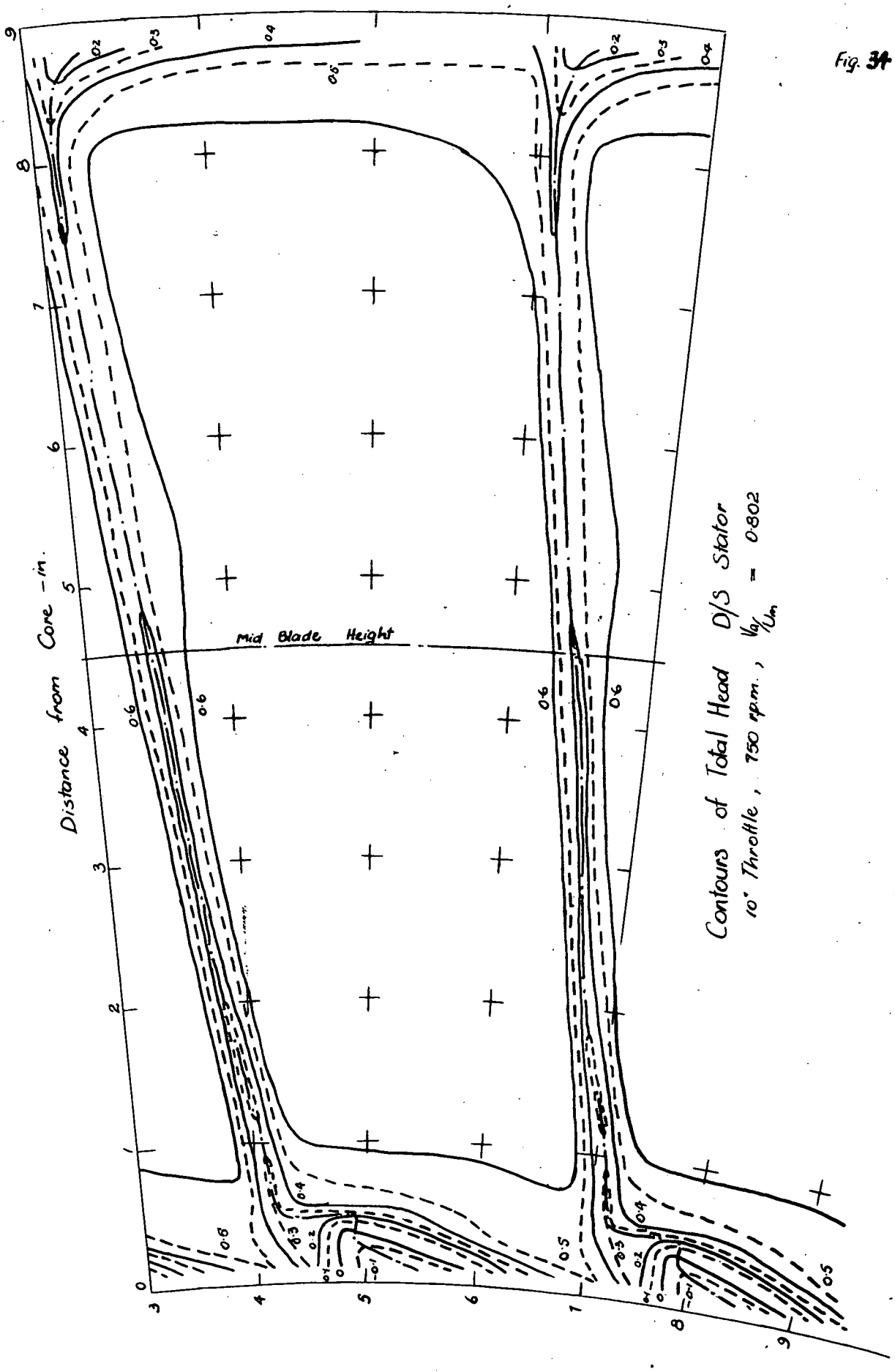
Distance from Core - in.
Mid Blade Height
Contours of Total Head D/S Stator
10° Throttle, 750 r.p.m., Va/Um = 0·802

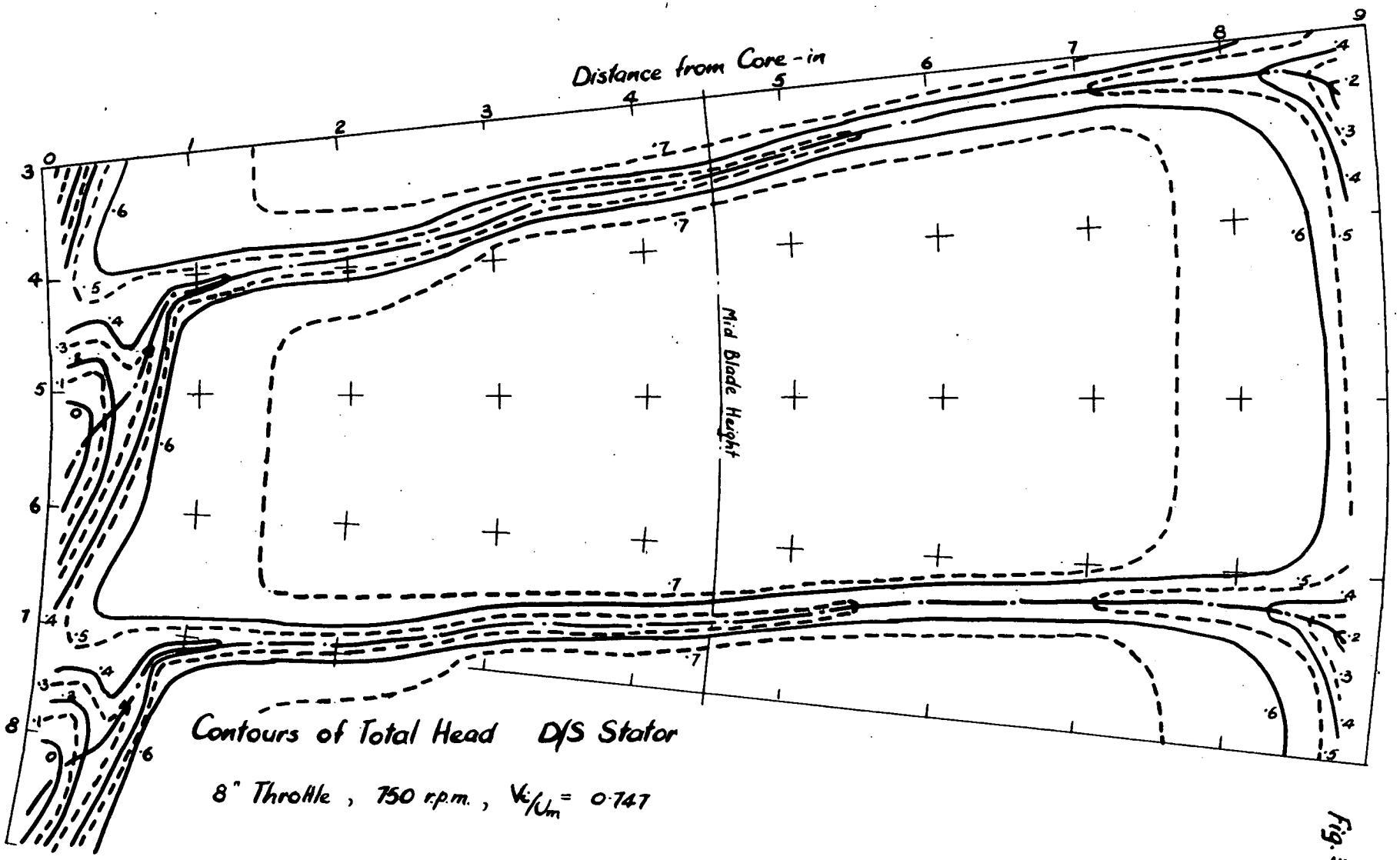

Contours of Total Head D/S Stator

8" Throttle , 750 r.p.m. , $V_x/U_m = 0.747$

Fig. 35

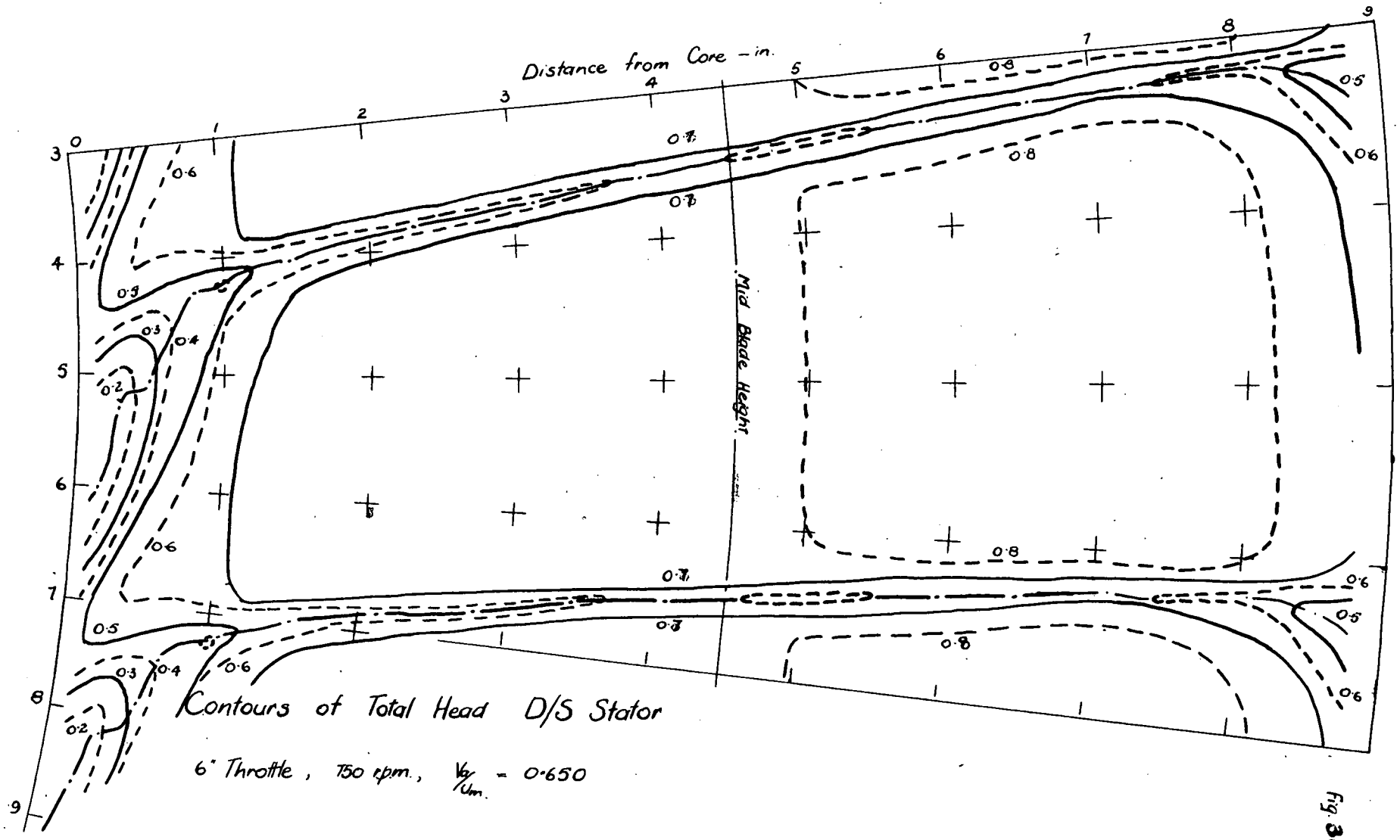

Contours of Total Head D/S Stator

6° Throttle, 750 r.p.m., V_z/U_m = 0·650

fig. 36

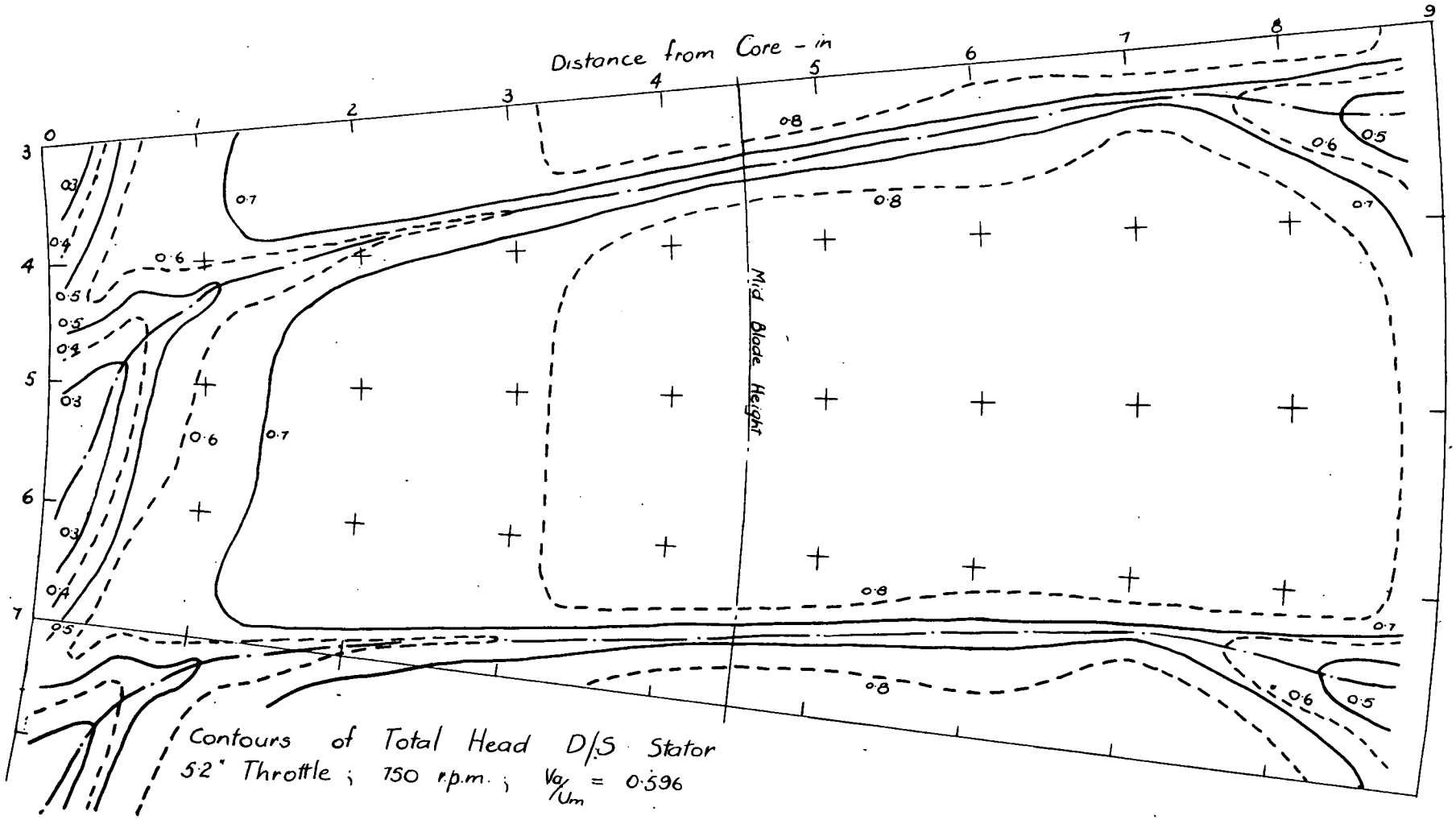

Contours of Total Head D/S Stator
5·2° Throttle ; 750 r.p.m. ; V_a/U_m = 0·596

Fig. 37

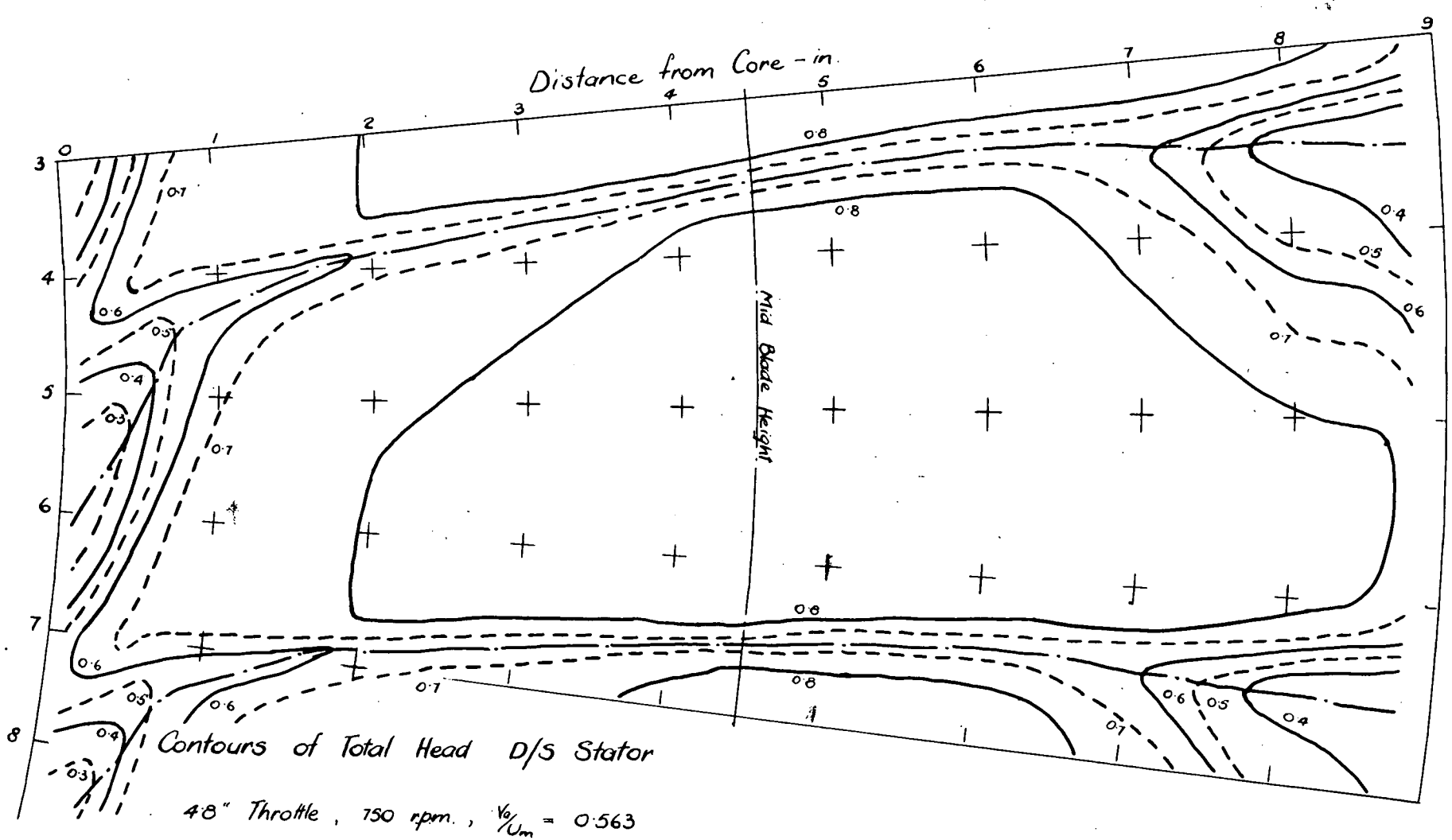

Contours of Total Head D/S Stator

4·8" Throttle, 750 r.p.m., V_o/U_m = 0·563

Fig. 38

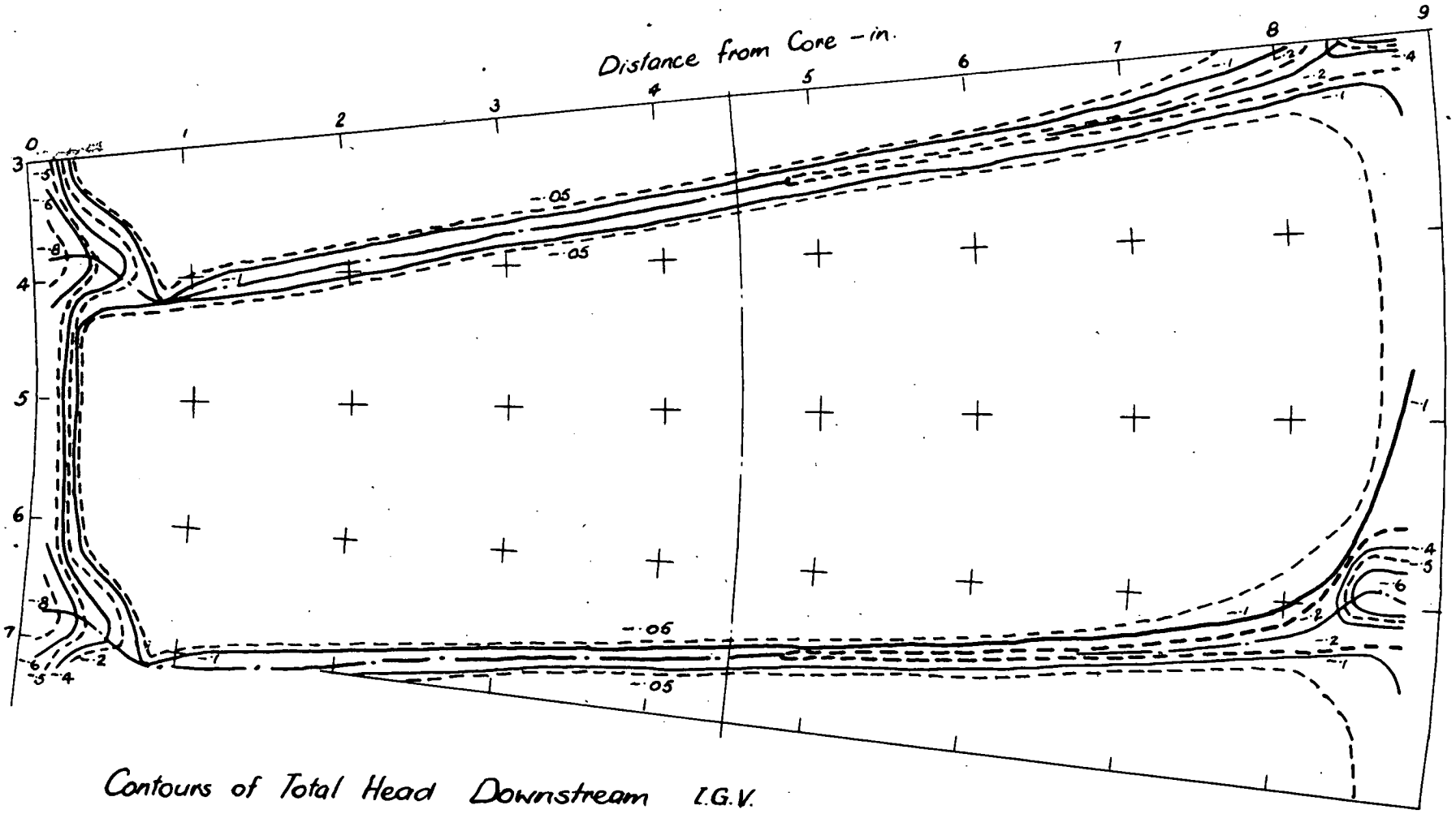

Contours of Total Head Downstream I.G.V.

22" Throttle, 750 r.p.m., $V_i/U_m = 0.905$

Fig. 39

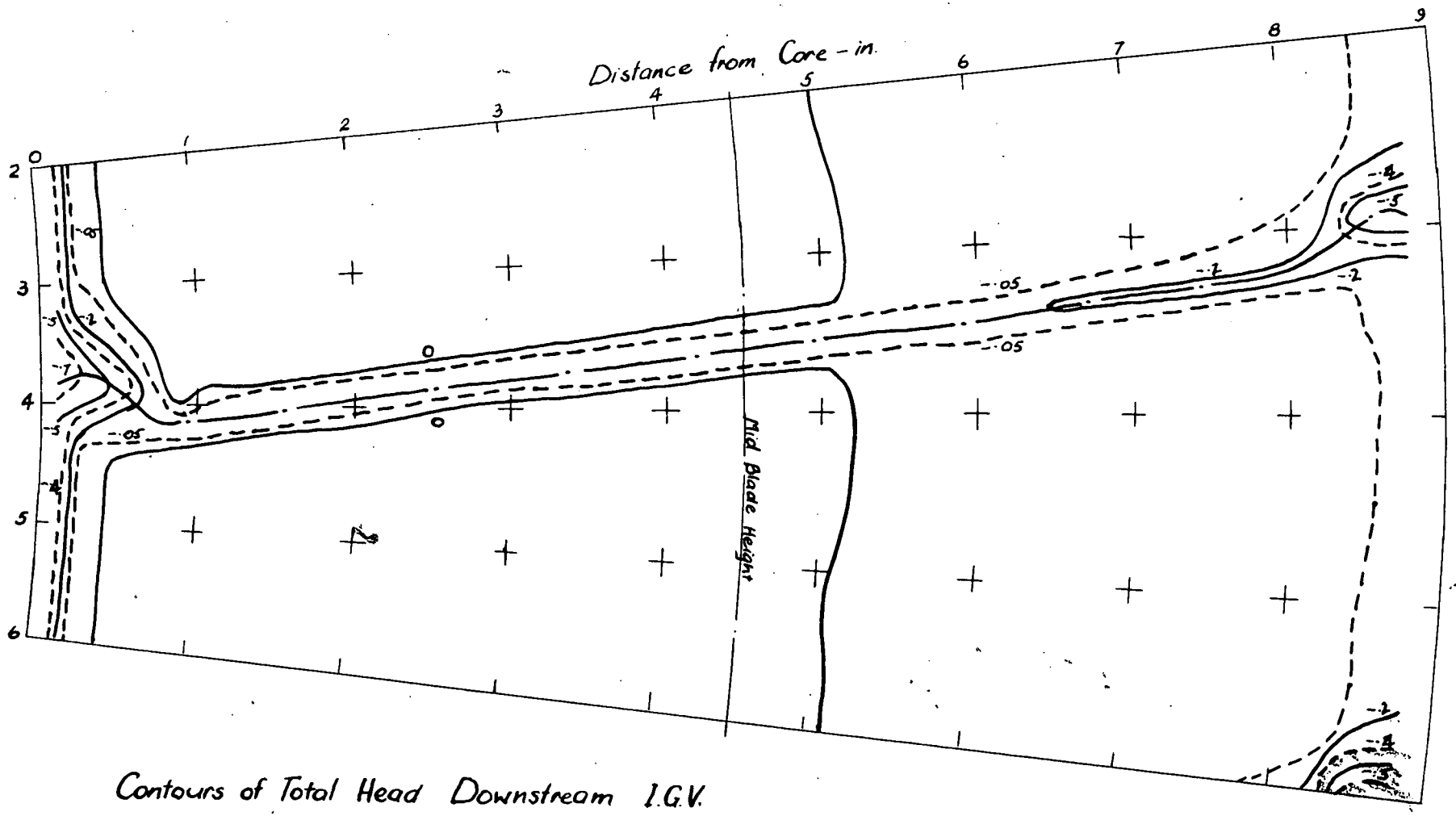

Contours of Total Head Downstream I.G.V.

13" Throttle , 750 r.p.m., V_i/U_m = 0·847

Fig. 40

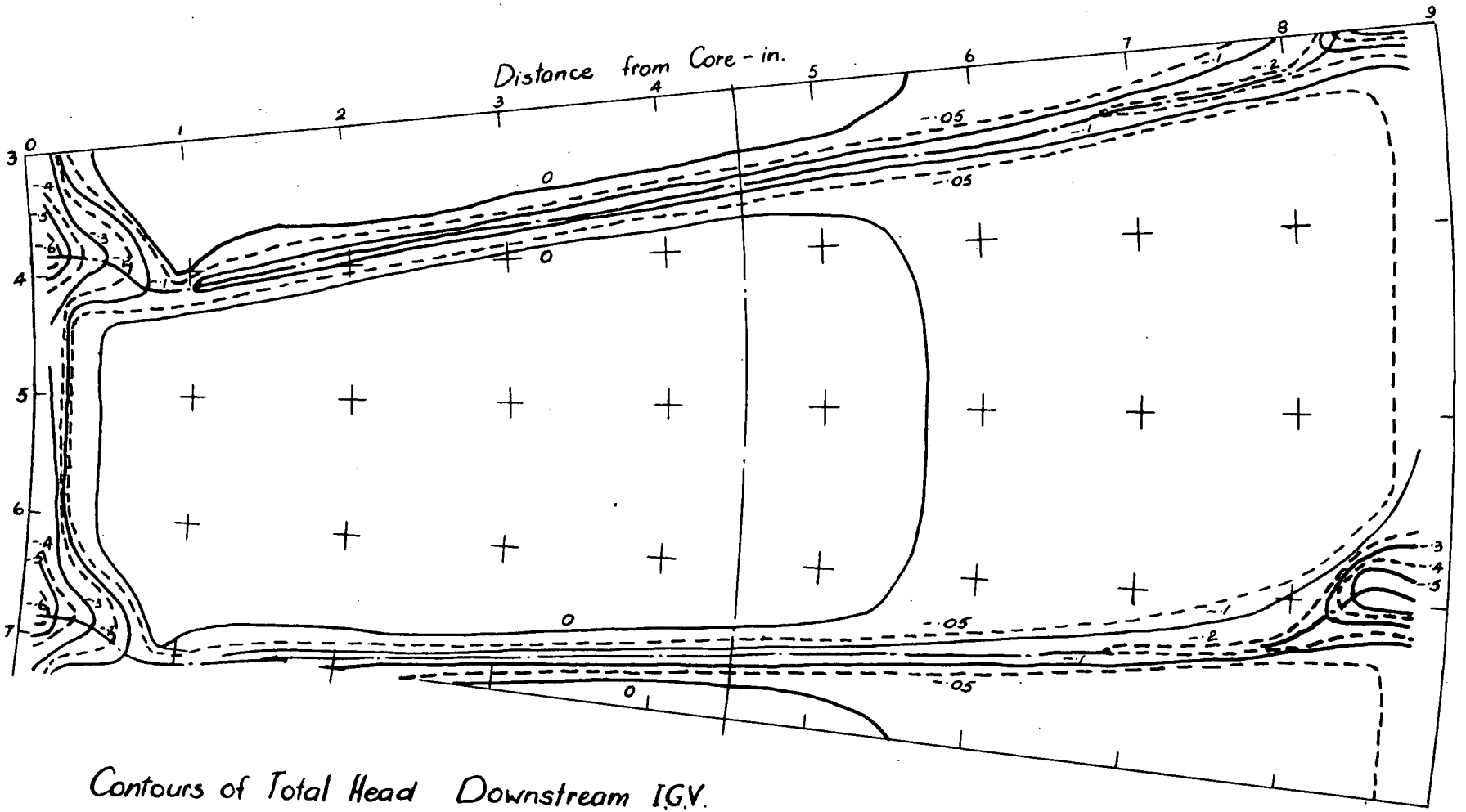

Contours of Total Head Downstream I.G.V.

10" Throttle, 750 r.p.m., $V_i/U_m = 0.799$

Fig. 41

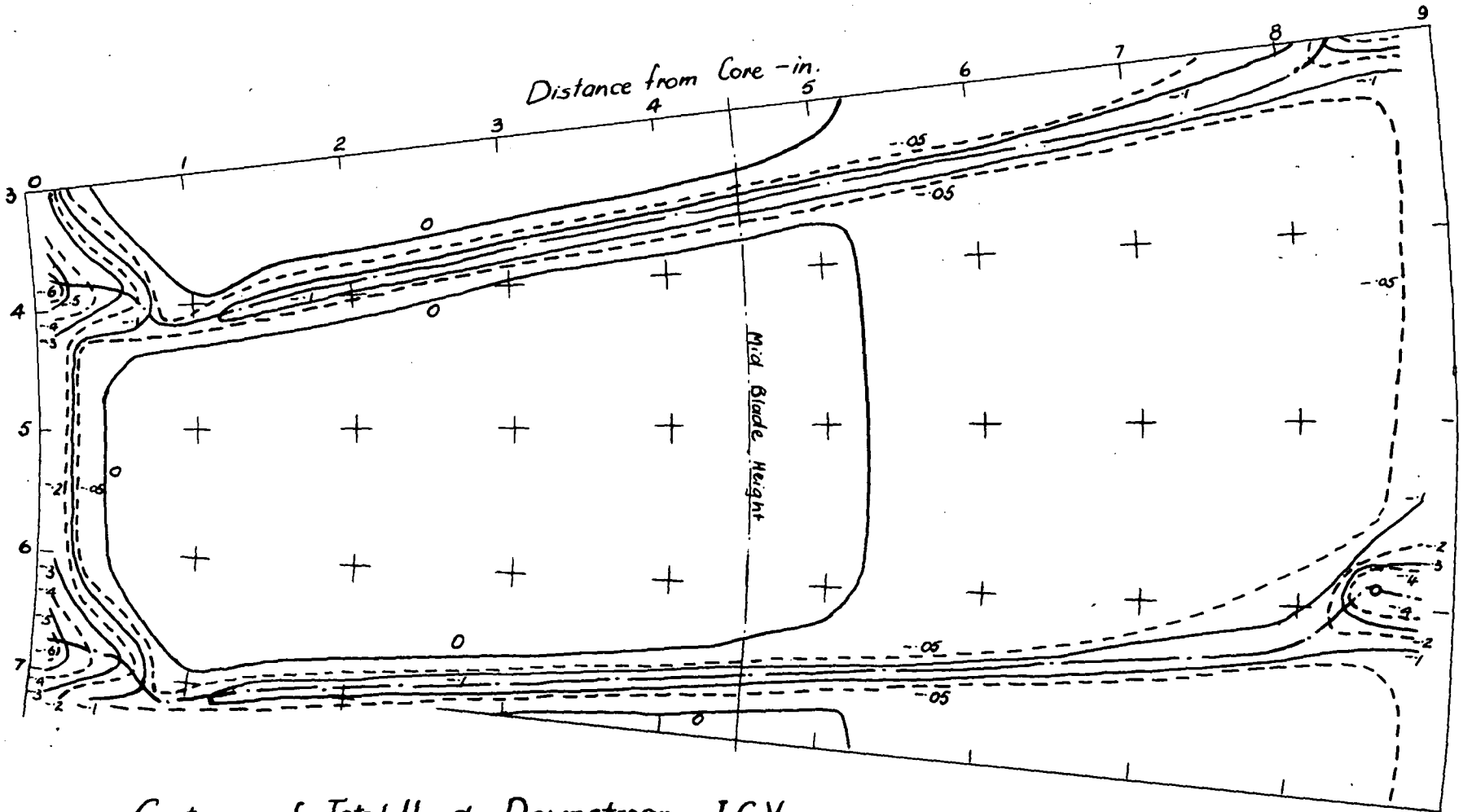

Contours of Total Head Downstream I.G.V.

8" Throttle , 750 r.p.m. , V_i/U_m = 0·744

fig 42

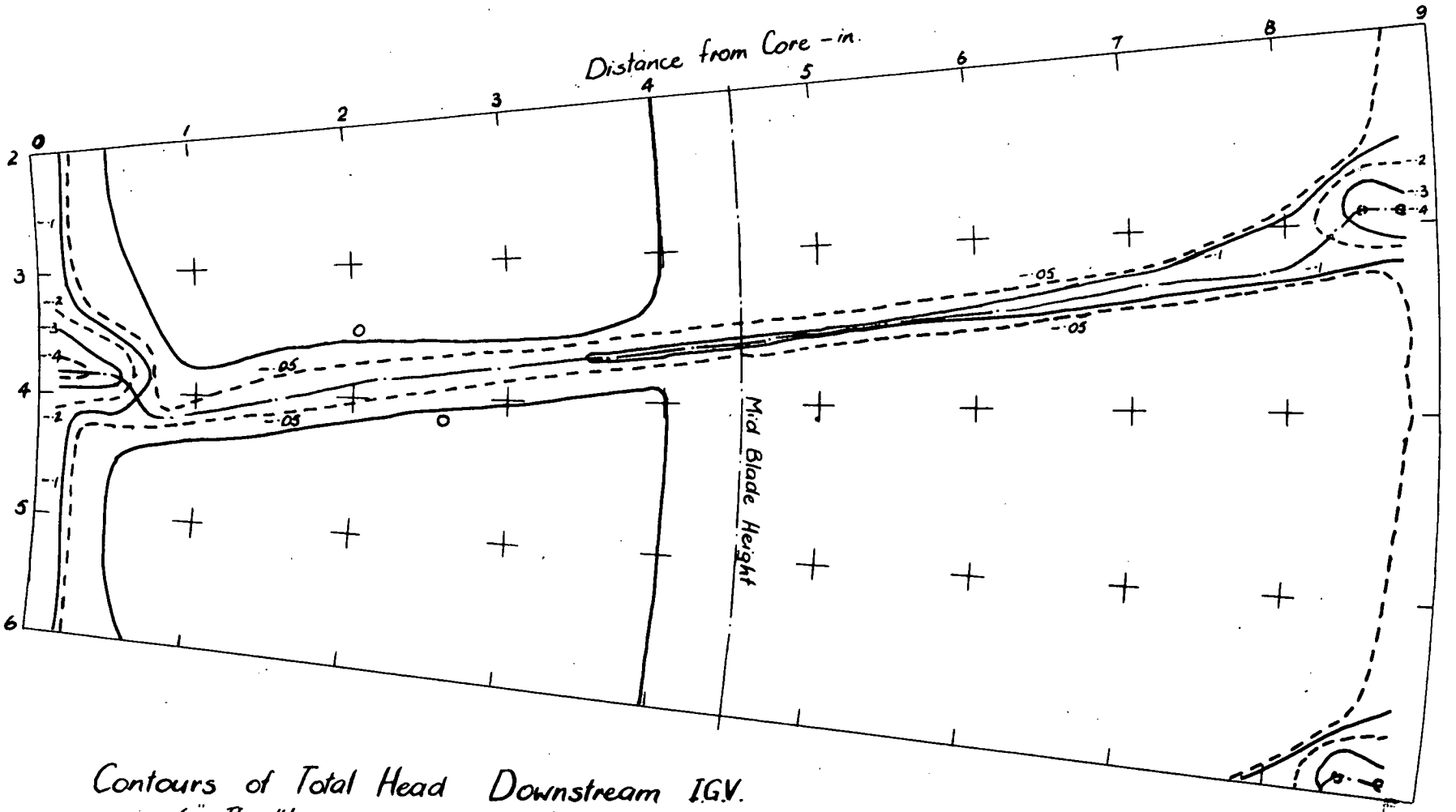

Contours of Total Head Downstream I.G.V.

6" Throttle , 750 r.p.m. , V_i/U_m = 0·651

Fig. 43

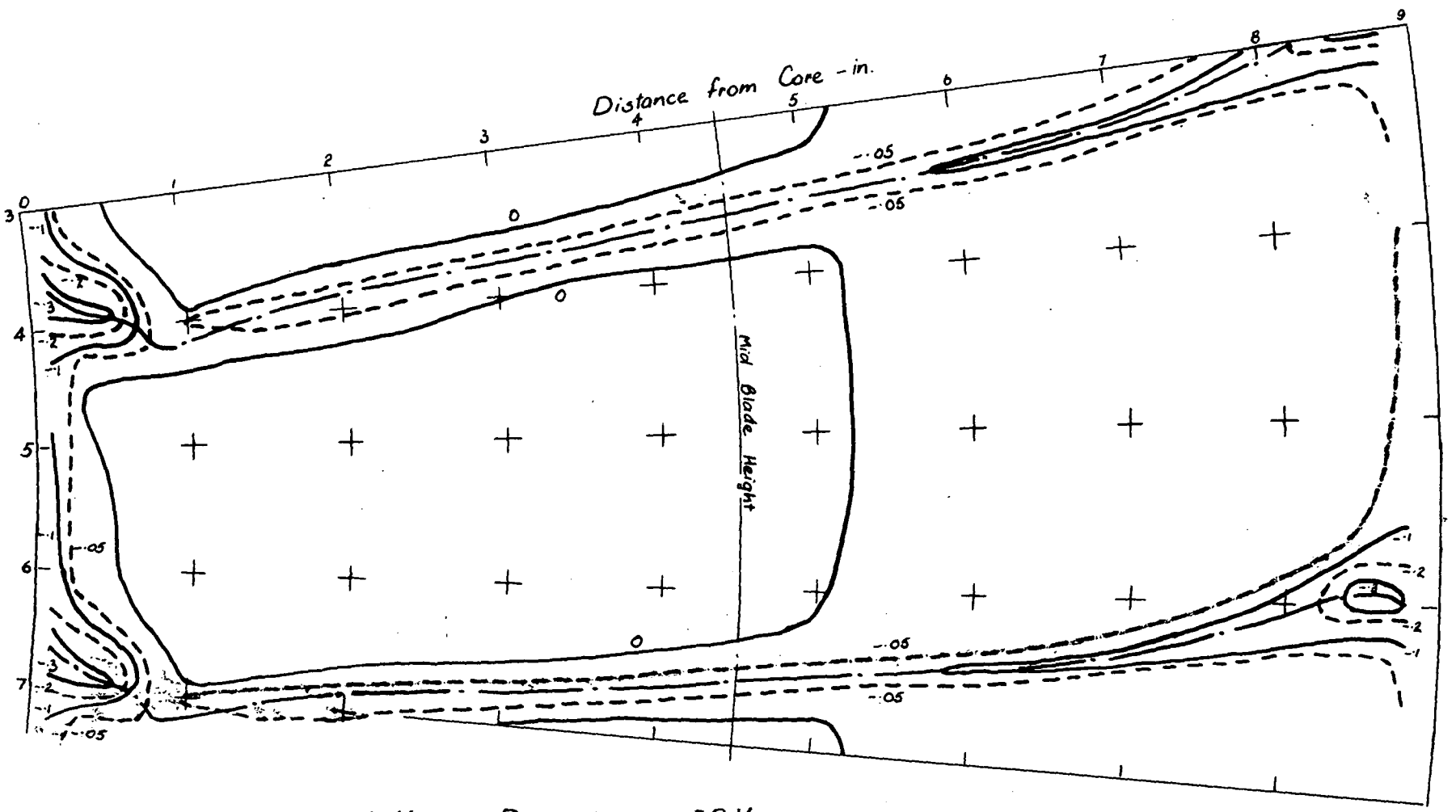

Contours of Total Head Downstream I.G.V.

5·2" Throttle , 750 r.p.m. , V_i/U_m = 0·597

Fig. 44

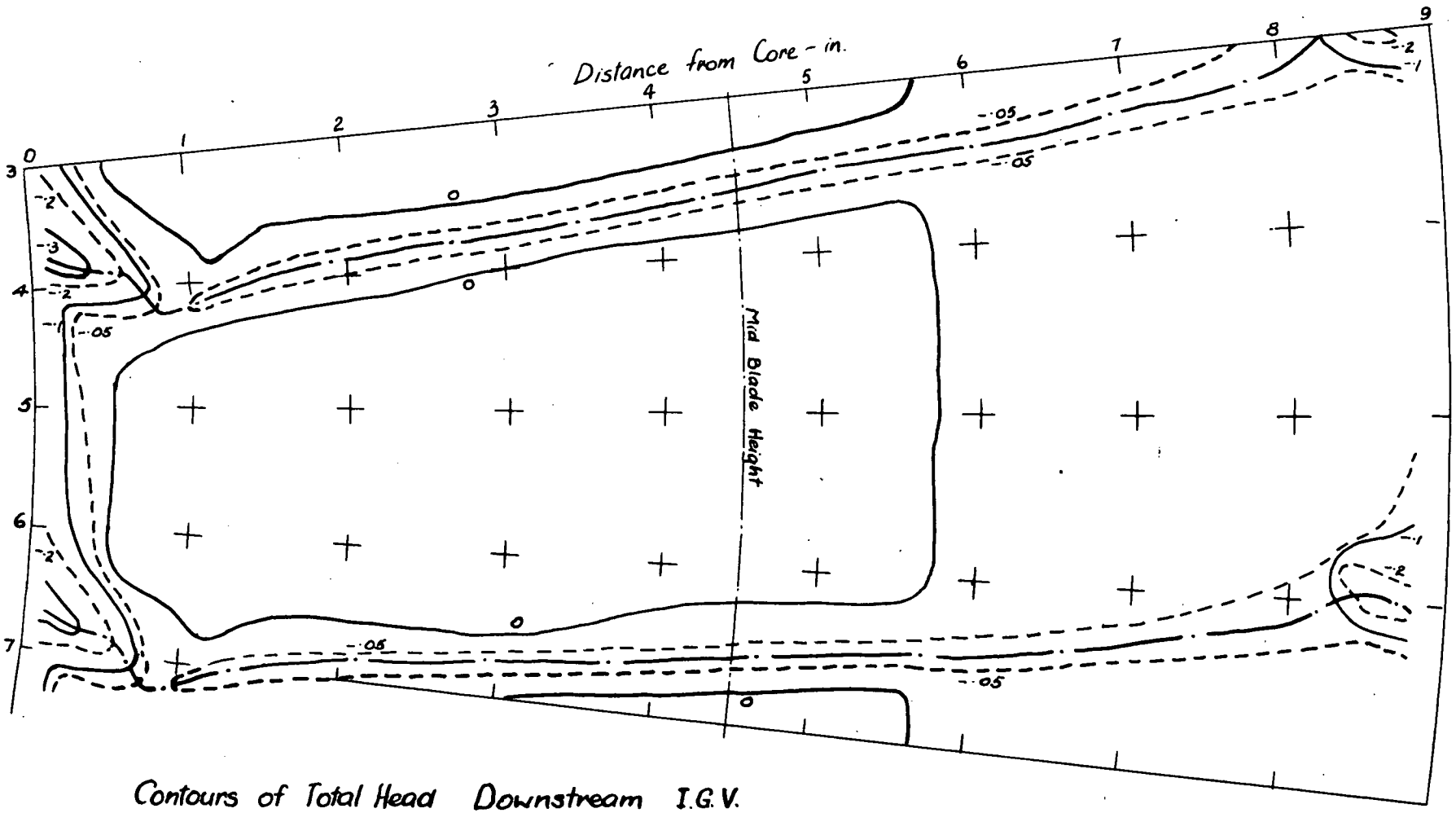

Contours of Total Head Downstream I.G.V.

4·8" Throttle , 750 r.p.m. , V_i/U_m = 0·516

Fig. 45

Fig. 46

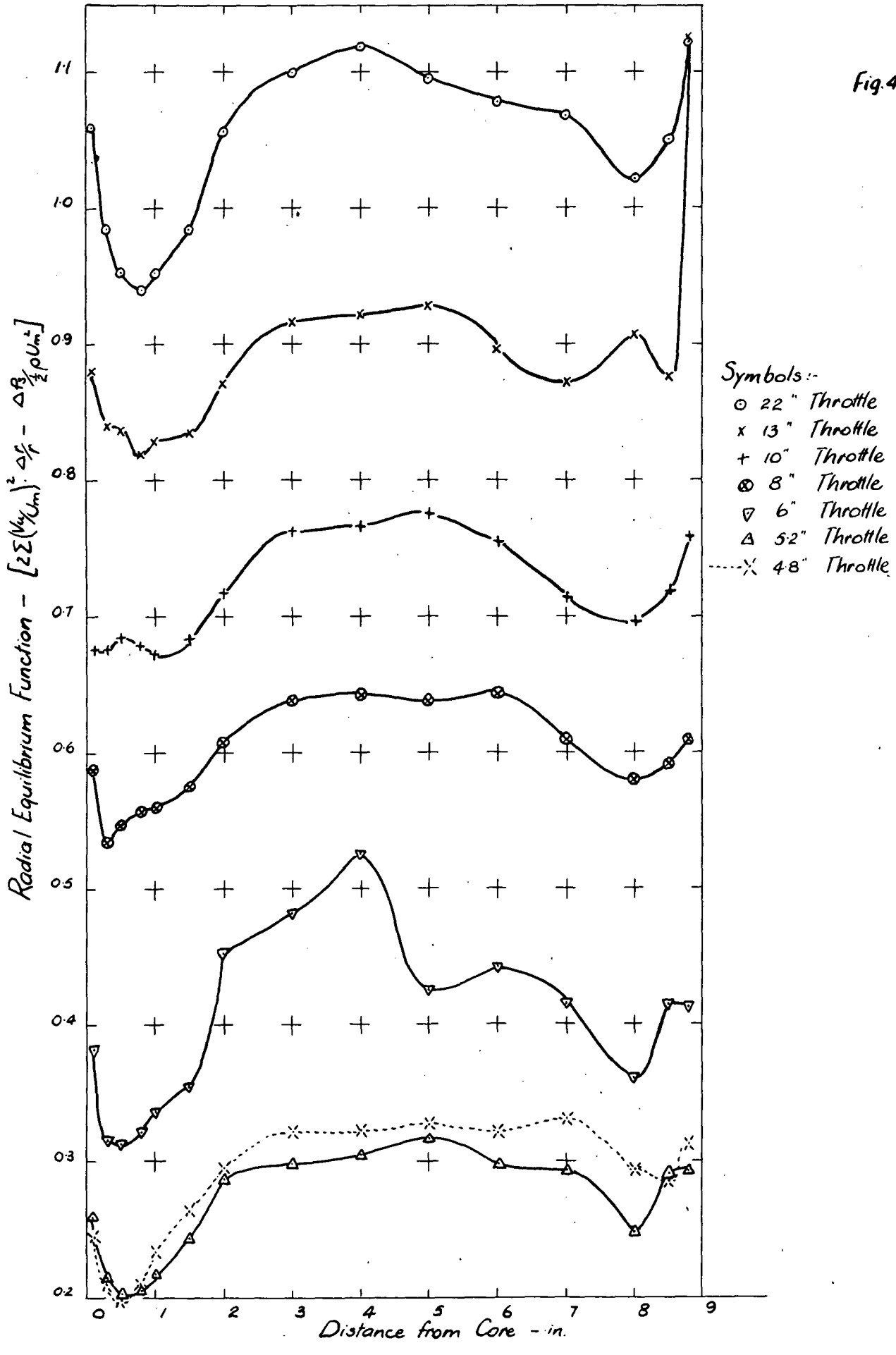

Curves Showing Degree of Radial Equilibrium Attained. Downstream Rotor

Fig. 47

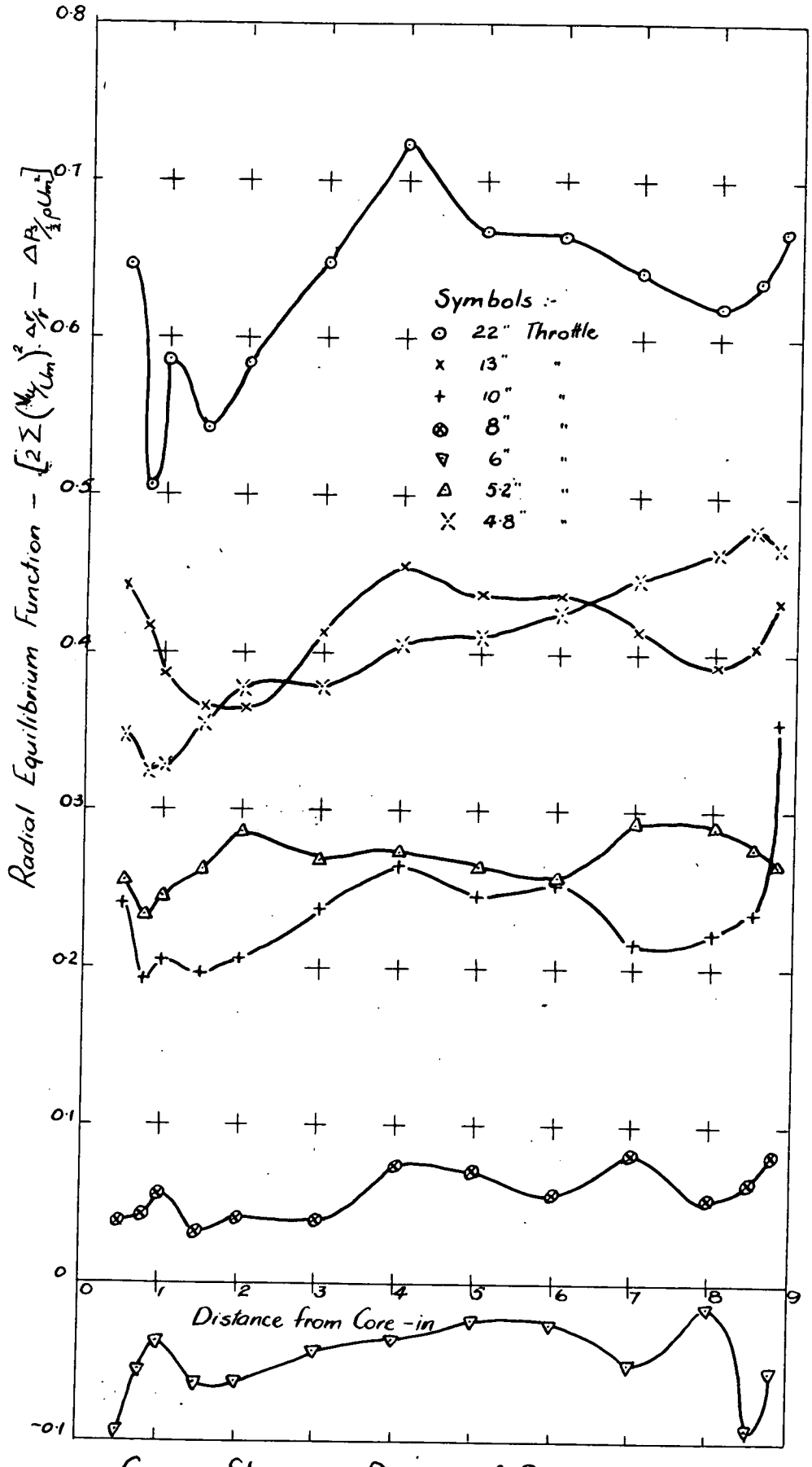

Curves Showing Degree of Radial Equilibrium Attained, Downstream Stator

Fig.48

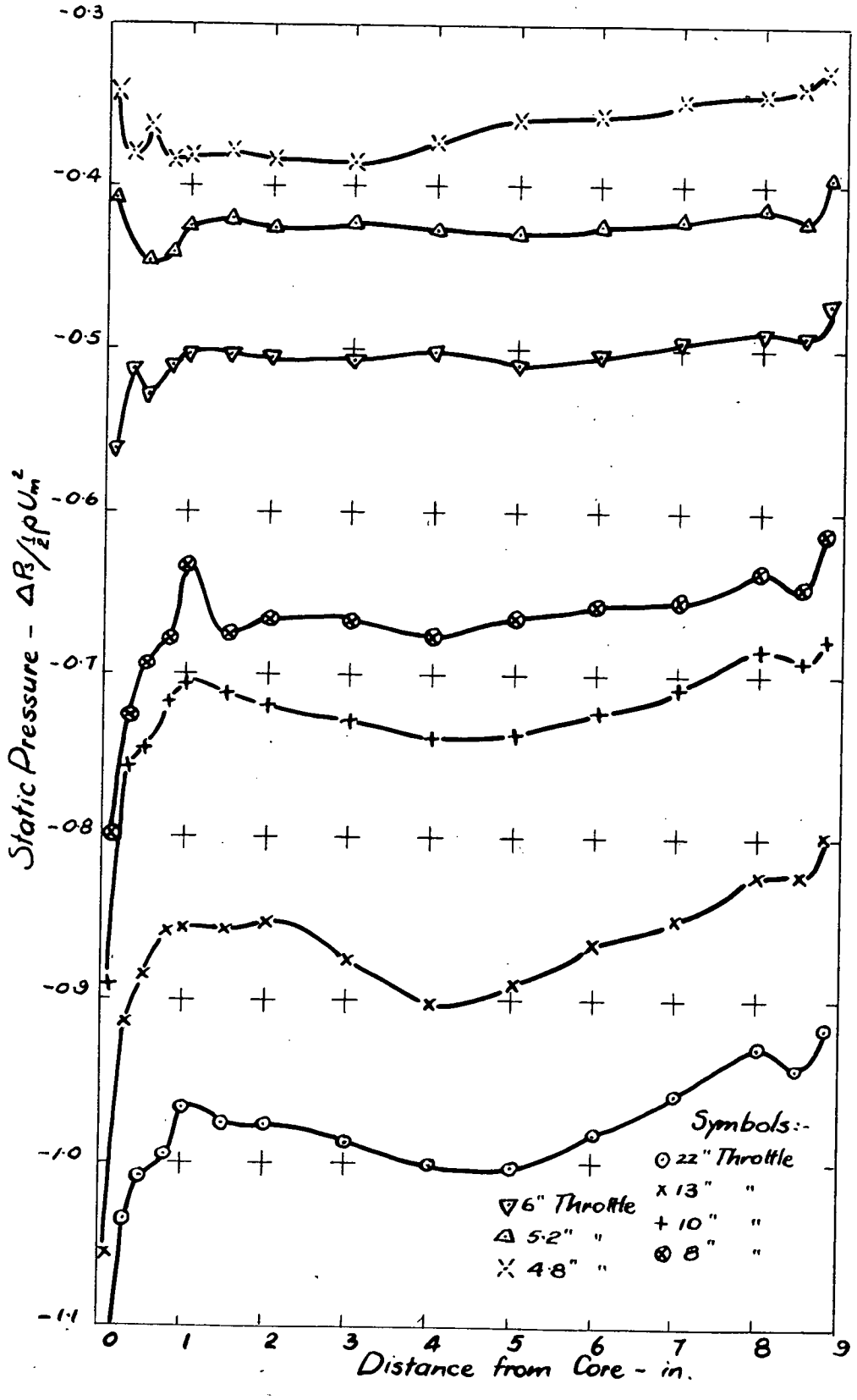

Static Pressure D/S Inlet Guide Vanes

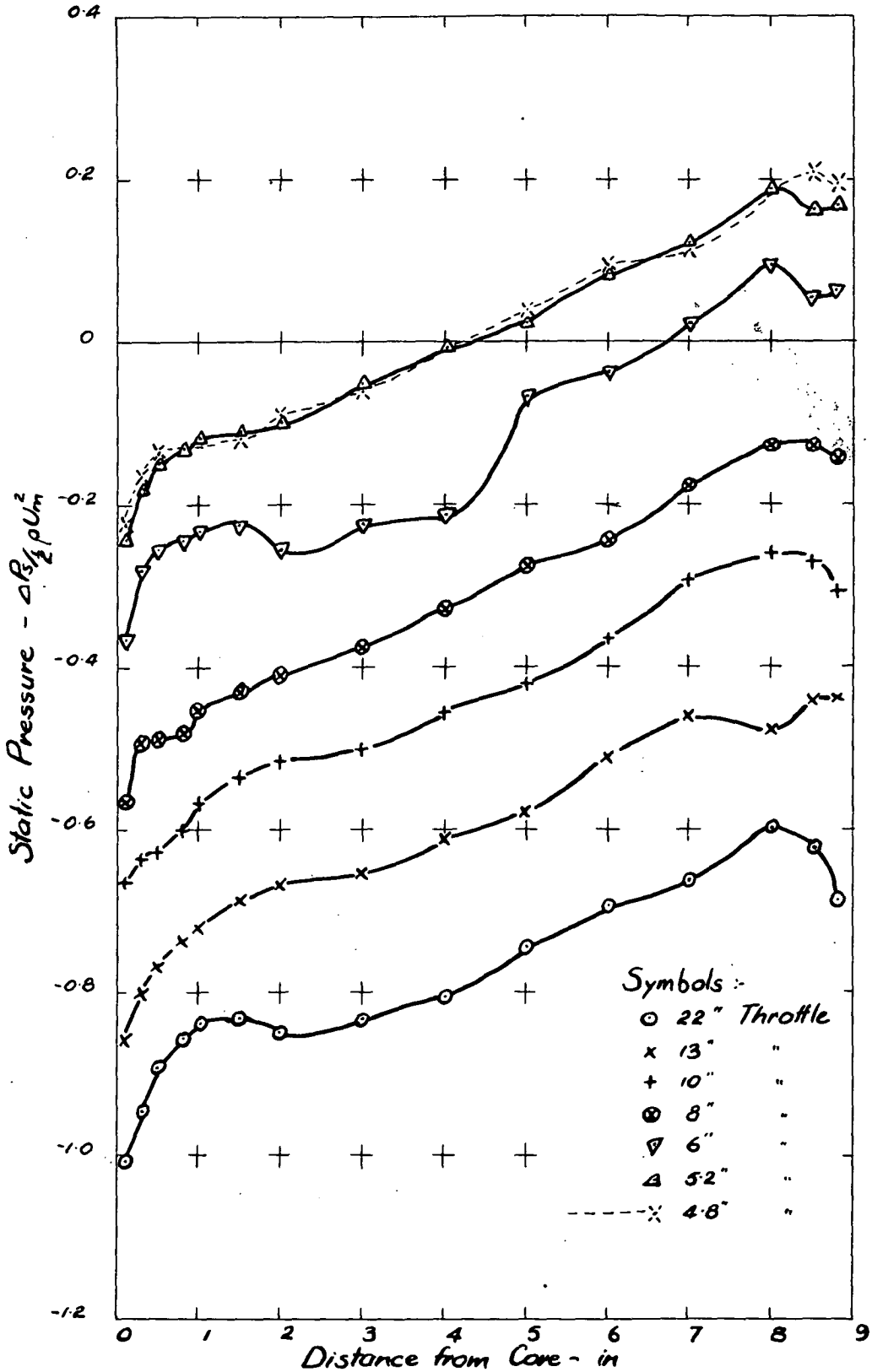

Static Pressure Downstream Rotor

Fig. 50

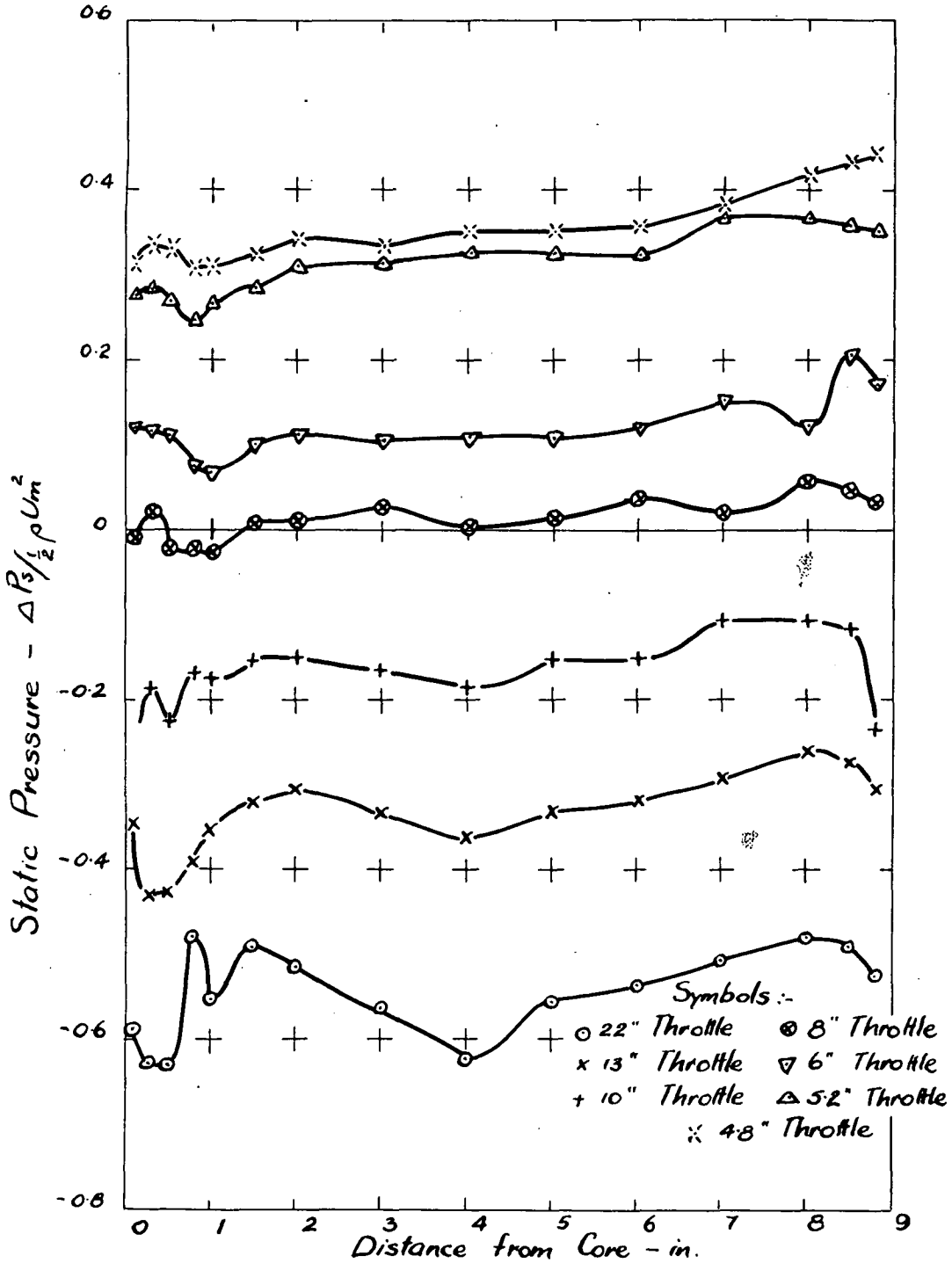

Static Pressure Downstream Stator

Fig.51

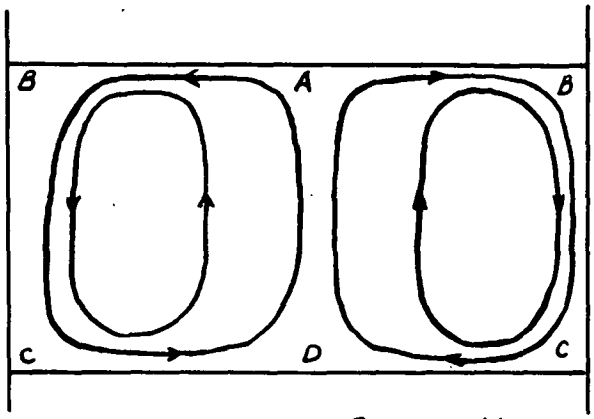

(a) Formation of Main Stream Vortices in a Cascade

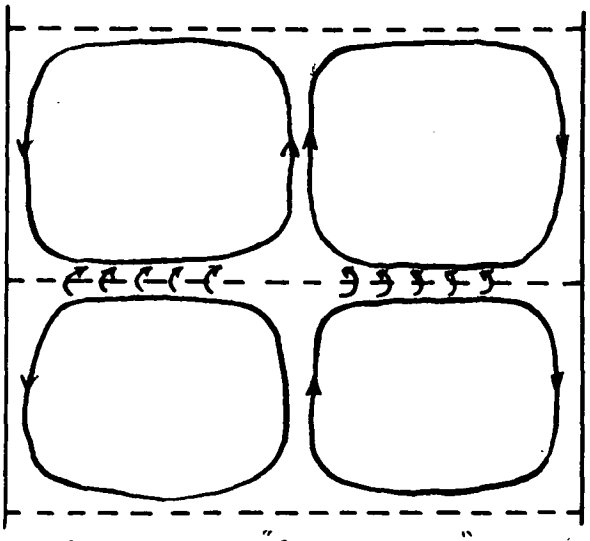

(b) Formation of "Ball Bearing" Vortices Downstream of the Cascade

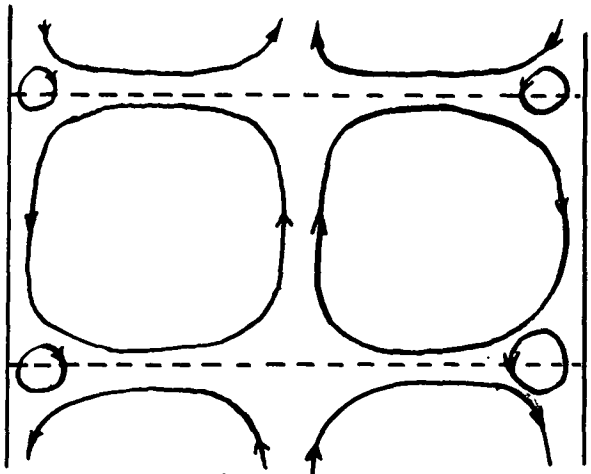

(c) "Rolling Up" of Ball Bearings Into "Trailing" Vortices

Formation of Main Stream and Trailing Vortices as in Ref. 10

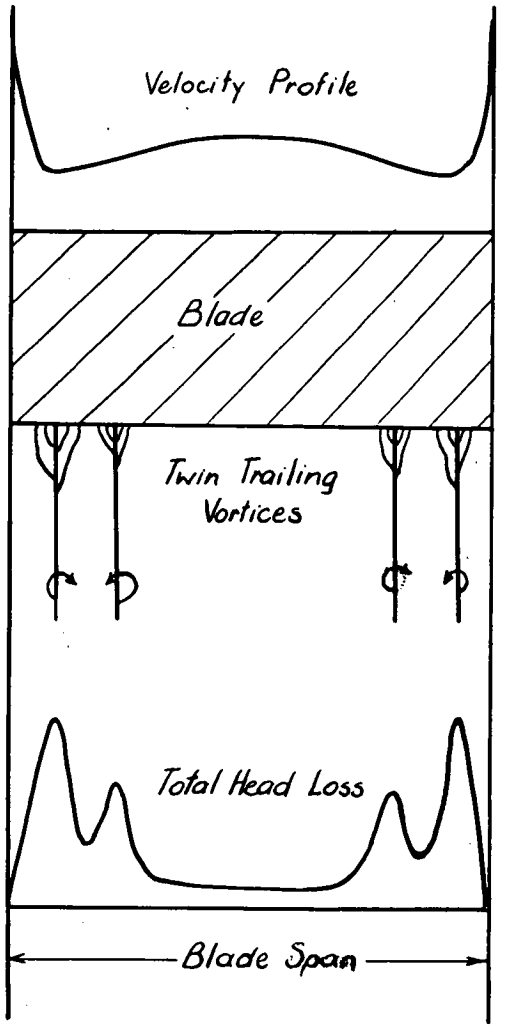

(a) Formation of Twin Vortices and Loss Peaks With M Shaped Velocity Distribution

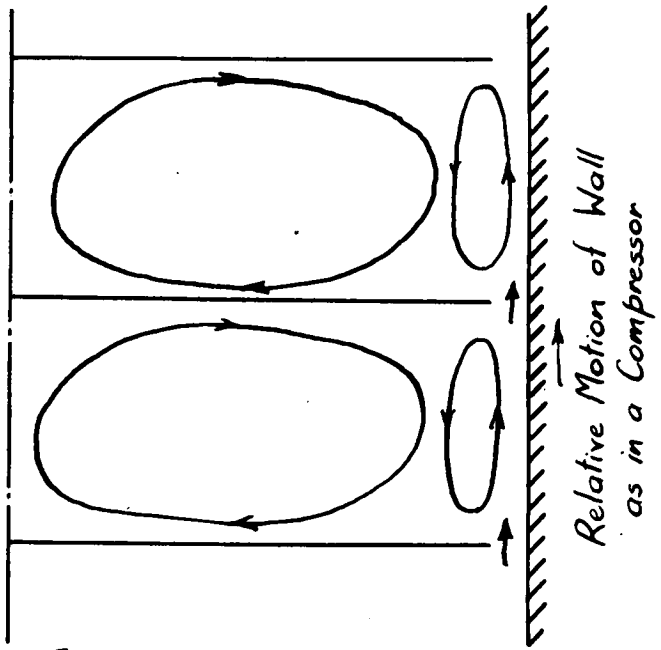

(b) Formation of Separate Main Stream Vortex With Tip Leakage and the Moving Wall.

Formation of Secondary Flows With and M Shaped Velocity Distribution, and Tip Leakage With Moving Wall

Fig. 52

Fig. 53

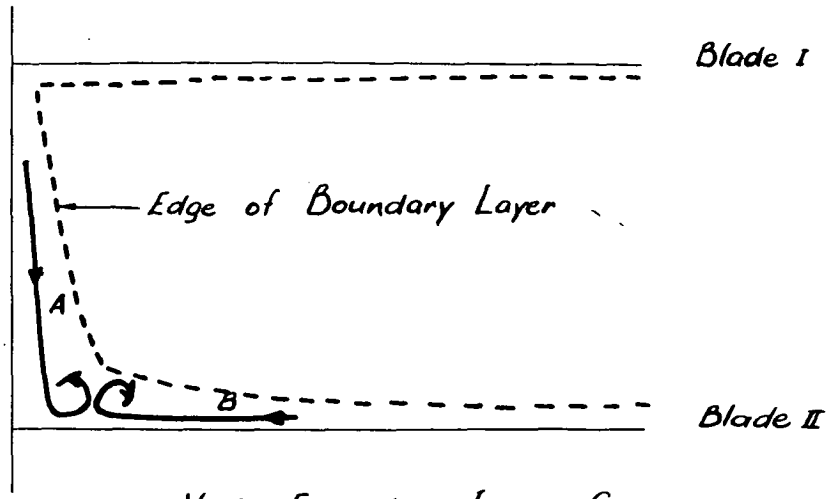

(a) Vortex Formation Inside Cascade

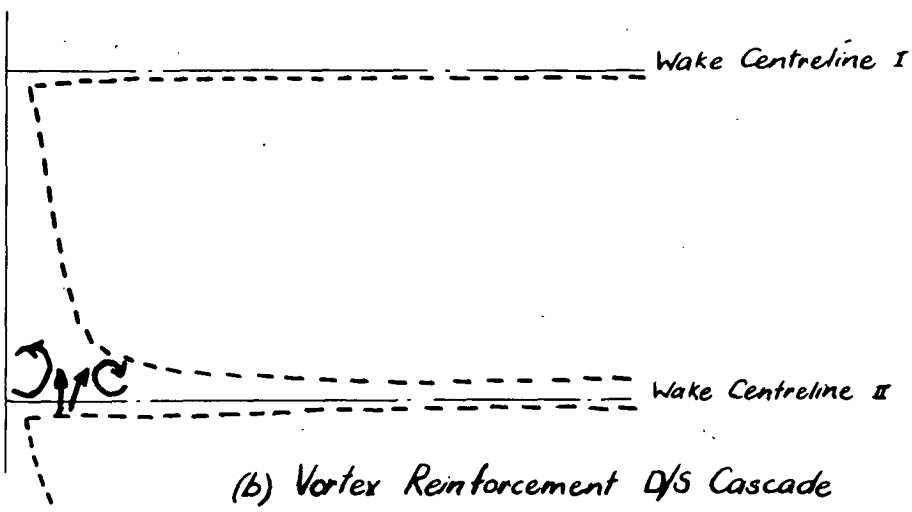

(b) Vortex Reinforcement D/S Cascade

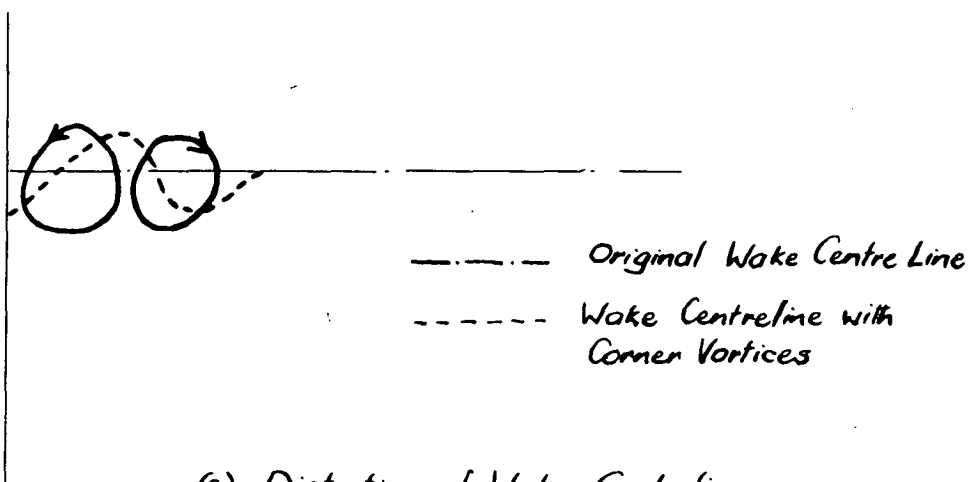

(c) Distortion of Wake Centreline Due to Twin Corner Vortices

Hypothetical Formation and Effects of Twin Corner Vortices in a Cascade

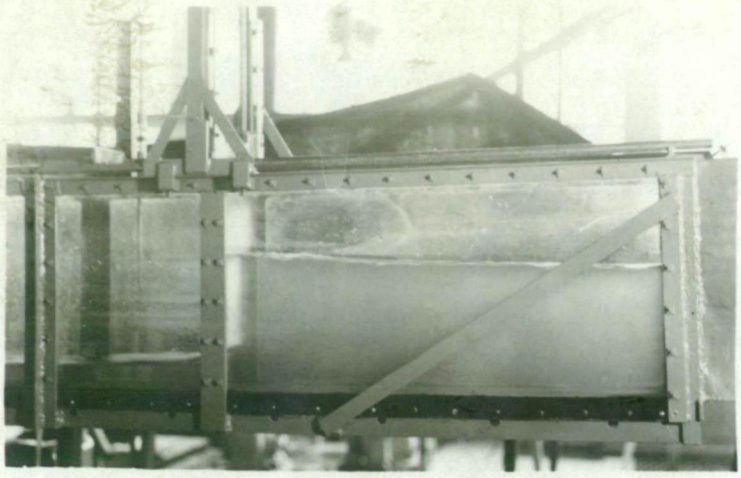

(a) Water Channel

(b) Main Stream Vortex

Actually this is a horseshoe vortex

(c) Corner Vortex Shown by Arrow A.

Vortex Formation on Upstream Side of Gate in Water Channel.